ABSTRACT

Title of Dissertation: ENERGY LOCALIZATION AND TRANSPORT IN BINARY ISOTOPICALLY DISORDERED FERMI-PASTA-ULAM CHAINS

Kenneth Alan Snyder, Doctor of Philosophy, 2005

Dissertation directed by: Professor T.R. Kirkpatrick
Department of Physics

Energy transport in binary isotopically disordered (BID) nonlinear Fermi-Pasta-Ulam (FPU) chains is a competition between localization and mode transitions. Starting from an arbitrary localized pulse, energy will dissipate ballistically until either Anderson localization (a disorder effect) or phonon scattering (a nonlinearity effect) slow the rate of dissipation. To reduce computational effort, we propose starting from a localized energy eigenstate so that in the absence of anharmonicity the energy is stationary and there is no transport. The second moment of the site energies is used to characterize an effective thermal conductivity as a function of impurity concentration and nonlinearity strength.

Calculating the properties of harmonic BID chains at arbitrary impurity concentration is complicated by the pure-disordered-pure transition that occurs as

the impurity concentration varies from zero to one. The localization length of dilute impurity harmonic BID chains is calculated exactly using scaling laws and the scattering cross section of a single impurity, which is calculated for discrete systems, differs from the continuum result. For arbitrary impurity concentration, the localization length is estimated by assuming independent contributions from the two limiting cases of pure material.

Information entropy was used to show that the number of modes excited by phonon scattering decreased with increasing impurity concentration, a fact that consistent with density of states calculations. At all impurity concentrations, the second moment of the site energies increases linearly in time, a fact that is corroborated by the number of masses participating in energy transport, as calculated from the localization parameter. The dilute concentration dependence of the effective thermal conductivity was consistent with kinetic theory. At the highest concentrations the thermal conductivity was proportional to the original localization length because mode suppression and dense impurities meant that the same length scale remained dominant over a long period of time.

ENERGY LOCALIZATION AND TRANSPORT IN BINARY ISOTOPICALLY DISORDERED FERMI-PASTA-ULAM CHAINS

by

Kenneth Alan Snyder

Dissertation submitted to the Faculty of the Graduate School of the
University of Maryland, College Park in partial fulfillment
of the requirements for the degree of
Doctor of Philosophy
2005

Advisory Committee:

Professor T.R. Kirkpatrick, Chairman/Advisor
Professor J.R. Dorfman
Professor A.B. Hassam
Professor C.J. Lobb
Professor D. Thirumalai
Dr. E.J. Garboczi (NIST)

ACKNOWLEDGEMENTS

Beginning in high school, I have always wanted to study physics and pursue a Ph.D. My path toward this goal has been long and tortuous. Along the way, a number of people have contributed in various ways toward this achievement.

My scientific career began as a research associate under Prof. Ken Hover (Cornell University). My interactions with Ken and his graduate students helped me learn to stand up for what I believed to be true. I later moved on to my current position within the Inorganic Group at the National Institute of Standards and Technology (NIST), where I have been given considerable freedom to explore ideas. My interactions with my NIST colleagues have taught me a lot about science and a lot about how scientists can work together in harmony toward a common goal. Most of all, I want to thank my Group Leader, Dr. Edward Garboczi, for both participating on my defense committee and for allowing me considerable latitude in finding the means necessary to finish.

I am also indebted to my advisor, Prof. Ted Kirkpatrick. His encouragement and reassurance kept me going. I learned a lot from our discussions that covered topics both inside and outside the field of physics.

Finally, I am deeply indebted to my wife Marcia and son David. Families have no choice but to share the burden of graduate studies. I am grateful for their patience, understanding, and encouragement.

TABLE OF CONTENTS

LIST OF TABLES

LIST OF FIGURES

LIST OF ACRONYMS

AS	Azbel and Soven
ATAF	Anderson, Thouless, Abrahams, and Fisher
BID	Binary Isotopically Disordered
BIDHC	Binary Isotopically Disordered Harmonic Chain
FPU	Fermi-Pasta-Ulam
FT	Fourier Transform
GF	Green's Function
GK	Green-Kubo
KAM	Kolmogorov-Arnol'd-Moser
KP	Kronig-Penney
NEMD	Non-Equilibrium Molecular Dynamics
SE	Standard Error of the sample mean
SHO	Simple Harmonic Oscillator
SIA4	Simplectic Integration Algorithm: 4-th Order
TBM	Tight Binding Model

Chapter 1

Introduction

This study investigates energy transport in disordered one-dimensional nonlinear chains. More specifically, the system of interest is a chain having binary, isotopic disorder; the impurities are single-valued. Starting from a homogeneous chain, disorder increases with increasing impurity concentration. Because these are discrete chains, as the impurity concentration increases beyond 1/2, the system becomes less disordered, becoming homogeneous at an impurity concentration of 1. This pure-disorder-pure transition is an important component to the response of these systems.

The harmonic behavior of the binary isotopic disordered (BID) chains is an important element in understanding the behavior of the anharmonic chains. The eigenstates of a disordered harmonic one-dimensional chain are localized, a phenomena referred to as Anderson localization. The length scale over which the eigenstates are localized is the localization length. The localization length of a harmonic BID chain decreases with increasing impurity concentration, up to a point. Above a certain impurity concentration, the localization length diverges toward infinity as the concentration approaches 1.

The objective here is to study energy localization and transport in nonlinear

disordered systems. Part of the far reaching appeal of the subject is its relevance to acoustic, electromagnetic, and quantum transport [1, 2]. Although considerable study has focused on the effects of solitary waves [3], here we are interested primarily in phonon behavior. Moreover, we want to study the behavior of systems that are otherwise at zero temperature, which presents its own problems. The system of interest is a one-dimensional discrete chain composed of masses that interact with nearest neighbors via both linear and cubic force terms. Starting from an eigenstate of the corresponding harmonic chain, we study energy dissipation and transport along the chain.

1.1 Outline

To study energy transport in disordered nonlinear systems, some preliminary discussion is needed to better understand the behavior of linear BID chains and the role of impurities in mode transitions. Information from both studies will be useful in comprehending the results from the study of energy transport.

Anderson Localization: In one-dimensional disordered systems, an electron wave function ψ is localized, meaning that $|\psi|^2$ decays exponentially to zero at either end of the system. The decay occurs over a length scale ξ, referred to as the Anderson localization length. In these systems, the zero amplitude of the electron wave function at each end means that these systems cannot conduct energy.

Fermi-Pasta-Ulam Chains: The Fermi-Pasta-Ulam (FPU) chain of masses connected to nearest neighbors via springs is a natural analog to the quantum system first studied by Anderson. Displacements along the chain ex-

hibit the same wave interferences that lead to localization and the entire system be described by a tight binding model analogous to the Anderson model. Moreover, nonlinear springs lead to a Hamiltonian that resembles the nonlinear Schrödinger equation.

Energy Transport: Energy transport through the FPU chain is analogous to electron transport through quantum systems. Quantitative studies of thermal conductivity in nonlinear disordered systems are performed at finite temperature. As such, these studies have a wealth of methods and techniques that can be borrowed from non-equilibrium thermodynamics. By contrast, here the system of interest is at zero temperature and the initial condition is a localized disturbance at one end of a system.

Each of these topics, in turn, requires an introduction. The following Sections introduce the relevant concepts in a logical order. Moreover, this Introduction is meant to be comprehensive so that the reader will be familiar with all the relevant issues, and their interdependencies, before reading the chapters that discuss the numerical experiments.

1.2 Anderson Localization

In the absence of disorder (and nonlinearity) in a quantum lattice, a quasi-particle wave function is a product of a periodic function and a plane wave [4]. Disorder destroys the spatial invariance, and the quasi-particles are no longer Bloch functions [4].

The first model to characterize localization in disordered materials was introduced by Anderson [5]. If the disorder is sufficiently strong, Anderson discovered

that the quasi-particle states are localized in their physical extent. Moreover, localized modes are incapable of contributing to overall transport if there is insufficient thermal energy to allow 'hopping' among eigenstates. Therefore, the metal-insulator transition [6] in a disordered system that occurs upon cooling a metal is referred to as an Anderson transition.

1.2.1 Anderson Tight Binding Model

The theory of localization was developed within the context of electrical conduction. Therefore, we need to characterize the spatial extent of the electron wave function at each site in the lattice. The governing equation for the system is the Schrödinger equation ($\hbar^2 = 1$) on a lattice with atoms located at $\mathbf{r}_n$:

$$\left[-\frac{1}{2m}\nabla^2 + \sum_n u_n(\mathbf{r} - \mathbf{r}_n)\right]\mathbf{\Psi}(\mathbf{r}) = E\mathbf{\Psi}(\mathbf{r}) \tag{1.1}$$

The atomic potential u_n is a random function, introducing disorder into the system.

Assuming that the electron wave functions at each atom are relatively independent, the wave function $\mathbf{\Psi}(\mathbf{r})$ can be approximated by a superposition of individual electron wave functions [7]:

$$\mathbf{\Psi}(\mathbf{r}) = \sum_n \psi_n \, \chi_n(\mathbf{r} - \mathbf{r}_n) \tag{1.2}$$

The function $\chi_n(\mathbf{r} - \mathbf{r}_n)$ is the atomic orbital at site $\mathbf{r}_n$, and ψ_n is its amplitude. The orbitals χ_n are the single-atom solutions:

$$\left[-\frac{1}{2m}\nabla^2 + u_n\right]\chi_n = \epsilon_n \chi_n \tag{1.3}$$

The quantity ϵ_n is the electron energy at the n-th atom.

For conduction, the individual electron wave functions must overlap. This information is contained in the orbital χ_n. Substituting Eq. (1.2) into Eq. (1.1), and using Eq. (1.3), gives

$$\sum_n \left[\epsilon_n - E + \sum_{p \neq n} u_p(\mathbf{r} - \mathbf{r}_p) \right] \psi_n \, \chi_n(\mathbf{r} - \mathbf{r}_n) = 0 \tag{1.4}$$

Multiplying the left hand side of Eq. (1.4) by χ_m^* and integrating over all space gives an equation for the amplitudes ψ_n [7]:

$$\sum_n \left[(\epsilon_n - E)\mathsf{A}_{m,n} + \sum_{p \neq n} \mathsf{B}_{m,p,n} \right] \psi_n = 0 \tag{1.5}$$

where the coefficients $\mathsf{A_{m,n}}$ and $\mathsf{B_{m,p,n}}$ are

$$\mathsf{A}_{m,n} = \int \mathrm{d}\mathbf{r} \; \chi_m^*(\mathbf{r} - \mathbf{r}_m) \, \chi_n(\mathbf{r} - \mathbf{r}_n) \tag{1.6a}$$

$$\mathsf{B}_{m,p,n} = \int \mathrm{d}\mathbf{r} \; \chi_m^*(\mathbf{r} - \mathbf{r}_m) \, u_p(\mathbf{r} - \mathbf{r}_p) \, \chi_n(\mathbf{r} - \mathbf{r}_n) \qquad (p \neq n) \tag{1.6b}$$

Eqs. (1.5) and (1.6) are valid for any arbitrary potential u_n. The coefficients A and B depend on the particular choice of u_n.

A solution to Eq. (1.5) can be found by making a few approximations. If the electrons are tightly bound to each atom, there will be negligible overlap among neighboring orbital functions χ, and $\mathsf{A}_{m,n}$ can be approximated by a Kronecker delta function $\delta_{m,n}$ [8]. For $\mathsf{B}_{m,p,n}$, given that $p \neq n$ and that χ_m is spatially localized, significant contributions can only come from $m = p$. Also, only lattice sites n that are nearest neighbors to m will contribute, so the only contributions to Eq. (1.6b) are $\mathsf{B}_{m,m,m+\mathbf{e}}$, where $\mathbf{e}$ represents the vector of nearest neighbors. Finally, the values $\mathsf{B}_{m,m,m+\mathbf{e}}$ are assumed to be a constant equal to V. Substituting for A and B in Eq. (1.5) gives

$$\epsilon_n \psi_n + V \sum_{\mathbf{e}} \psi_{n+\mathbf{e}} = E \psi_n \tag{1.7}$$

This is the Anderson tight binding model (TBM) that appeared in his seminal work [5].

Typically, the hopping potential V is absorbed into the other terms:

$$\epsilon_n \psi_n + \sum_{\mathbf{e}} \psi_{n+\mathbf{e}} = E\psi_n \tag{1.8}$$

For the case of a one-dimensional lattice, the summation contains two terms:

$$\epsilon_n \psi_n + \psi_{n-1} + \psi_{n+1} = E \psi_n \tag{1.9}$$

This is the TBM for which we will seek an analogy from the discrete chain.

1.2.2 Localized Eigenstates

For a one-dimensional chain composed of N sites, Eq. (1.9) is an eigenvalue problem with N degrees of freedom, yielding N eigenvalues and N eigenvectors. A homogeneous system having $\epsilon_n = -2$ will have eigenvalues in the range $-4 \leq E \leq 0$, and all the eigenvectors will span the system.

The addition of impurities gives rise to eigenvectors that have (virtually) zero amplitude at the ends of the system. These eigenvectors, therefore, cannot contribute to transport. An example eigenvector from a disordered system is shown in Fig. 1.1 for a system having 100 sites. Disorder site energies $\epsilon_n = -2.2$ were chosen at random with probability 0.10. The eigenvalue for the eigenvector shown in Fig. 1.1 is $E = -4.06$. Although this system is too short to represent a disordered system, the behavior of the eigenvector shown is characteristic of disordered systems.

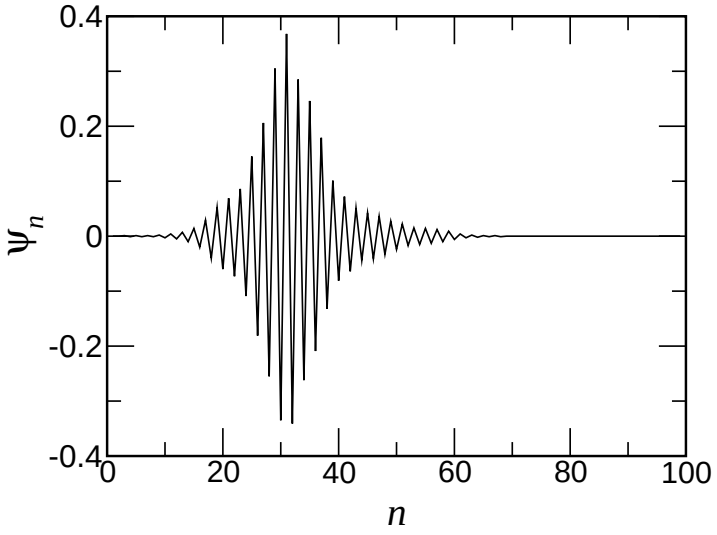

Figure 1.1: An eigenstate for disordered system of length 100 and homogeneous site energy $\epsilon_n = -2$. The system obeys the Anderson TBM in Eq. (1.9). Disorder site energy $\epsilon_n = -2.2$ at sites chosen at random with probability 0.10.

1.3 Localization Length

Localization length refers to the spatial extent of eigenstates in the disordered system. In Fig. 1.1, it is the distance over which $|\psi_n|^2$ decays to zero. Halperin [9] showed that if the electron eigenfunction is localized, there can be no static conductivity. Simply put, there cannot be transport if the eigenvector amplitude is zero at both ends of the system. Mott and Twose [10] first conjectured that all the eigenstates of a disordered one-dimensional system are localized, having exponentially decreasing amplitudes. Therefore, none of the eigenstates can have finite amplitude at both ends of a disordered system.

Having established that the eigenstates have zero amplitude at both ends, the next objective was to characterize the spatial behavior analytically. Borland

[11] used quantum liquids (delta function array) to show that the wave function envelop grows exponentially with distance from the boundary. In Fig. 1.1, it is analogous to starting from the end of the system and working towards the middle.

The subsequent development for the wave function amplitude exploited properties of random matrices. Although Schmidt [12] was probably the first to formalize the transfer matrix approach to a tight binding model, Matsuda and Ishii [13] initiated the formal proof of exponentially decaying eigenfunctions by applying Furstenberg's [14] theorem on noncommuting random matrices to the one-dimensional disordered harmonic chain. Ishii [15] then generalized the result for a number of classical and quantum one-dimensional lattices. It is this work that is usually cited as the proof of exponentially decaying eigenfunctions in disordered harmonic lattices.

1.3.1 Lyapunov Exponents

The Lyapunov exponent γ is the (inverse) length scale over which the eigenfunctions decay. The value of γ is found directly from Furstenberg's [14] theorem. Consider a one-dimensional system that obeys the Anderson TBM:

$$\psi_{n+1} = (E - \epsilon_n)\psi_n - \psi_{n-1} \tag{1.10}$$

Given that $|\psi_0|^2 + |\psi_1|^2 \neq 0$, the solution can be expressed in terms of a transfer matrix T_n:

$$\begin{pmatrix} \psi_{N+1} \\ \psi_N \end{pmatrix} = \mathsf{T}_N \, \mathsf{T}_{N-1} \cdots \mathsf{T}_1 \begin{pmatrix} \psi_1 \\ \psi_0 \end{pmatrix} \tag{1.11}$$

where

$$\mathsf{T}_n = \begin{pmatrix} (E - \epsilon_n) & -1 \\ 1 & 0 \end{pmatrix} \tag{1.12}$$

For a random distribution of ϵ_n, Furstenberg's theorem states that [13–15]

$$\lim_{N\to\infty} \frac{1}{N} \ln\left[|\psi_N|^2 + |\psi_{N-1}|^2\right] = 2\gamma > 0 \tag{1.13}$$

with probability 1. The Lyapunov exponent γ is positive because the calculation begins at the edge of the system, so the amplitudes ψ_n grow exponentially.

The localization length ξ is defined in relation to the Lyapunov exponent. As the Lyapunov exponent γ characterizes the exponentially increasing eigenfunction amplitude, the localization length ξ characterizes the exponentially decaying amplitude envelop. They are reciprocal length scales, and one's choice for the precise relationship between the two is somewhat arbitrary. Generally, they are defined as follows:

$$\xi = \frac{1}{2\gamma} \tag{1.14}$$

1.3.2 Scaling Theory

The scaling theory used to describe conduction through disordered materials is based on theories developed for critical phenomena. Close to the transition between localized and extended states (metal-insulator transition) there exists a single relevant scaling variable that is sufficient to describe the critical behavior [16]. For metallic systems, the scaling parameter is the dimensionless conductivity and for dielectrics it is the ratio of the variation of the distance between energy levels to the variation in the boundary conditions of a long but finite system [1]. To characterize the dimensionless conductance g of a system having length L, the logarithmic derivative β' was introduced [17]:

$$\beta' = \frac{\mathrm{d}\ln g}{\mathrm{d}\ln L} \tag{1.15}$$

In the metallic regime β' is positive, and in the insulating regime it is negative.

To make this result meaningful, one must be able to calculate the conductivity of a disordered system from some macroscopic property. A calculation of the conductivity using the Kubo-Greenwood formula applied to a disordered system led to a conductivity that is directly proportional to the transmission probability T [18, 19]. Thouless [20] pointed out that one must also consider the leads of the system when performing the calculation; there must exist an electric field in the leads to maintain charge neutrality. Doing so adds an additional term to the Kubo-Greenwood calculation, and the corrected result is identical to that of Landauer [21]:

$$g = \frac{T}{R} \tag{1.16}$$

This result was corroborated by Anderson, Thouless, Abrahams, and Fisher (ATAF) [22] and developed further by Anderson and Lee [23].

System Conductance

The formulation of the system conductance by Landauer and ATAF is instructive, so it is summarized briefly here. Consider a disordered material, as depicted in Fig. 1.2 by the grey region. On each end are leads having no impurities. The labels i and r represent incident and reflected waves to the left of a disordered region; likewise for i' and r' on the right side. For an incident wave having amplitude A, there will be a reflection amplitude r, and a transmission amplitude t. The reflection probability R is $|r|^2/|A|^2$ and the transmission probability T is $|t|^2/|A|^2$, such that $R + T = 1$.

An oscillatory electrical potential Φ is applied, from left to right, across the system. The Fermi energy (chemical potential) E_F of the reservoir on the left is greater than that on the right by an amount $e\Phi$, where e is the charge of an

electron. The excess electron density $\widetilde{n}$ is proportional to E_F:

$$\widetilde{n} = \frac{\mathrm{d}n}{\mathrm{d}E_F}\, e\Phi \tag{1.17}$$

The excess density $\widetilde{n}$ is also proportional to the difference in the electron currents j, divided by the respective velocities:

$$\widetilde{n} = \frac{j_i + j_r}{v} - \frac{j_{r'} + j_{i'}}{v'} \tag{1.18}$$

$$= \frac{2R(j_i - j_{i'})}{\partial E_F / \partial P_x} \tag{1.19}$$

The total current is $I/e = (j_i + j_{i'})T$, and the conductance G is

$$G = \frac{I}{\Phi} = \frac{T}{2R}\, e^2\, \frac{\mathrm{d}n}{\mathrm{d}E_F}\, \frac{\partial E_F}{\partial P_x} \tag{1.20}$$

Given that $\mathrm{d}n/\mathrm{d}E_F = (1/\pi\hbar)(\partial P_x/\partial E_F)$, the velocity and the density of states factors cancel, giving

$$G = \frac{e^2}{2\pi\hbar}\, \frac{T}{R} \tag{1.21}$$

This is the Landauer [21] result. To generalize this result for any of the models enumerated by Ishii [15], a dimensionless conductivity g and a dimensionless resistivity ρ are defined.

$$g = \frac{1}{\rho} = \frac{T}{R} \tag{1.22}$$

Exponential Scaling

Having established a proper expression for the system conductance, the next step is to determine what particular function of the conductance scales exponentially with system length. Landauer [21] averaged the total system resistivity ρ_T. For a system composed of two regions, one having resistivity ρ_1 and the other having

Figure 1.2: Schematic of a section of disordered material with incident (i) and reflected (r) waves at both ends.

resistivity ρ_2, the total resistivity does not exhibit classical linear scaling:

$$\begin{aligned} \rho_T &= \left\langle \frac{|r|^2}{|t|^2} \right\rangle \\ &= \langle \rho_1 \rangle + \langle \rho_2 \rangle + 2\langle \rho_1 \rangle \langle \rho_2 \rangle \end{aligned} \tag{1.23}$$

This scaling gives rise to the desired exponentially increasing resistivity.

The exponential growth of ρ_T can be demonstrated by assuming that system ρ_1 has added to it a much smaller system ρ_2. Let ρ_2 be an infinitesimal quantity such that

$$\rho_2 = \alpha \, \mathrm{d}L \tag{1.24}$$

Starting at a length scale L_o for which the resistance is classical, which is to say that $\rho_o \ll 1$, α represents the classical resistivity ρ_o / L_o. Substituting Eq. (1.24) into Eq. (1.24) gives

$$\rho_T - \rho_1 = \alpha \, \mathrm{d}L + 2\rho_1 \, \alpha \, \mathrm{d}L \tag{1.25}$$

To leading order, it can be assume that $\rho_T \approx \rho_1$:

$$\mathrm{d}\rho_T \approx (1 + 2\rho_T) \, \alpha \, \mathrm{d}L \tag{1.26}$$

The final expression for the length dependence of ρ_T was originally given by

Landauer [21]:

$$\rho_T \approx \frac{\mathrm{e}^{2\alpha L} - 1}{2} \tag{1.27}$$

This result was confirmed by ATAF [22], who then demonstrated that other scaling schemes are possible:

$$\rho_T = \frac{1}{\langle g_T \rangle} = |\rho_1 - \rho_2| \tag{1.28}$$

$$\rho_T = \frac{1}{\langle |t|^2 \rangle} - 1 = \rho_1 + \rho_2 \tag{1.29}$$

The first relation is not a rational scaling law, and the second, although consistent with classical scaling, would not lead to exponential behavior, as would be expected. Therefore, a clear answer cannot be found by seeking desirable scaling relations from averaged quantities.

ATAF [22] postulated that the distribution must be considered along with the average. The variance of the scaling variable should increase slower than L^2 with increasing length. This is required to ensure that the distribution converges.

ATAF showed that the quantity $\langle \ln(1+\rho) \rangle$ could satisfy these criteria. There is additive scaling,

$$\langle \ln(1 + \rho_T) \rangle = \langle \ln(1 + \rho_1) \rangle + \langle \ln(1 + \rho_2) \rangle \tag{1.30}$$

that implies

$$\ln(1 + \rho_T) = \alpha L \tag{1.31}$$

The quantity α is the inverse localization length [22]

$$\alpha = 1/\xi \tag{1.32}$$

and is the meaningful scaling quantity. This leads to exponentially increasing resistivity with system length [22]:

$$\rho = \mathrm{e}^{\alpha L} - 1 \tag{1.33}$$

This differs from the Landauer [21] result by an important factor of 2.

The relationship between the ATAF classical resistivity α and the Lyapunov exponent γ can be made using an alternate form of Eq. (1.13) that uses the system transmission probability T [16]:

$$2\gamma = -\lim_{L\to\infty} \frac{1}{L} \ln T \tag{1.34}$$

Using $T = 1 + \rho$ and Eq. (1.31) gives an expression for α:

$$2\gamma = \alpha \tag{1.35}$$

This leads to the scaling equation expressed as a function of the Lyapunov exponent:

$$\ln(1 + \rho_T) = 2\gamma L \qquad \rho = \mathrm{e}^{2\gamma L} - 1 \tag{1.36}$$

Alternatively, using Eq. (1.14),

$$\ln(1 + \rho_T) = L/\xi \qquad \rho = \mathrm{e}^{L/\xi} - 1 \tag{1.37}$$

More precisely, these quantities are meaningful only in an averaged sense:

$$2\langle\gamma\rangle = \langle \ln(1 + \rho_T)\rangle \tag{1.38}$$

The brackets $\langle\cdots\rangle$ denote ensemble averages.

Logarithmic Derivative

The logarithmic derivative β' in Eq. (1.15) can be evaluated for one-dimensional systems. Using the fact that the transmission probability $T = 1 - \rho_T$ and Eq. (1.37), the dimensionless conductance g is

$$g = \frac{\mathrm{e}^{-L/\xi}}{1 - \mathrm{e}^{-L/\xi}} \tag{1.39}$$

The logarithmic derivative β' can be expressed as a function of the conductance g [22]:

$$\begin{aligned} \beta' = \frac{L}{g}\frac{\partial g}{\partial L} &= -(1+g)\,\frac{L}{\xi} \\ &= -(1+g)\,\ln\left(\frac{1+g}{g}\right) \end{aligned} \tag{1.40}$$

Because g is a positive definite quantity, the logarithmic derivative β' is strictly less than zero. Therefore, harmonic one-dimensional systems having finite disorder are insulators, and can never transition to a metallic (conducting) state.

1.3.3 BID Scaling

The ATAF additive scaling relation in Eq. (1.30) can be used to estimate the total resistivity of a BID system. Because the impurities in a BID system are identical, so are the individual impurity resistivities ρ_i. The total resistivity ρ_T is a sum over all the impurities:

$$\langle \ln(1+\rho_T)\rangle = \sum_{i=1}^{N} \langle \ln(1+\rho_i)\rangle = N\langle \ln(1+\rho)\rangle \tag{1.41}$$

This leads to an exact expression for the localization length ξ for the system:

$$\langle \xi \rangle = \frac{L}{N}\,\frac{1}{\ln(1+\rho)} = \frac{1}{c\ln(1+\rho)} \tag{1.42}$$

In the limit of weak scattering ($\rho \to 0$), the localization length approaches the mean free path Λ:

$$\xi(\rho \to 0) = \frac{1}{c\rho} \approx \frac{1}{c\sigma} = \Lambda \tag{1.43}$$

1.3.4 Numerical Methods

One of the first things to be done is to establish the properties of disordered harmonic systems. This requires calculating localization lengths as a function

of system parameters such as impurity cross section and impurity concentration. These calculations will both confirm expected results for a system of weak scatterers and be used to establish relationships for the systems having strong disorder: high impurity scattering cross section and high impurity concentration.

Kronig-Penney Liquid

The first method is a direct calculation on a continuum analog. The Kronig-Penney [24] liquid model approximates the impurities as point scatterers. Between the scatterers are freely propagating waves. The localization length is calculated from the system transmission coefficient T.

A solution $\Psi(x)$ is sought for a system obeying Eq. (1.1) and having a potential that is a sum over N delta function impurities, each having strength ϵ_n:

$$\left[-\frac{\partial^2}{\partial x^2} + \sum_{n=1}^{N} \epsilon_n \, \delta(x - x_n)\right] \Psi(x) = k^2 \, \Psi(x) \tag{1.44}$$

where $k^2 = E$. The total function $\Psi(x)$ is a sum of partial solutions between the scatterers:

$$\Psi(x) = \sum_{n=0}^{N} \psi_n(x) \qquad\qquad x_n \leq x \leq x_{n+1} \tag{1.45}$$

where $x_0 = -\infty$ and $x_{N+1} = +\infty$. Each $\psi_n(x)$ is the solution to the homogeneous equation, and is a sum of counter-propagating waves:

$$\psi_n = A_n \mathrm{e}^{+\mathrm{i}kx} + B_n \mathrm{e}^{-\mathrm{i}kx} \tag{1.46}$$

At each impurity, the adjacent functions are continuous,

$$\psi_{n-1}(x_n) = \psi_n(x_n) \tag{1.47}$$

but the slopes are discontinuous:

$$\left.\frac{\partial \psi_n}{\partial x}\right|_{x_n} - \left.\frac{\partial \psi_{n-1}}{\partial x}\right|_{x_n} = \epsilon_n \qquad\qquad 1 \leq n \leq N \tag{1.48}$$

Equations (1.47) and (1.48), along with the boundary conditions A_0 (specified) and $B_N = 0$ result in $2N$ equations with $2N$ unknowns. The equations can be solved numerically using a linear algebra routine such a LAPACK.

The system resistivity can be calculated from the system reflection amplitude r and transmission amplitude t:

$$r = B_0 \qquad t = A_N \qquad \rho = \frac{|r|^2}{|t|^2} \tag{1.49}$$

This entire process can be repeated for a new collection of impurities, and the ensemble-averaged localization length is calculated from $\langle \ln(1+\rho) \rangle$.

MacKinnon and Kramer

The method of MacKinnon and Kramer [25–27] is used to calculate the localization length (Lyapunov exponent) of a discrete system have localized impurities. The method is based on the Anderson tight binding Hamiltonian [5]:

$$\widehat{H} = \sum_n |n\rangle \, \epsilon_n \, \langle n| + \sum_{n,m} |n\rangle \, V_{n,m} \, \langle m| \tag{1.50}$$

where the second summation is over nearest neighbors. Each state $|n\rangle$ is an orbital centered at site n. Formally, the Green's function (GF) is

$$G(E) = \frac{1}{E - \widehat{H}} \tag{1.51}$$

The matrix elements of $G(E)$ are

$$G_{m,n}(E) = \langle m| \, G(E) \, |n\rangle = \sum_k \frac{\langle m \,|\, k\rangle \, \langle k \,|\, n\rangle}{E - \epsilon_k} \tag{1.52}$$

Therefore, $G_{1,n}$ is the coupling between atoms at opposite ends of lattice and can be used to calculate the localization length ξ [25, 26]:

$$\frac{2}{\xi} = -\lim_{n\to\infty} \frac{1}{n} \ln |G_{1,n}|^2 \tag{1.53}$$

This result is based on the Herbert and Jones [28] relationship between spectral density and the range of localization, later generalized by Thouless [29] for the method of energy level shifting in dielectrics.

By exploiting the fact that on a one-dimensional lattice there is only one self-avoiding path between site 1 and site n [30], $G_{1,n}$ can be calculated by iteration:

$$G_{1,n+1} = G_{1,n}\, G_{n+1,n+1} \tag{1.54a}$$

$$G_{n+1,n+1} = [E - \epsilon_{n+1} - G_{n,n}]^{-1} \tag{1.54b}$$

Now all that remains is determining $G_{1,1}$

Returning to the Anderson TBM in Eq. (1.9), the nearest neighbor wave amplitudes are interdependent:

$$A_{n+1} = (E - \epsilon_n)\; A_n - A_{n-1} \tag{1.55}$$

One could, in principal, assign $A_0 = 0$ and $A_1 = 1$, and then iterate along the chain for each subsequent amplitude. This iteration scheme is identical to the GF iterations in Eqs. (1.54) if $G_{1,n} = A_{n+1}^{-1}$.

This development, however, was not new. The contribution of MacKinnon and Kramer was to develop an algorithm that improved measurement statistics by periodically rescaling the amplitudes. If the scaling is done at the n-th iteration, the subsequent scaled values, denoted $\overline{A}$, are:

$$\overline{A}_{n-1} = A_{n-1}\, A_n^{-1} \tag{1.56}$$

$$\overline{A}_n = 1 \tag{1.57}$$

$$\overline{A}_{n+1} = A_{n+1}\, A_n^{-1} \tag{1.58}$$

$$\tag{1.59}$$

The third relation comes from Eq. (1.55). By rescaling the amplitudes, information is not lost due to roundoff error, as would occur otherwise.

1.3.5 Nonlinearity

Given that linear one-dimensional disordered system are exponentially localized, one expects that nonlinearity will lead to mode transitions into channels that are not immediately localized, thereby leading to transport. As a result, the expectation is that nonlinearity will, in some way, either reduce or destroy any form of localization in disordered chains.

The effect of nonlinearity on disordered systems was studied in detail by Devillard and Souillard [31] using the nonlinear Schrödinger equation:

$$\left[\frac{\partial^2}{\partial x^2} + V(x) - \alpha(x)|\Phi|^2\right]\Phi = E\Phi \tag{1.60}$$

They used the theory of random matrices [14, 32] to calculate the transmission coefficient as a function of system length L. For a conserved probability flux, there is one and only one solution for a given transmission probability. They concluded that for short systems having weak nonlinearity, the transmission decays exponentially. For long enough systems, the transmission fell off as L^{-1}.

Doucot and Rammal [33] used a dynamical systems point of view to study localization in disordered anharmonic systems. They found that for short lengths, transmission decays exponentially. For large systems, transmission decays as a power law, in agreement with Devillard and Souillard [31]. For their system, the crossover occurred for system lengths on the order of a few times that of the localization length.

These results corroborate the conclusion that nonlinearity destroys localization in disordered systems [34]. Given that the average resistivity is related

directly to the transmission coefficient,

$$\langle \rho \rangle = \left\langle \frac{1}{T} \right\rangle - 1 \tag{1.61}$$

a power law decay in transmission T corresponds to a power law increase in resistivity ρ. The persistent length dependence results from the fact that although mode transitions lead to new modes that are capable of immediate transmission, these new modes will also undergo competition between transmission and localization. It is not obvious from these results, however, whether localization is suppressed sufficiently in nonlinear disordered systems that the systems will exhibit diffusive energy transport.

1.4 Disorder Model

There are two kinds of disorder relevant to this study. One is structural disorder:

$$U(x) = \sum_i u_i \, \delta(x - x_i) \tag{1.62}$$

The sum is taken over the number of impurities. The other type of disorder is substitutional disorder:

$$U(x) = \sum_n u_n \, \delta(x - an) \tag{1.63}$$

The sum is taken over all sites, and a is the distance between nearest neighbors.

The substitutional disorder model can be used to develop a discrete Schrödinger equation. The solution to the continuous Schrödinger equation ($\hbar^2 = 2m = 1$)

$$-\nabla^2 \psi + U(\mathbf{r})\psi = E\psi \tag{1.64}$$

Using the Green's function for the one-dimensional Helmholtz equation [8], the solution is [1]

$$\psi(x) = -\frac{\mathrm{i}}{2\kappa} \sum_n u_n \mathrm{e}^{\mathrm{i}\kappa|x-na|} \, \psi(na) \qquad\qquad \kappa^2 = E \tag{1.65}$$

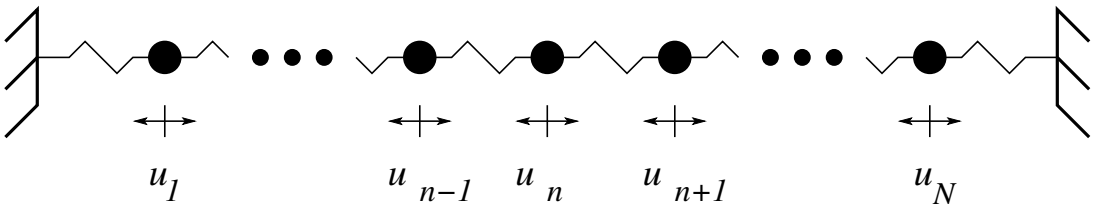

Figure 1.3: Schematic of FPU chain. Masses have displacement u from the equilibrium position, and interact with nearest neighbors through springs. The ends have zero displacement.

Solving for ψ at $x = na$, and using the notation $\psi_n = \psi(na)$ gives

$$\left(1 + \frac{\mathrm{i}u_n}{2\kappa}\right)\,\psi_n = -\,\frac{\mathrm{i}}{2\kappa}\sum_{m\neq n}\,u_m\psi_m\,\mathrm{e}^{\mathrm{i}\kappa a|n-m|} \tag{1.66}$$

After multiplying both sides by $\cos\kappa a$ and subtracting out similar expressions for ψ_{n+1} and ψ_{n-1} leads to a discrete analog to the Schrödinger equation: [1]

$$\psi_{n+1} + \psi_{n-1} - 2\left(\cos\kappa a + \frac{u_n}{2\kappa}\,\sin\kappa a\right)\,\psi_n = 0 \tag{1.67}$$

1.5 Fermi-Pasta-Ulam Chains

For this study, the physical model is the discrete chain composed of masses interacting with nearest neighbors via linear and cubic force terms. The first numerical experiment to use this type of model was performed by Fermi, Pasta, and Ulam [35] at Los Alamos Laboratory in 1955. This was such a seminal work that these systems bear the authors' names: Fermi-Pasta-Ulam (FPU) chains. A schematic of an FPU chain is shown in Fig. 1.3. For a system composed of N masses, the

Hamiltonian H is a function of the momentum p_n and the displacement (about its equilibrium position) u_n of the n-th mass:

$$H = \sum_{n=1}^{N} \frac{p_n^2}{2m_n} + \frac{K}{2}(u_{n+1} - u_n)^2 + \frac{\alpha}{3}(u_{n+1} - u_n)^3 + \frac{\beta}{4}(u_{n+1} - u_n)^4 \qquad (1.68)$$

The quantity K is the familiar Hooke's constant. Researchers typically express lengths in units of the equilibrium mass spacing a. Although one could, in principle, vary the interaction parameters K, α, and β, in this study, disorder is effected through changes in mass. This way, one can at least express results as a ratio of the nonlinear parameters α and β to the harmonic coefficient K.

Often, FPU experiments use either the cubic (α) term as a lowest order nonlinear approximation or the quartic (β) term for its symmetry. To distinguish between these two, a shorthand has developed that refers the particular choice by using a suffix: FPU-α or FPU-β. Here, we choose the FPU-β system for its symmetry.

From the Hamiltonian in Eq. (1.68), the equation of motion for the FPU-β chain is

$$m_n \ddot{u}_n = K(u_{n+1} - 2u_n + u_{n-1}) + \beta \left[(u_{n+1} - u_n)^3 - (u_n - u_{n-1})^3\right] \qquad (1.69)$$

This expression shows that we can assign $K = 1$ with no loss of generality. In addition, in the absence of impurities, the masses all have the same value: $m_\circ = 1$.

The time dependence of the displacements u_n is calculated using numerical integration. Two different integration schemes were used. A 4-th order Adams-Bashford-Moulton [36–38] predictor-corrector algorithm was used for the earlier work. Both 4-th order [39] and 6-th order [40] symplectic integration were used for the later work. The energy fluctuation for predictor-corrector and the symplectic algorithms depends upon the step size, and both avoid energy drift. A discussion

of numerical integrators is given in Appendix B.

1.5.1 Harmonic Chain TBM

There is a corresponding tight binding model for the disordered harmonic chain. The equation of motion for the harmonic ($\beta = 0$) chain is

$$m_n \ddot{u}_n = K\left(u_{n+1} - 2u_n + u_{n-1}\right) \tag{1.70}$$

As this is a harmonic equation, the solution is separable and the displacements are sinusoidal: $u_n(t) = \phi_n \, \mathrm{e}^{-\mathrm{i}\omega t}$. Substituting this solution for u_n into Eq. (1.70) gives the harmonic chain TBM:

$$\frac{m_n \omega^2}{K}\phi_n + \sum_{e=\pm 1} \phi_{n+e} = 2\phi_n \tag{1.71}$$

By analogy to the Anderson TBM in Eq. (1.9), $m_n\omega^2/K$ corresponds to the electron energy, the hopping potential V is 1, and the energy E is 2. Through this correspondence, we can avail ourselves to the tools and results developed for the Anderson TBM.

1.5.2 Dispersion Relation

The vibrations of discrete objects such as chains and crystals are constrained. As a result, they have a nonlinear dispersion relation. The dispersion relation for the harmonic chain is an important quantity, so it will be given first. The dispersion relation for the anharmonic chain is calculated by analogy.

Harmonic Chains

Using the equation of motion for the harmonic chain in Eq. (1.69), the equation of motion for the homogeneous harmonic portion of the chain is

$$m_\circ \ddot{u_n} = K\left(u_{n+1} - 2u_n + u_{n-1}\right) \tag{1.72}$$

The lack of disorder means that both the spatial and temporal solutions can be expressed succinctly:

$$u_n = A\mathrm{e}^{+\mathrm{i}\theta_n} \tag{1.73}$$

where

$$\theta_n = kan - \omega t \qquad\qquad k = \frac{2\pi q}{Na}$$

for some integer q. Substituting this solution into the equation of motion gives

$$-m_\circ \omega^2 u_n = 2Ku_n\left(\cos ka - 1\right) \tag{1.74}$$

Solving for ω gives the dispersion relation for a discrete chain[41]:

$$\omega = 2\sqrt{\frac{K}{m_\circ}}\,\left|\sin\left(ka/2\right)\right| \tag{1.75}$$

The maximum frequency ($2\sqrt{K/m_\circ}$) occurs for the shortest possible wavelength: $2a$. The dispersion relation in Eq. (1.75) is plotted in Fig. 1.4 over the first Brillouin zone [42].

The phase velocity v_p of a propagating wave along a homogeneous chain was first calculated by Newton [*Principia*, Book II (1686)] [42]:

$$v_p = a\sqrt{\frac{K}{m_\circ}} \tag{1.76}$$

This is the velocity that a phase angle propagates along the chain. The group velocity v_g is a differential quantity that characterizes the "center of gravity"

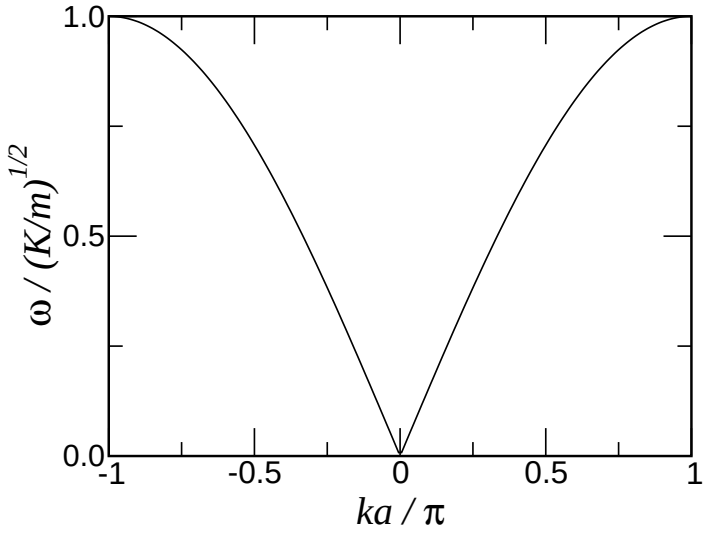

Figure 1.4: Dispersion relation for homogeneous harmonic chain having spring constant K and mass m.

velocity of a group of waves:

$$v_g = \frac{\partial \omega}{\partial k} = \sqrt{\frac{Ka^2}{m_\circ}} \cos\frac{ka}{2} = v_p \cos\frac{ka}{2} \tag{1.77}$$

The group velocity is the velocity at which energy is transported along the chain.

Anharmonic Medium

The dispersion relation for the FPU-β chain can be calculated using its continuum analog. A continuous elastic medium having mass density μ and Youngs modulus Y has a Langrange density $\mathcal{L}$ [43, 44]:

$$\mathcal{L} = \frac{\mu}{2}\left(\frac{\partial u}{\partial t}\right)^2 - \frac{Y}{2}\left(\frac{\partial u}{\partial x}\right)^2 - \frac{\beta}{4}\left(\frac{\partial u}{\partial x}\right)^4 \tag{1.78}$$

u represents displacement and ∇u represents strain. The equation of motion is

$$\ddot{u} = \frac{Y}{\mu}\frac{\partial^2 u}{\partial x^2} + \frac{\beta}{\mu}\frac{\partial}{\partial x}\left(\frac{\partial u}{\partial x}\right)^3 \tag{1.79}$$

This equation is recognizable as the wave equation with phase velocity $\sqrt{Y/\mu}$, with an additional term that contributes the anharmonic dispersion.

The cubic terms gives rise to dispersion. The dispersion relation for a nonlinear system is calculated by assuming counter-propagating harmonic waves:

$$u = A\mathrm{e}^{+\mathrm{i}(kx-\omega t)} + A^*\mathrm{e}^{-\mathrm{i}(kx-\omega t)} \tag{1.80}$$

The calculation proceeds as for the harmonic case. The cubic term, however, requires special consideration. First, the derivative is evaluated:

$$\frac{\partial u}{\partial x} = (\mathrm{i}kA)\mathrm{e}^{+\mathrm{i}(kx-\omega t)} + (\mathrm{i}kA)^*\mathrm{e}^{-\mathrm{i}(kx-\omega t)} \tag{1.81}$$

As a shorthand, let $B = (\mathrm{i}kA)$. The cube of the derivative is

$$\begin{aligned}\left(\frac{\partial u}{\partial x}\right)^3 &= (B)^3\mathrm{e}^{+3\mathrm{i}(kx-\omega t)} + (B^*)^3\mathrm{e}^{-3\mathrm{i}(kx-\omega t)} \\ &\quad +3(B)^2B^*\mathrm{e}^{+\mathrm{i}(kx-\omega t)} + 3(B^*)^2B\mathrm{e}^{-\mathrm{i}(kx-\omega t)} \\ &\approx 3\left|B\right|^2\left(\frac{\partial u}{\partial x}\right)\end{aligned} \tag{1.82}$$

This approximation, known as the rotating wave approximation (RWA), assumes that only the harmonic frequencies contribute significantly. With this approximation, the dispersion relation becomes [44–46]:

$$\omega^2 = \frac{Y}{\mu}k^2 + \frac{3\beta}{\mu}|A|^2k^4 = \omega_o^2\left(1 + \frac{3\beta\mu}{Y^2}\left|A\right|^2\omega_o^2\right) \tag{1.83}$$

where $\omega_o^2 = k^2Y/\mu$. The dispersion relation is expressed in powers of k^2 and, alternatively, in powers of ω_o^2. The apparent result is that changes in frequency are proportional to the anharmonicity β. Moreover, the frequency shift ($\Delta\omega = \omega - \omega_o$) is proportional to ω_o^3.

Anharmonic Chain

The expansion in ω_o^2 on the right hand side of Eq. (1.83) guides one to the corresponding solution for a discrete chain. Substituting the dispersion relation for the harmonic chain in Eq. (1.74) into ω_o in Eq. (1.83) above, the dispersion relation for the anharmonic chain is [45, 46]:

$$\omega_o^2 = \frac{2K}{m_\circ}\,(1-\cos Ka)\,\left[1+\frac{6\,\beta\,|A|^2}{K}\,(1-\cos Ka)\right] \tag{1.84}$$

1.5.3 Spectral Density

The FPU equation of motion in Eq. (1.71) for a chain of N masses can be expressed succinctly in matrix notation [47, 48]:

$$\mathsf{A}\mathbf{u} = \omega^2\mathbf{u} \tag{1.85}$$

This is an eigenvalue problem having N eigenvalues $\nu_n = \omega_n^2$. The eigenvalues are the solution to the secular equation

$$\mathrm{Det}\,|\mathsf{A}-\nu\mathsf{I}| = 0 \tag{1.86}$$

The distribution of the N values ν_n represents the spectrum of the system. As the system length increases, the spectrum approaches a continuous function, and the fraction of eigenvalues between ν and $\nu+\mathrm{d}\nu$ is the spectral density $D(\nu)$.

The spectral density of the homogeneous chain is [41, 47, 48]

$$\begin{aligned} D(\nu) &= \frac{N}{\pi}\,\frac{1}{\sqrt{\nu}\sqrt{\nu_{max}-\nu}} \\ &= \frac{N}{\pi}\,\frac{1}{\omega\sqrt{\omega_{max}^2-\omega^2}} \end{aligned} \tag{1.87}$$

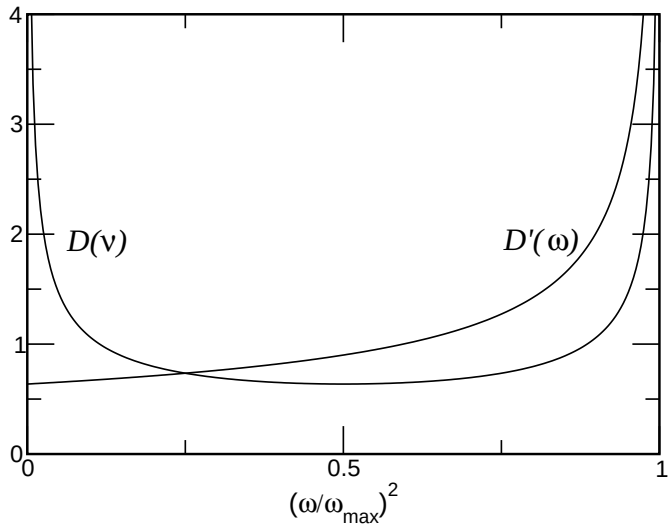

Figure 1.5: Spectral density $D(\nu)$ and $D'(\omega)$ of homogeneous linear chains.

The spectral density in ω space is

$$\begin{aligned} D'(\omega) &= D(\omega^2)\,\frac{\mathrm{d}\nu}{\mathrm{d}\omega} \\ &= \frac{2N}{\pi}\,\frac{1}{\sqrt{\omega_{max}^2-\omega^2}} \end{aligned} \tag{1.88}$$

Both $D(\nu)$ and $D'(\omega)$ are plotted in Fig. 1.5 as a function of $(\omega/\omega_{max})^2$. Typically, one sees the eignevalue spectral density $D(\nu)$ in discussions of disordered systems.

For disordered systems, the spectral density can only be calculated numerically. Typically, the negative factor counting method of Dean [49, 50] is used, and consists of factoring the secular determinant

$$\mathrm{Det}\,|S(\nu)| = \prod_{m=1}^{N} Q_m(\nu,\nu_m) \tag{1.89}$$

The product is over the N possible eigenvalues. The number of negative values Q_m is the number of eigenvalues less than ν_m.

A discussion of spectral density in the context of Green's function formalism is given in Appendix A.

1.5.4 Mode Transitions

Mode transitions are an important aspect of energy transport in anharmonic chains. In the absence of anharmonicity, the response frequency is equal to the driving frequency. Anharmonicity excites additional modes that can then propagate and scatter.

Consider a single simple harmonic oscillator (SHO) that has a mass $m_\circ$ that experiences a time-dependent displacement $u(t)$, driven with force F at frequency ω. The equation of motion is

$$\ddot{u} + \omega_o^2 u \left(1 + \frac{\beta}{K} u^2\right) = \frac{F}{m_\circ} \cos \omega t \tag{1.90}$$

where $K/m_\circ = \omega_o^2$. Based on the symmetry of the problem and orthogonality, the solution for u must also be sinusoidal:

$$u = \sum_n u_n \cos n\omega t \tag{1.91}$$

The symmetry requires that n must be odd. The entire left hand side of Eq. (1.90) must reduce to the form $A_n \cos n\omega t$, and orthogonality dictates that $A_1 = F/m_\circ$ and all other $A_n = 0$.

Limiting the expansion in Eq. (1.91) to the first two terms ($u = u_1 \cos \omega t + u_3 \cos 3\omega t$) and using the trigonometric relation ($4\cos^3 \omega t = 3\cos \omega t + \cos 3\omega t$) gives the coefficients for the first two terms:

$$F/m_\circ = (1 - \Omega^2)u_1 + \frac{3}{4}\Theta u_1 \left(u_1^2 + u_1 u_3 + 2u_3^2\right) \tag{1.92}$$

$$A_3 = (1 - 9\Omega^2)u_3 + \frac{1}{4}\Theta \left(u_1^3 + 6u_1^2 u_3 + 3u_3^3\right) \tag{1.93}$$

where the substitutions $\Omega = \omega/\omega_o$ and $\Theta = \beta/K$ have been made. There are additional terms in ωt that can be ignored if $\Theta \ll 1$ and $|u_3| \ll |u_1|$. Consequently, terms with Θu_3 in Eqs. (1.93) can also be ignored, yielding an amplitude

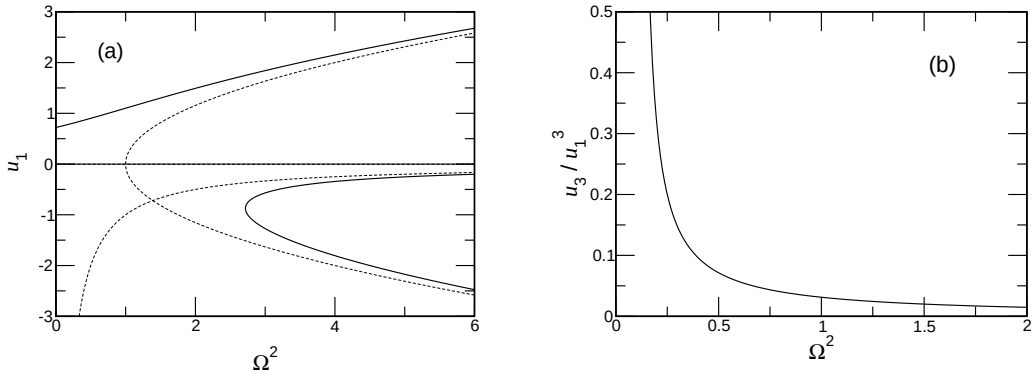

Figure 1.6: Mode transition plots as a function of Ω^2 for systems having $\beta/K = 1$: (a) Amplitude-frequency plot (solid lines) and (b)u_3/u_1^3.

frequency response relationship [43]:

$$1 - \Omega^2 + \frac{3}{4}\Theta u_1^2 = \frac{1}{u_1} \qquad\qquad u_3 = -\frac{\Theta u_1^3}{4(1 - 9\Omega^2)} \tag{1.94}$$

The amplitude-frequency plot of u_1 and the ratio u_3/u_1^3 as a function of Ω^2 are shown as solid lines in Fig. 1.6. The dotted lines in Fig. 1.6(a) are $\Omega^2 = 1 + (3/4)u_1^2$ and $\Omega^2 = -1/u_1$. Negative values of u_1 in Fig. 1.6(a) correspond to mode transitions having opposite phase.

For a driving frequency $\Omega^2 > 2.7$, the amplitude u_1 is multi-valued. As a consequence, oscillations at these frequencies can jump spontaneously from one value to another [43]. Noting that this behavior occurs at frequencies above the natural frequency of the SHO (ω_o), at low driving frequencies, the behavior of the system will remain well behaved and predictable.

The behavior of u_3 shown in Fig. 1.6(b) is somewhat opposite to that of u_1. The amplitude u_3 decreases with increasing driving frequency ω. Therefore, at higher frequencies the behavior of u_1 can become erratic and the transfer of energy to higher harmonics can decrease.

1.5.5 Ergodicity

The primary purpose of the original FPU experiment [35] was to investigate ergodicity in anharmonic systems. They used a lattice of 64 masses and excited the lowest mode. In time, the displacement become more irregular. Eventually, however, the energy returned to the initial excited mode. To explain this behavior, the Kolmogorov-Arnol'd-Moser (KAM) theorem (see Ref. [51]) asserts that even if a Hamiltonian is non-integrable, there may be conserved integrals other than energy that can lead to states that will not go to equipartition. As a result, small systems with weak anharmonicity are more likely to have recurrences.

In contrast to the FPU experiment, the systems of interest here are very long and have stronger anharmonicity. It is fully expected that the systems will tend toward ergodic behavior. The degree to which a system is ergodic can be quantified by a number of different measures.

Localization Parameter

The localization parameter Γ was introduced by Cretegny et a. [52] to study the transient state that precedes equipartition in FPU-β chains. It can be used to estimate the number of sites over which energy is distributed, and it is solely a function of the site energy E_i:

$$\Gamma = N \frac{\sum_i^N E_i^2}{\left(\sum_i^N E_i\right)^2} \tag{1.95}$$

If the energy is localized at one site, $\Gamma = N$, and if the energy is evenly distributed among all the sites $\Gamma \approx 1$. Due to thermodynamic fluctuations, the energy is never uniformly distributed among all the masses. As a result, the value of Γ at very long time differs from one.

The asymptotic ($t \to \infty$) value Γ_∞ depends upon site energy fluctuations:

$$\Gamma_\infty = \frac{\langle E_i^2 \rangle}{\langle E_i \rangle^2} \tag{1.96}$$

The configurational partition function is ($\beta_T = 1/k_B T$)

$$F(\beta_T) = \int \exp\left[-\beta_T V(x)\right] \, \mathrm{d}x \tag{1.97}$$

The moments of E_i can be expressed as functions of $F(\beta_T)$ [53]:

$$\langle E_i \rangle = \frac{1}{2\beta_T} - \frac{1}{F}\frac{\partial F}{\partial \beta_T} \tag{1.98}$$

$$\langle E_i^2 \rangle = \frac{3}{4\beta_T^2} - \frac{1}{\beta_T F}\frac{\partial F}{\partial \beta_T} + \frac{1}{2F^2}\left(\frac{\partial F}{\partial \beta_T}\right)^2 + \frac{1}{2F}\frac{\partial^2 F}{\partial \beta_T^2} \tag{1.99}$$

In the pure harmonic case, $\langle E_i \rangle = 1/\beta_T$ and $\langle E_i^2 \rangle = 7/4\beta_T^2$. In the pure quartic case $\langle E_i \rangle = 3/4\beta_T$ and $\langle E_i^2 \rangle = 19/16\beta_T^2$. The asymptotic value Γ_∞ is 7/4 for the harmonic case and 19/9 for the pure quartic case, both of which are independent of temperature. For the systems in which both K and β are not zero, the value of Γ_∞ is between these two values.

An example of the behavior of Γ is shown in Fig. 1.7 as a function of time t. For the system shown, $K = \beta = 1$. The system is a hoop having $N = 512$ masses, and the initial displacement is $k = \pi$, with a very small amount of randomness, as was done be Cretegny et al. [52]. The error bars represent the standard deviation from 50 systems, and the asymptotic value is approximately $\Gamma_\infty = 1.8$.

Participating Modes

The idea for estimating the number of participating harmonic modes at a particular site was proposed by Luca et al. [54, 55]. It is an extension to the concept of spectral entropy, which was first proposed by Livi et al. [56, 57]. Spectral

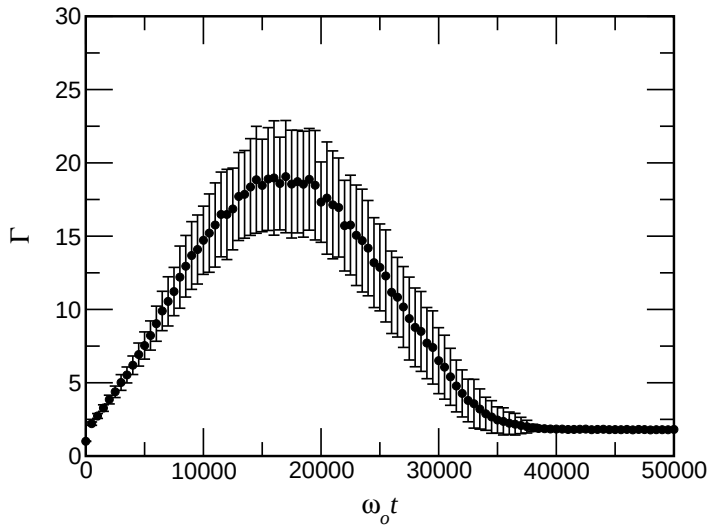

Figure 1.7: Localization parameter Γ as a function of scaled time $\omega_o t$ for the $\beta = 1$ system initially in the $k = \pi$ mode. Error bars represent one standard deviation from 50 systems.

entropy, in turn, is based on information entropy, first proposed by Shannon and Weaver [58] and formalized by Brillouin [59].

At a particular site along the chain, the harmonic approximation can be used to express the energy at the site as a function of frequency ω. The Fourier transform of both the displacement and the momentum gives the Fourier coefficients Q_ω and P_ω, respectively. The energy at the site can be expressed as a function of these coefficients:

$$E_\omega = \frac{1}{2}\left(m\omega^2 Q_\omega^2 + \frac{P_\omega}{m}\right) \tag{1.100}$$

Equivalently, the total energy at the site is $E_T = \sum_\omega E_\omega$. The fraction of energy with frequency ω is $e_\omega = E_\omega / E_T$.

Livi et al. [56] were studying equipartition in FPU chains and sought a means to quantify the degree of equipartition. The measure had three criteria: 1) the

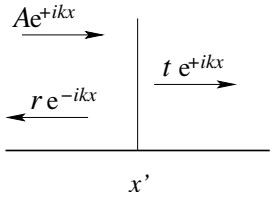

Figure 1.8: Schematic of a wave with amplitude A scattering from impurity located at x'. The reflected amplitude is r and the transmitted amplitude is t.

measure must be stable over time and fluctuation in the spectral distribution; 2) the measure must be reliable and insensitive to the initial conditions that may involve many modes; and 3) the measure must select the inverse square law in the power spectrum, denoting equipartition of energy. A suitable solution was found in the spectral entropy S [56]:

$$S = -\sum_{\omega}^{N_\omega} e_\omega \ln e_\omega \tag{1.101}$$

If all the energy is in a single mode, $S = 0$. Alternatively, if the energy is evenly distributed among all the modes, $S = \ln N_\omega$. The effective number of harmonic modes present at a site is $\exp(S)$.

1.6 Impurity Cross Section

Because the systems to be studied have single-valued impurity, the frequency-dependent cross section $\sigma(\omega)$ of each impurity is the same. Moreover, the cross section will be a useful quantity for characterizing the system. A schematic of scattering is shown in Fig. 1.8 for an incident wave having amplitude A. There is a single impurity located at x' that induces scattering, resulting in a reflected and transmitted wave. The reflection and transmission amplitudes are r and

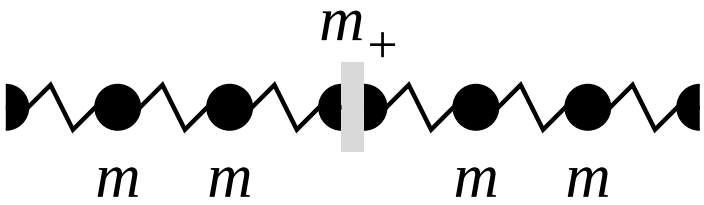

Figure 1.9: Schematic of physical model for impurity. An equilibrium mass m is divided in two and a mass m_+ is placed between the halves.

t, respectively. By definition, the scattering cross section is the ratio of the energy scattered to the incident energy. For one-dimensional systems, this ratio is proportional to the reflection probability:

$$\sigma = \frac{|r|^2}{|A|^2} \tag{1.102}$$

It follows, by conservation of energy, that $|A|^2 = |r|^2 + |t|^2$. It is a reasonably straightforward task to calculate the cross section. The answer found, however, depends upon one's physical model.

1.6.1 Impurity Model

The isotopic impurities used in this study are effected by changing the value of a particular mass. Conceptually, the material properties of the chain change in the proximity of the impurity. It would be useful to treat the impurity as a small (in its spatial extent) object placed between two systems that are homogeneous right up to the impurity.

For the FPU chain, this is achieved by thinking of the impurity as a mass m_+ between two sections of "pure" chain. Sections of pure chain can be created by taking sections of chain, terminated with a mass, and divide the end masses into two equal halves. The impurity can then be placed between two such sections.

This is depicted in Fig.1.9. Conceptually, the mass m_+ in Fig. 1.9 would have zero spatial extent. This conceptual model lends itself to solution via a continuum approximation.

1.6.2 Continuum Approximation

The scattering cross section can be calculated from a continuum approximation for the chain. In the limit that the mass spacing a approaches zero, the ratio m/a is the mass density μ. Similarly, the product Ka is the Youngs modulus Y. In this continuum limit, longitudinal waves along the chain are analogous to plane waves through an infinite medium having mass density μ and Youngs Modulus Y. The implicit assumption is that the displacement wavelength λ is much longer than the mass spacing a.

Between impurities, waves with amplitude $\psi(x, t|\omega)$ traveling along a harmonic material will satisfy the wave equation:

$$\mu \frac{\partial \psi^2}{\partial t^2} - Y \frac{\partial \psi^2}{\partial x^2} = 0 \tag{1.103}$$

An impurity located at x' will give rise to a reactive force due to the impurity impedance Z:

$$\mu \frac{\partial \psi^2}{\partial t^2} - Y \frac{\partial \psi^2}{\partial x^2} = -Z(\omega)\, \delta(x - x') \frac{\partial \psi}{\partial t} \tag{1.104}$$

Consistent with the physical model, the spatial extent of the impurity is modeled by a delta function.

Equation (1.104) is harmonic. Therefore, the frequency channels are separate, and the solution can be expressed as a function of angular frequency ω:

$$\psi(x, t|\omega) = \phi(x|\omega)\, \mathrm{e}^{-\mathrm{i}\omega t} \tag{1.105}$$

Substitution into Eq. (1.104) leads to a stationary equation for the spatial component of the amplitude ϕ:

$$\left[\frac{\partial^2}{\partial x^2} + \kappa^2 = -\frac{\mathrm{i}\omega}{Y} Z(\omega)\delta(x - x')\right] \phi(x|\omega) \tag{1.106}$$

where $\kappa = \omega\sqrt{\mu/Y}$.

Equation (1.106) can be solved using the Green's function $G(x, x')$ satisfying

$$\left[\nabla^2 + \kappa^2\right] G(x, x') = -\delta(x - x') \tag{1.107}$$

In one-dimension, the Green's function is [8, 60]

$$G(x, x') = \frac{\mathrm{i}}{2\kappa} \mathrm{e}^{\mathrm{i}\kappa|x-x'|} \tag{1.108}$$

The function ϕ can be solved for from the following integral equation:

$$\phi(x) = \phi^{\circ}(x) + \int G(x, x'') \frac{\mathrm{i}\omega}{Y} Z(\omega)\delta(x'' - x')\phi(x'')\mathrm{d}x'' \tag{1.109}$$

The function ϕ° is the solution to the homogeneous equation. Substituting for $G(x, x')$ gives

$$\phi(x) = \mathrm{e}^{+\mathrm{i}\kappa x} - \frac{\omega Z}{2Y\kappa} \mathrm{e}^{+\mathrm{i}\kappa|x-x'|}\phi(x') \tag{1.110}$$

The value of $\phi(x')$ is found by evaluating this equation at $(x = x')$:

$$\phi(x') = \frac{\mathrm{e}^{\mathrm{i}\kappa x'}}{1 + \frac{Z}{2Y\kappa/\omega}} \tag{1.111}$$

This can now be used to express the solution for $\phi(x)$:

$$\phi(x) = \mathrm{e}^{\mathrm{i}\kappa x} - \left(\frac{Z}{Z + \sqrt{4Y\mu}}\right) \mathrm{e}^{\mathrm{i}\kappa|x-x'|} \mathrm{e}^{\mathrm{i}\kappa x'} \tag{1.112}$$

This is a more general solution than the one by Morse and Ingard [43, Eq. 4.5.8]. After substituting for κ, the scattering cross section σ for 1-D systems is calculated from the reflection probability:

$$\sigma = |r|^2 = \frac{|Z|^2}{|Z|^2 + 4Y\mu} \tag{1.113}$$

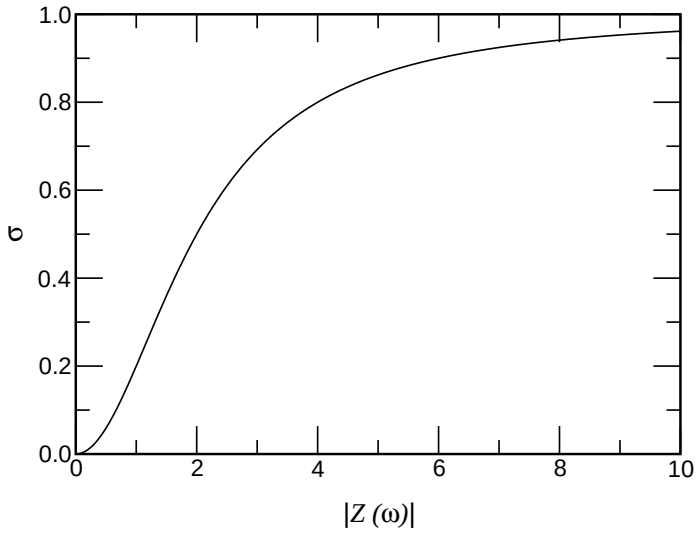

Figure 1.10: Scattering cross section σ as a function of impurity impedance $Z(\omega)$.

In the continuum limit, $Y\mu = Km_\circ$:

$$\sigma = \frac{|Z|^2}{|Z|^2 + 4Km_\circ} \tag{1.114}$$

As the spring constant K and the equilibrium mass $m_\circ$ are both equal to 1 for all the calculations, the scattering cross section σ of a single impurity can be expressed as a function of the impurity impedance $Z(\omega)$. Equation (1.114) is plotted in Fig. 1.10 as a function of $|Z(\omega)|$. This relationship holds as long as the continuum approximation is accurate for the discrete chain.

1.7 Thermal Transport

One goal of this work is to study energy transport along BID FPU chains. In the absence of translation, this corresponds to transport of heat energy, characterized by a thermal conductivity. Interestingly, the question of diffusive energy transport in one-dimensional chains is still a subject of study. In general, these studies

involve placing thermostats at each end of the system, calculating the thermal flux, and determining the thermal conductivity via Fourier's law.

It has been shown that a harmonic chain having thermostats at each end cannot support a thermal gradient, so the thermal conductivity is proportional to the system length [61]. This behavior is due to the extended, non-interacting phonons in the system traveling without attenuation. It was thought that maybe impurities could cause sufficient phonon scattering to give a finite thermal conductivity. The addition of impurities to the harmonic chain does lead to a thermal gradient [62, 63], but the thermal conductivity κ diverges as $L^{1/2}$ [13]. The only way to obtain a finite thermal conductivity in a disordered harmonic system was to either place each mass in contact with a thermal reservoir [64], or employ a time-dependent perturbative force [65, 66].

Nonlinearity is thought to be the key ingredient for normal heat conduction [67]. Nonlinearities will cause freely propagating phonons to scatter spontaneously, thereby slowing the rate of energy transport. FPU-β chains (without disorder) having thermostats at both ends exhibited finite thermal gradients, but the thermal conductivity still diverges as $L^{1/2}$ [68].

Experiments on disordered nonlinear systems have shed some light on the problem. Some of the first numerical experiments on disordered nonlinear systems have used isotopic disorder [69] and force constant disorder [70]. Although both experiments observed a thermal gradient, both experiments suffered from boundary effects, and neither established whether the thermal conductivity was a function of system length. A recent study of a disordered FPU-β chain observed a constant thermal conductivity for both large L and low temperature [71]. This is consistent with the assertion that Fourier's law is satisfied when there are

phonon-lattice interactions in addition to the phonon-phonon interactions [72].

For systems at zero temperature, the thermal conductivity is not defined in any strict sense. Instead, studies have focused on the properties of pulses traveling through the system. Most experiments have as a boundary condition either a localized (over one or a few masses) pulse or a Gaussian pulse. The system is integrated numerically, and experiments measure either the pulse position [73–75] or the pulse dispersion [76, 77].

1.7.1 Finite Temperature Methods

The specific technique for calculating the thermal conductivity in thermostated systems depends upon whether one seeks to characterize equilibrium or nonequilibrium systems. Fortunately, both types of systems are characterized by the same transport coefficient. The Onsager regression hypothesis [78, 79] states that the coefficient controlling regression of microscopic thermal fluctuations at equilibrium are the same that control relaxation of nonequilibrium disturbances.

Green-Kubo Relations

The Green-Kubo (GK) relations can be used to calculate the thermal conductivity κ from the fluctuations of a system in equilibrium at temperature T. The coefficient is calculated from an integral of the autocorrelation of a flux J:

$$\kappa = \frac{1}{k_B T^2 V} \int_0^\infty dt \langle J(t) J(0) \rangle \tag{1.115}$$

Whether one uses the heat flux J^q [80] or the energy flux J^e [81] depends upon whether one uses the grand canonical ensemble (J^q) or the microcanonical ensemble (J^e). The correct choice of ensemble and flux is that which yields the

proper result with the ensemble-independent calculation in which one takes the fluid volume to infinity before taking $k \to 0$ [82, Section 2.5].

Helfand Moments

The thermal conductivity of a collection of freely moving particles in thermal equilibrium can be determined from energy fluctuations. The energy fluctuation $\widetilde{E}_i$ for the i-th particle is the difference between the instantaneous site energy e_i and the ensemble averaged value $\langle e_i \rangle$:

$$\widetilde{E} = e_i - \langle e_i \rangle \tag{1.116}$$

If the energy fluctuation is conserved, and the energy flux has a linear dependence on $\nabla \widetilde{E}$, the quantity $\widetilde{E}_i(x,t)$ will satisfy the diffusion equation. For the boundary conditions that the initial value $\widetilde{E}_i(x,0)$ is localized about x_{i0}, and that $\widetilde{E}_i(\pm\infty, t) = 0$, the solution for $\widetilde{E}_i(x,t)$ is Gaussian, and the measure of spread is the second moment of $\widetilde{E}_i$:

$$2\kappa t\, \widetilde{E}_i(x,0) \sim \int (x - x_{i0})^2\, \widetilde{E}(x,t)\; dx \tag{1.117}$$

where κ is the thermal conductivity.

As $\widetilde{E}_i$ represents the fluctuation for a single particle, a bulk expression requires an ensemble integral of the second moment. Making no assumption about the independence of particle energies, the thermal conductivity can be calculated from a double sum over particle positions: [83]

$$H^p = \left\langle \sum_{i,j} (x_i - x_{j0})^2\, \widetilde{E}_i(x,t)\, \widetilde{E}_j(x,0) \right\rangle \sim 2\kappa t \tag{1.118}$$

Replacing conservation of momentum with conservation of energy yields an equiv-

alent alternative expression: [83]

$$H^e = \left\langle \left[\sum_i (x_i \widetilde{E}_i - x_{i0} \widetilde{E}_{i0}) \right]^2 \right\rangle \sim 2\kappa t \tag{1.119}$$

Equations (1.118) and (1.119) are the Helfand moments for calculating the thermal conductivity of a bath of particles.

Nonequilibrium Molecular Dynamics

There are a number of practical difficulties that arise when trying to perform a GK calculation. They are difficult to perform [84] and thermostats usually lead to heterogeneities at the bounaries, yielding nonuniform temperature gradients. These "jumps" at the boundaries are due to end resistances, which depend upon the thermostat response time [68].

Zhang, Isbister, and Evans [85] use the Evans nonequilibrium molecular dynamics (NEMD) heat flow algorithm to compute the thermal conductivity in one-dimensional lattices. Studies using thermal reservoirs and calculating thermal flux have a number of disadvantages. The system is spatially inhomogeneous and one cannot define an intrinsic temperature for the system due to the large temperature gradient. Consequently, it is impossible to obtain the temperature dependence of the heat conductivity in these systems. In addition, the problems associated with using the Nosé-Hoover thermostat for boundary particles (insufficient chaotic behavior to yield the canonical distribution, leading to periodic structure in phase space) have been discussed by Fillipov et al. [86].

The thermal conductivity of the FPU-β chain at temperature T is calculated as follows. The thermal conductivity is calculated from the Green-Kubo relation

for thermal conductivity:

$$\kappa = \lim_{\tau\to\infty} \frac{L}{k_B T^2} \int_0^\tau \mathrm{d}t \, \langle J_x(t)\, J_x(0)\rangle_{eq} \tag{1.120}$$

L is the system length: $L = Na$. The notation $\langle \ldots \rangle_{eq}$ denotes an equilibrium ensemble average. The heat flux J_x is given by

$$J_x(t) = \frac{-1}{2N} \sum_i \frac{p_i}{m_i} \left[U'(q_{i+1} - q_i) + U'(q_i - q_{i-1})\right] \tag{1.121}$$

In the Evans NEMD algorithm, the N particles are coupled to a "heat field" $\mathbf{F}_e$. The coupling is defined in such a way that the energy dissipation is proportional to $J_x \cdot \mathbf{F}_e$ ($\mathrm{d}H/\mathrm{d}t = LJ_xF_e$), and that the adiabatic incompressibility of phase space condition is satisfied [84, 87]. From this, the thermal conductivity coefficient can be calculated from the ratio of the heat flux to the applied heat field:

$$\kappa = \lim_{F_e\to 0} \lim_{t\to\infty} \frac{\langle J_x(t)\rangle}{TF_e} \tag{1.122}$$

Here, $\langle J_x(t)\rangle$ is, in principle, a nonequilibrium ensemble average. In practice, it can be replaced by a time average of $J_x(t)$ if the nonequilibrium steady state is unique. In addition, this heat flow algorithm is only valid in the linear regime: $F_e \to 0$ [84].

1.8 Research Plan

The following three chapters address the issues enumerated previously. The core of each chapter originates from both published and submitted journal papers:

Chapter 2: K.A. Snyder and T.R. Kirkpatrick, "Wave localization in binary isotopically disordered one-dimensional harmonic chains with impurities having arbitrary cross section and concentration," Phys. Rev. B **70**, 104201 (2004).

Chapter 3: K.A. Snyder and T.R. Kirkpatrick, "Influence of Anderson localization on the mode decay of excited nonlinear systems," Ann. Phys. (Leipzig) **8**, SI 241–244 (1999).

Chapter 4: K.A. Snyder and T.R. Kirkpatrick, "Energy transport along Fermi-Pasta-Ulam chains containing binary isotopic disorder: Zero temperature systems," (Submitted) Phys. Rev. B (2005).

Chapter 2 summarizes results from an experiment on harmonic BID chains. Scaling is used to calculate the localization length of chains having arbitrary impurity cross section and impurity concentration. In addition, a minimum system length can be determined from the Lyapunov exponent statistics. Because BID systems are "pure" at the extrema of impurity concentration, the localization length passes through a minimum with increasing impurity concentration. An interesting *ansatz* was the approximation for $\xi(c)$ that is a linear sum of the dilute scattering result for the extrema "pure" systems.

Chapter 3 was a study of the effects impurities have on mode decay in anharmonic BID systems. Although the initial effect of the impurities is to accelerate the rate of mode decay, the long term effect depended on the impurity mass. More specifically, impurities that add mass to the chain slow the ultimate rate that energy leaves the initial mode. Impurities that remove mass from the chain ($m_+ < 0$) can lead to more rapid energy loss from the initial mode. The primary explanation is that heavy masses capture energy and oscillate at lower amplitudes, thereby "holding on" to energy. Impurities for which $m_+ < 0$ oscillate at larger amplitudes, thereby expelling energy more quickly.

Chapter 4 summarizes the experiment to quantify the rate of energy transport along an anharmonic BID chain that is at zero temperature. The initial condi-

tion is an eigenstate of the harmonic chain, so that in the absence of nonlinearity, the energy is stationary. The addition of anharmonicity can lead to transport, quantified by the second moment M of the site energies. The effective transport coefficient was the proportionality between M and time. The time exponent of M for most of the systems was near to one, so an effective transport coefficient was estimated from the slope of $M(t)$ for an ensemble of systems. The effective transport coefficient was inversely proportional to impurity concentration for weak disorder. For strongly disordered systems having impurity concentrations $c\lambda > 1$, the effective transport coefficient was proportional to the original localization length.

Chapter 2

Equilibrium Harmonic Behavior

The localization length for isotopically disordered harmonic one-dimensional chains is calculated for arbitrary impurity concentration and scattering cross section. The localization length depends on the scattering cross section of a single scatterer, which is calculated for a discrete chain having a wavelength dependent pulse propagation speed. For binary isotopically disordered systems composed of many scatterers, the localization length decreases with increasing impurity concentration, reaching a mimimum before diverging toward infinity as the impurity concentration approaches a value of one. The concentration dependence of the localization length over the entire impurity concentration range is approximated accurately by the sum of the behavior at each limiting concentration. Simultaneous measurements of Lyapunov exponent statistics indicate practical limits for the minimum system length and the number of scatterers to achieve representative ensemble averages. Results are discussed in the context of future investigations of the time-dependent behavior of disordered anharmonic chains.

2.1 Introduction

The length scale over which Anderson localization [5] occurs in harmonic disordered chains can be expressed as a function of the ensemble-averaged system resistivity [21, 22]. Using scaling arguments, [22] the ensemble-averaged resistivity of harmonic systems having binary isotopic disorder (single-valued impurities) can be expressed as a function of the scattering cross section of a single impurity and the impurity concentration. Binary isotopically disodered harmonic chains (BIDHC) also have the property that in the limit that the impurity concentration approaches unity, the system is once again "pure," and the Anderson localization length diverges toward infinity. As a result, the Anderson localization length passes through a minimum at intermediate concentrations [88]. These properties of a BIDHC make these systems both tractable and interesting.

In this work, an approximation is developed for the localization length of a BIDHC with arbitrary impurity cross section and concentration. In addition, the result incorporates the discrete nature of the chain. Similar studies have been performed previously, but with important differences. Bourbonnais and Maynard [73] studied energy transport in one-dimensional systems having isotopic disorder, but the impurity masses were not single-valued. The results of Azbel and Soven [89] on quantum systems having binary isotopic disorder were based on a continuum solution for impurity locations constrained to exist on lattice sites. Although the Azbel and Soven result applied to short wavelengths that may exist between the impurities, the results do not incorporate the additional features of a discrete mechanical system.

This study serves as an introduction to future work on energy transport in binary isotopically disordered anharmonic chains. To perform that work, numer-

ical integration will be used to study the time-dependent nature of these systems. To be practical, the initial conditions will require sufficiently short wavelengths and high impurity concentrations to keep integration times manageable. In addition, the results of the study will incorporate the discrete nature of the mechanic chains so that these effects can accounted for in the results.

In this study, the energy localization in a BIDHC is studied for arbitrary displacement wavelength, impurity concentration and scattering cross section. Disorder is effected by changing randomly selected masses by a fixed amount. A continuum Kronig-Penney (KP) model [24] is used to develop a general expression for scattering cross section, and the continuum impurity impedance is corrected for wavelength dependent pulse propagation speed in discrete systems. The resulting expression is verified by direct numerical integration. The localization length of systems with strong scatterers is calculated using both the continuum KP model and the MacKinnon and Kramer [25] (MK) method. The distribution of Lyapunov exponents is studied using the continuum KP model, and the minimum requirements are found for system length and number of scatterers to achieve proper scaling statistics. The localization length concentration dependence is studied using the MK method, and an analytical expression is found for its behavior. For arbitrary impurity concentration and impurity cross section, the localization length in a BIDHC can be approximated by invoking a simple *ansatz* based on an analogy to electrical systems. The result is tested on systems having displacement wavelengths as short as four lattice spacings long.

2.2 Model System

The physical model used here is the harmonic version of the Fermi-Pasta-Ulam (FPU) [35] chain that is composed of discrete springs and masses. The masses m_i are on a lattice with spacing a and interact via nearest neighbor springs with force constant K. Disorder is effected by changing the background mass $m_\circ$ by a fixed amount m_+ with probability c. To simplify the results, all lengths are scaled by the lattice spacing a.

For a system composed of N masses, each characterized by a displacement u_i about the equilibrium location and a momentum p_i, the Hamiltonian is separable:

$$H = \frac{1}{2} \sum_{i}^{N} \frac{p_i^2}{m_i} + K \, (u_{i+1} - u_i)^2 \tag{2.1}$$

The real space equation of motion is

$$\frac{m_i}{K} \, \ddot{u}_i = u_{i+1} - 2u_i + x_{i-1} \tag{2.2}$$

The Fourier transform leads to the corresponding equation of motion for the energy eigenstate amplitudes $u_i(\omega)$:

$$u_{i+1} = \left[2 - \frac{\omega^2 m_i}{K} \right] \, u_i - u_{i-1} \tag{2.3}$$

This is the corresponding Anderson tight-binding model for the chain.

2.2.1 Discrete Analysis

The time-dependent properties of the system were determined by numerical time integration of Eq. (2.2) using a fourth-order symplectic integrator algorithm (SIA4) for separable Hamiltonians. The coefficients were taken from Candy and Rozmus [39], and the time step was 1/200 of the natural period.

The localization length was calculated from Eq. (2.3) using the method of MacKinnon and Kramer (MK) [25]. This method exploits the statistical properties of the u_i so that periodic rescaling can be used to improve overall statistics.

2.2.2 Continuum Analysis

A Kronig-Penney model [24] is used to develop an expression for the scattering cross section of an impurity and to study the statistics of the scaling parameter [22]. The continuum system analogous to the discrete chain is a homogeneous elastic medium having mass density μ and Youngs modulus Y. In the absence of impurities, a longitudinal displacement amplitude $\psi(x,t|\omega)$ with angular velocity ω will propagate down the rod with phase velocity $v_p = \sqrt{Y/\mu}$.

A harmonic oscillator impurity located at x' will give rise to a reactive force due to the impurity impedance Z for a wave with angular velocity ω:

$$\left[\mu\frac{\partial^2}{\partial t^2} - Y\frac{\partial^2}{\partial x^2} = -Z(\omega)\,\delta(x-x')\frac{\partial}{\partial t}\right]\,\psi(x,t|\omega) \tag{2.4}$$

We assume the solution has a time dependence given by an exponential of angular velocity ω ($\psi = \phi(x|\omega)\,\mathrm{e}^{-\mathrm{i}\omega t}$) to obtain

$$\left[\frac{\partial^2}{\partial x^2} + \kappa^2 = \frac{-\mathrm{i}\omega}{Y}\,Z(\omega)\,\delta(x-x')\right]\,\phi(x|\omega) \tag{2.5}$$

where $\kappa = \omega/v_p$. Equation 2.5 can be solved analytically for a single scatterer or can be solved numerically for a system composed of an arbitrary number of scatterers. From this numerical solution, one can determine the system resistivity, which can be used to calculate the localization length. A more complete discussion of calculating the initial condition is given in Appendix E.

2.3 Cross Section

The scattering cross section σ for a single impurity can be calculated from the continuum system of Eq. (2.5). The Green's function for the 1-D Helmholtz equation [60] can be used to solve for the admittance $\phi(x)$:

$$\phi(x) = \mathrm{e}^{\mathrm{i}\kappa x} - \left(\frac{Z(\omega)}{Z(\omega) + \sqrt{4\mu Y}} \right) \mathrm{e}^{\mathrm{i}\kappa|x-x_i|}\, \mathrm{e}^{\mathrm{i}\kappa x_i} \tag{2.6}$$

The scattering cross section in 1-D is equivalent to the reflection probability:

$$\sigma = \frac{|Z(\omega)|^2}{|Z(\omega)|^2 + 4\mu Y} \tag{2.7}$$

To apply this equation to the discrete chain, it must be converted from the continuum result to the corresponding discrete equation.

For an FPU system having masses spaced a distance a apart, the continuum coefficients can be expressed as a function of the discrete properties in the limit $a \to 0$ [90]:

$$\mu = \frac{m_\circ}{a} \qquad\qquad Y = Ka \tag{2.8}$$

The scattering cross section can now be expressed as a function of the discrete system components:

$$\sigma = \frac{|Z(\omega)|^2}{|Z(\omega)|^2 + 4Km_\circ} \tag{2.9}$$

The impedance $Z(\omega)$ of a mass impurity along a one-dimensional chain is proportional to the mass m_+ that is added to the background mass $m_\circ$ [43]:

$$Z(\omega) = -\mathrm{i}\, m_+ \omega \tag{2.10}$$

A numerical experiment was performed to test the applicability of Eqs. (2.9) and (2.10) to FPU systems, and a schematic of the experiment is shown in Fig. 2.1. The system had fixed ends and length L. One impurity was located at $L/3$, and

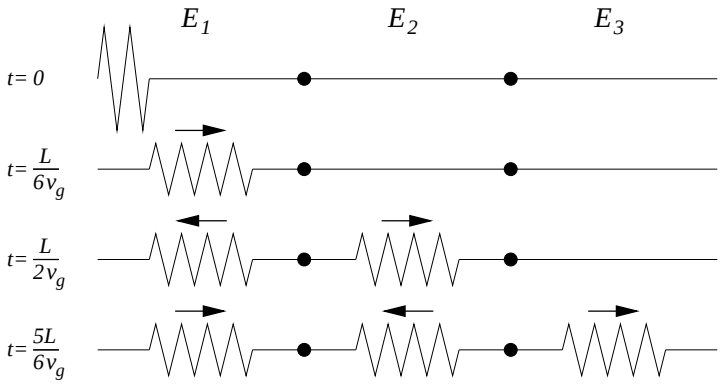

Figure 2.1: Schematic of cross section numerical experiment; each line represents the state of the system at the time of measurement. The time t, shown along left side, is expressed as a function of the system length L and group velocity v_g. The large dots denote the location of two impurities.

another impurity was located at $2L/3$. An initial displacement was made with wavelength λ and total length 16λ, and the hyperbolic tangent function was used to taper the oscillation amplitude from A to zero. Initially, the pulse was located at one end of the system. It had length 8λ, amplitude $2A$, and zero initial velocity. The time-dependent behavior was determined by numerical integration using the SIA4 algorithm.

The measured scattering cross section was determined from the energy located in the three regions separated by the impurities. The pulse energy located in each three regions, denoted by E_1, E_2, and E_3 in Fig. 2.1, was calculated at four separate times: $t = 0$, $L/6v_g$, $L/2v_g$, and $5L/6v_g$, where v_g is the group velocity $(\partial\omega/\partial k)$. At these times, the pulses are located near the center of a region. Although redundant with respect to the initial total energy, determining the energy at $t = L/6v_g$ provided a consistency check. In each case, the difference between $E_1(t = 0)$ and $E_1(t = L/6v_g)$ was less than one part in 10^4.

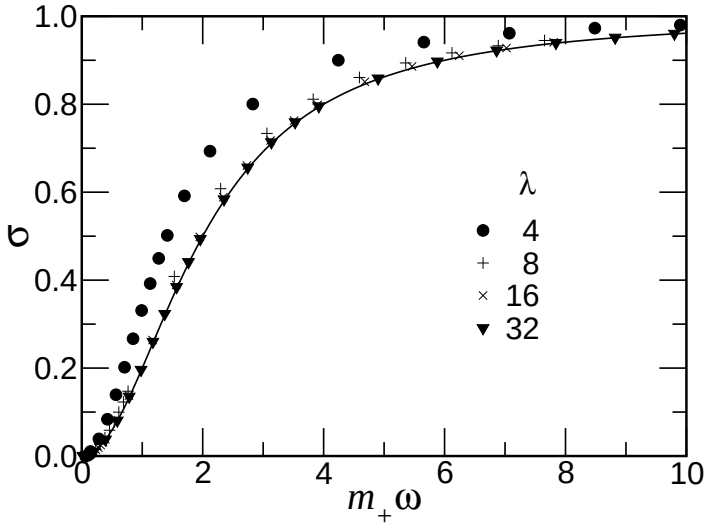

Figure 2.2: Cross section σ as a function of $m_+\omega$ for different wavelengths λ. The solid curve is the analytical result in Eq. (2.15).

The scattering cross section in FPU systems is the reflection coefficient. In this experiment, the reflection coefficient R is calculated from the ratio of energies in the first two intervals after one scattering event:

$$R = \frac{E_1(L/2v_g)}{E_1(0)} \tag{2.11}$$

Although the transmission coefficient T could have been determined from $E_2(L/2v_g)$, a second scatterer was used as a more rigorous test of the experiment design and numerical integrator. The transmission coefficient T for a single scatterer was calculated using the energy after two scattering events:

$$T = \sqrt{\frac{E_3(5L/6v_g)}{E_1(0)}} \tag{2.12}$$

In all cases, the magnitude of $1 - R - T$ was less than 10^{-3}.

The results of the numerical experiment are shown in Fig. 2.2 for different wavelengths. As can be seen in the figure, Eq. (2.10) is accurate for long wave-

lengths only. For shorter wavelengths, a correction is needed to account for the discrete nature of the chain.

There are two possible ways to approach the correction. In a discrete chain, the obvious difference among waves having varying wavelength is the group velocity v_g. To correct the scattering cross section equation, the correction needs to be dimensionless. The likely choice is the relative group velocity c_s, expressed as a function of the wave number k:

$$c_s = \frac{v_g}{v_p} = \cos(ka/2) \qquad\qquad k = \frac{2\pi}{\lambda} \tag{2.13}$$

If the value of κ in Eq. (2.5) should have been $\kappa = \omega/v_g$, the quantity $4Km_\circ$ in the denominator of Eq. (2.9) would become $4Km_\circ c_s^2$. Alternatively, the impedance of a mass in a discrete chain can be adjusted for the speed of the oncoming wave:

$$Z(\omega) = -\mathrm{i}\, m_+\omega/c_s \tag{2.14}$$

Substituting this value of $Z(\omega)$ into Eq. (2.9) gives the scattering cross section of a mass impurity in a one-dimensional discrete chain:

$$\sigma = \frac{(m_+\,\omega/c_s)^2}{(m_+\,\omega/c_s)^2 + 4Km_\circ} \tag{2.15}$$

The correction due to c_s also appears in the solution for the corresponding NLS system [91].

A comparison of the corrected cross section σ in Eq. (2.15) to the measured reflection coefficient R in Eq. (2.11) is shown in Fig. 2.3 for different displacement wavelengths λ. The results demonstrate that Eqn. 2.15 is an accurate estimate for the scattering cross section σ for displacement wavelengths as short as $4a$. Moreover, the symmetry about zero for scattering cross section for negative values of m_+ is shown in the inset of Fig. 2.3.

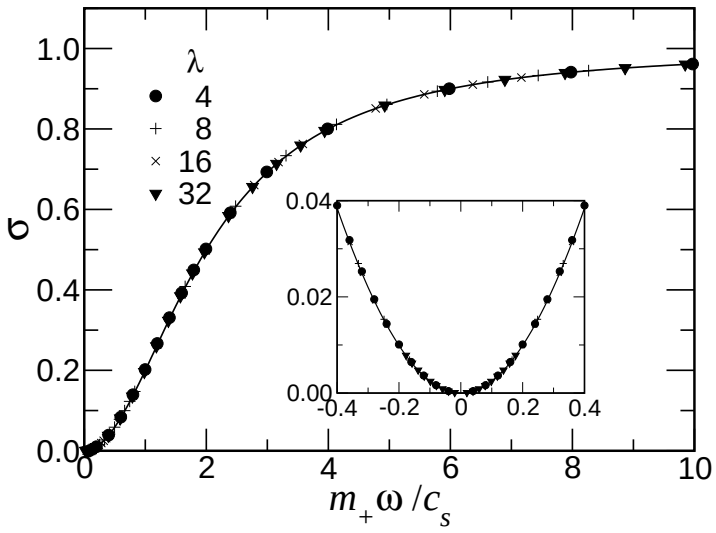

Figure 2.3: Cross section σ as a function of $m_+\omega/c_s$ for different wavelengths λ. The solid curve is the analytical result in Eq. (2.15). The inset shows additional data near zero.

2.4 Localization Length

The resistivity ρ_N of a system composed of N scatterers is the ratio of the system reflection coefficient R_N to the system transmission coefficient T_N [21]:

$$\rho_N = \frac{R_N}{T_N} \tag{2.16}$$

Using scaling arguments [22] that achieve proper statistical properties, the system resistivity ρ_N can used to define the Lyapunov exponent γ:

$$\gamma = \frac{\ln(1+\rho_N)}{L} \tag{2.17}$$

The factor of two normally appearing in this equation is omitted here for convenience. The localization length ξ for a system having length L and N scatterers

is defined from the ensemble averaged Lyapunov exponent:

$$\xi^{-1} = \langle\gamma\rangle = \frac{\langle \ln(1+\rho_N)\rangle}{L} \tag{2.18}$$

Unless otherwise noted, the symbol γ shall imply the ensemble averaged quantity.

2.4.1 Strong Scatterers

To perform future numerical experiments on anharmonic systems of manageable length, the scatters will need to be relatively strong. Therefore, weak scattering results will not be applicable. Moreover, a means is needed to predict the average localization behavior of a system using only single scatterer information. Because the impurities are identical, the scaling law [22] can be exploited to express system behavior as a function of the resistivity of a single scatterer ρ:

$$\langle \ln(1+\rho_N)\rangle = N \ln(1+\rho) \tag{2.19}$$

where ρ is related to the scattering cross section σ:

$$\rho = \frac{\sigma}{1-\sigma} \tag{2.20}$$

Substituting from Eq. (2.18) above yields an unbiased estimate for the ensemble averaged localization length (dilute limit) as a function of impurity concentration c:

$$\xi_\circ^{-1} = c\langle \ln(1+\rho)\rangle \tag{2.21}$$

In the limit of weak scattering ($c, \rho \to 0$), one recovers the expected result $\xi_\circ^{-1} = c\sigma = \Lambda^{-1}$, where Λ is the classical mean free path.

To demonstrate both the effect of strong scatterers ($\sigma \to 1$) and the accuracy of Eq. (2.19), the ensemble average $\langle \ln(1+\rho_N)\rangle$ was calculated from 10 000

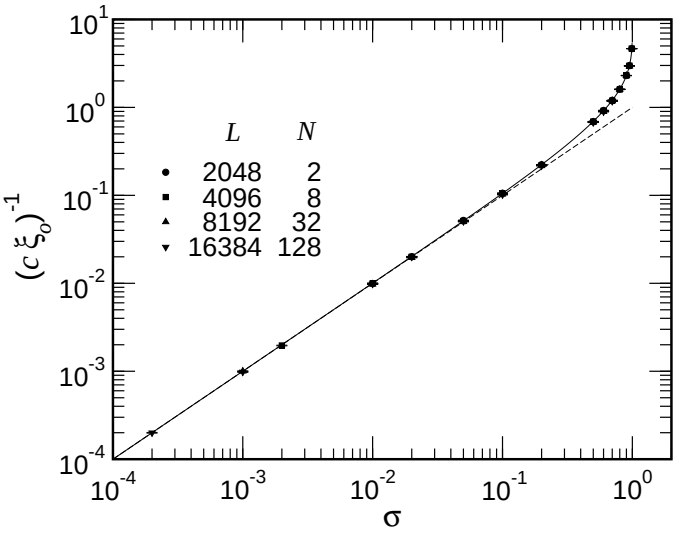

Figure 2.4: Localization length $\xi_\circ$, scaled by impurity concentration c, as a function of impurity scattering cross section σ for systems having length L and N impurities. The solid line is $\ln(1+\rho)$ and the dashed line represents the mean free path estimate. The error bars represent the standard error. (Many of the symbols lie upon one another and the error bars are typically smaller than the symbols.)

systems, each having length L and N impurities. The displacement wavelength was 32, and the scattering cross section of each impurity was σ. The results from the calculation are shown in Fig. 2.4 as a function of the impurity cross section σ. In the figure, the error bars represent the standard error (SE) [92], which, for an ensemble composed of W systems, is the population standard deviation s divided by $\sqrt{W}$. As can be seen, all the systems have the $\ln(1+\rho)$ dependence that deviates from the mean free path approximation for cross sections ≥ 0.2, and for all combinations of system size and number of scatterers.

2.4.2 Statistics

The results shown in Fig. 2.4 demonstrate that, in the mean, systems having a finite density of scatterers have the expected behavior. Recent results suggest that systems having relatively few scatterers do not exhibit Gaussian behavior and, therefore, do not obey scaling laws. For systems having sufficient length and number of scatterers, the population of Lyapunov exponents is normally distributed [22], with variance s_γ^2 [22, 93]

$$s_\gamma^2 = \frac{2}{L^2} \langle \ln(1+\rho_N) \rangle \tag{2.22}$$

Returning to the data of Fig. 2.4, the population of Lyapunov exponents γ was compared to the expectations of Eq. (2.22). To assess the "normality" of the data, the intervals, both above and below the mean, having coverage factors [94] corresponding to one and two standard deviations, were determined from the population. In addition, the population standard deviation Δ is shown so that it could be compared to both its estimated value in Eq. (2.22) and to the corresponding coverage interval.

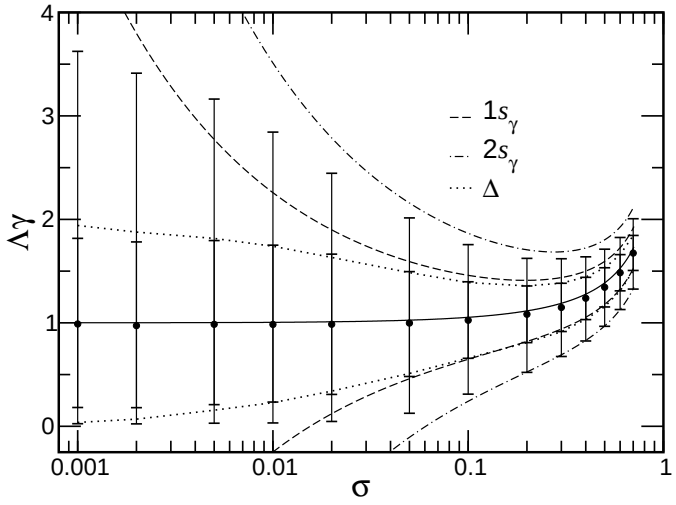

Figure 2.5: Lyapunov exponent γ statistics as a function of scattering cross section σ for a system with $L = 16\ 384$, $N = 128$, and $\lambda = 32$. Error bars represent coverage factors corresponding to one and two standard deviations of a normal distribution. The predicted intervals $\pm 1 s_\gamma$ and $\pm 2 s_\gamma$ from Eq. (2.22) are shown as dashed and dotted lines, along with observed population standard deviation Δ.

The results of the Lyapunov exponent statistics calculation, from an ensemble with a population of 10 000, are shown in Fig. 2.5 for systems having length $L = 16\ 384$, $N = 128$ impurities, and displacement wavelength $\lambda = 32$. (Results for other systems were similar, and are omitted for brevity.) The data are shown as a function of the single impurity cross section σ. The filled symbols are the average value, and the solid line is the estimated average value. The error bars represent the intervals that have the same coverage factor as one and two standard deviations in a normal distribution. The two pairs of dashed lines are the estimated standard deviations from Eq. (2.22). The dotted line is the population standard deviation Δ.

For small scattering cross sections, the distribution of γ is asymmetric, with zero as a lower bound for the coverage intervals. Interestingly, only the outer intervals are asymmetric about the mean. The inner intervals are nearly symmetric about the mean, and they have a value nearly equal to the population standard deviation.

As the scattering cross section increases, the results begin to exhibit Gaussian behavior. Above a 0.2 scattering cross section, the measured intervals, the predicted intervals s_γ, and the population standard deviation Δ all agree. Therefore, agreement between the population standard deviation Δ and the estimated standard deviation s_γ is as much as measure of "normality" as is a careful analysis of the population coverage intervals.

Exploiting this relationship, the population standard deviation Δ for all the data from the Lyapunov exponent statistics experiment are shown in Fig. 2.6 as a function of the system length. For normally distributed populations, the estimated coefficient of variation can be determined from Eq. (2.18) and Eq. (2.22),

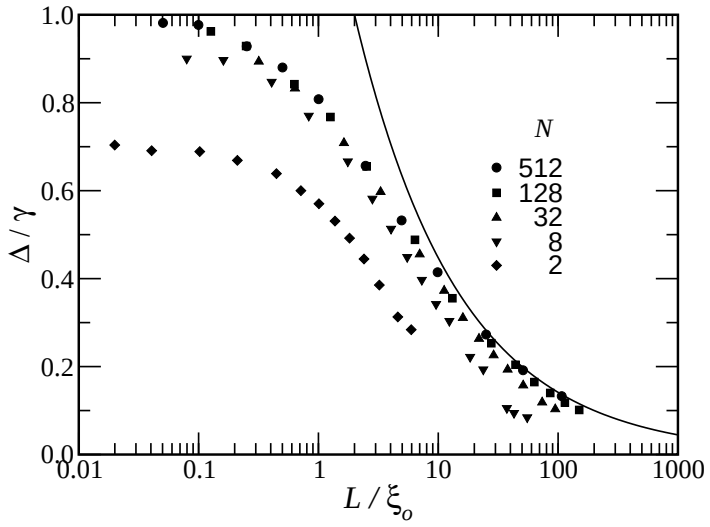

Figure 2.6: Lyapunov exponent coefficient of variation Δ/γ as a function of the ratio of system length L to the localization length $\xi_\circ$ for systems having different numbers of scatterers N. The solid curve is Eq. (2.23).

and has the following convenient form:

$$\frac{s_\gamma}{\langle\gamma\rangle} = \sqrt{\frac{2}{L/\xi_\circ}} \tag{2.23}$$

This equation is shown as a solid line in Fig. 2.6. One can conclude from the figure that in order for the observed Lyapunov exponents to be normally distributed, the system length must be at least 10 times the localization length, and the number of scatterers must be ≥ 32.

2.5 Concentrated Impurities

For dilute impurity concentrations, the localization length decreases with increasing impurity concentration. As the impurity concentration c approaches unity, however, the FPU system will become a pure system composed entirely of masses $m_\circ + m_+$. At $c = 1$, the system is once again devoid of impurity and the localization length goes to infinity. At intermediate impurity concentrations, the localization length passes through a minimum. Therefore, the behavior of a system at arbitrary impurity concentration cannot be fully characterized by the relation in Eq. (2.21).

For dilute systems, the localization length $\xi_{c\to 0}$ is that of Eq. (2.21):

$$\xi_{c\to 0}^{-1} = \xi_\circ^{-1} = c\,\langle\ln(1+\rho)\rangle \tag{2.24}$$

At high concentrations, the localization length $\xi_{c\to 1}$ has a concentration dependence that is proportional to $(1-c)$:

$$\xi_{c\to 1}^{-1} = (1-c)\langle\ln(1+\rho')\rangle \tag{2.25}$$

The adjusted resistivity ρ' is for a system having background mass $m_\circ + m_+$ and impurities with mass $m_\circ$. By the nature of the solution using the MK method,

and given that the systems are harmonic, the frequency ω is the same for both systems, but the wavenumber and the corresponding relative group velocity are different:

$$k' = \frac{2}{a}\,\mathrm{Sin}^{-1}\left[\frac{\omega}{2}\sqrt{\frac{m_\circ + m_+}{K}}\right] \tag{2.26a}$$

$$c_s' = \cos\left(k'/2\right) \tag{2.26b}$$

$$\rho' = \frac{(-m_+\omega/c_s')^2}{4K(m_\circ + m_+)} \tag{2.26c}$$

The behavior of the system for all values of impurity concentration is conjectured from the electrical analogy: as Lyapunov exponent is to resistivity, localization length is to conductivity. If one assumes that at some intermediate concentration the behavior is simultaneously expressing itself as two systems with localization lengths $\xi_{c\to 0}$ and $\xi_{c\to 1}$, these two systems should contribute independently to the overall behavior, like two conductors in parallel. By this analogy, the total localization length ξ would be additive:

$$\xi = \xi_{c\to 0} + \xi_{c\to 1} \tag{2.27}$$

This equation represents a more complete estimate for the localization length that is valid for both strong and concentrated scatterers.

2.5.1 Positive m_+

The accuracy of the approximation in Eq. (2.27) is demonstrated in Fig. 2.7 for systems having impurity scattering cross section $\sigma = 0.20$ and displacement wavelength λ ranging from 8 to 128. The localization length ξ for these systems was calculated using the MK method. As can be seen, the approximation in Eq. (2.27) is reasonably accurate. The inset shows the same data, plotted as a

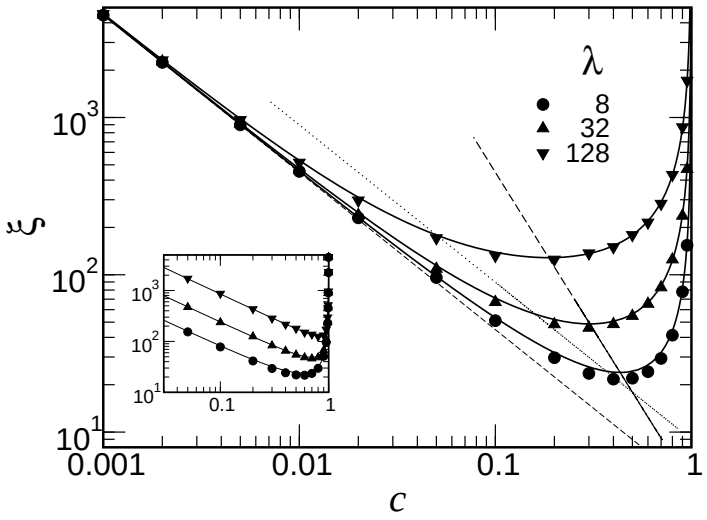

Figure 2.7: Localization length ξ as a function of impurity concentration c in a discrete system having scatterers with cross section 0.2. The solid lines are from Eq. (2.27), the dashed line is the locus of minima, and the dotted line denotes equal contribution from $\xi_{c\to 0}$ and $\xi_{c\to 1}$. Inset shows same data as a function of (1-c).

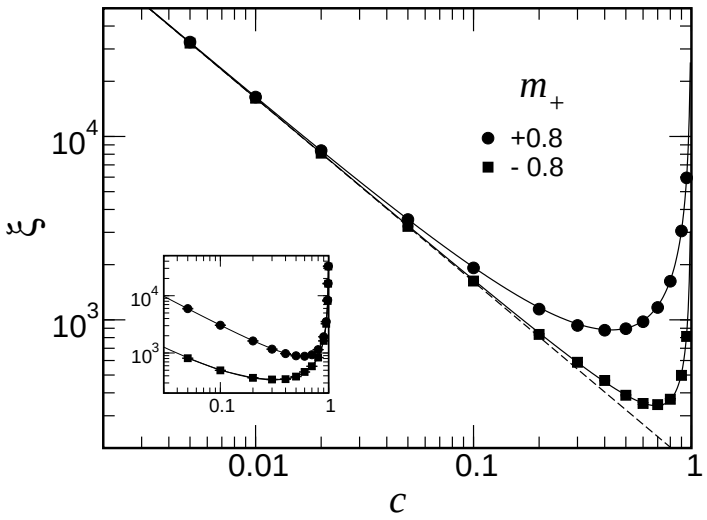

Figure 2.8: Localization length ξ as a function of impurity concentration c for $m_+ = \pm\ 0.8$. Inset shows same data as a function of (1-c).

function of $(1-c)$, highlighting the separate behavior near $c \to 1$ for the different wavelengths.

Also shown in Fig. 2.7 are a dashed line and a dotted line. The dashed line is the locus of localization length minima as a function of displacement wavelength. Not only does the minimum localization length increase with increasing wavelength, the concentration at which this happens decreases with increasing wavelength. The dotted line in Fig. 2.7 is the locus of points where $\xi_{c\to 0} = \xi_{c\to 1}$. This locus of points is meant to delineate the cross-over point as the system passes from one dominate phase to the other. The cross-over point has a stronger concentration dependence than the locus of minima.

2.5.2 Negative m_+

The impurity scattering cross section σ depends only upon the magnitude $|m_+|$. For small impurity concentrations, the localization length will be the same whether m_+ is positive or negative. At higher concentrations, however, the behavior of the systems with positive m_+ will differ from those with negative m_+ because Eqs. (2.26) will give different results for the two systems.

As an example, the localization concentration dependence was calculated for two systems with displacement wavelength $\lambda = 32$. The added impurity masses were $+0.8$ and -0.8, and the localization length was determined by the MK method. The results of the calculation are shown in Fig. 2.8 as a function of the impurity concentration c. The estimate from Eq. (2.27) for each system is shown as a solid line. Within the inset are the data plotted as a function of $(1-c)$. The dashed line is the dilute limit value in Eq. (2.21). As expected, the behavior of the two systems diverge at higher concentrations.

2.5.3 Cut-Off Frequency

If the conceptual model of independent harmonic systems that led to the adjusted values given in Eqs. (2.26) is correct, Eq. (2.26a) suggests that there exists a cut-off frequency for the harmonic system in the limit of $c \to 1$. If the argument of Sin^{-1} is greater than one, k' becomes a complex number. The real component of k' is $2/a$, which is a wave with a zero group velocity. An imaginary component to k' means that the wave is localized. Under these conditions, the localization length $\xi_{c\to 1} = 0$, and the system behaves according Eq. (2.21), meaning that the system localization length is a monotonically decreasing function of impurity concentration.

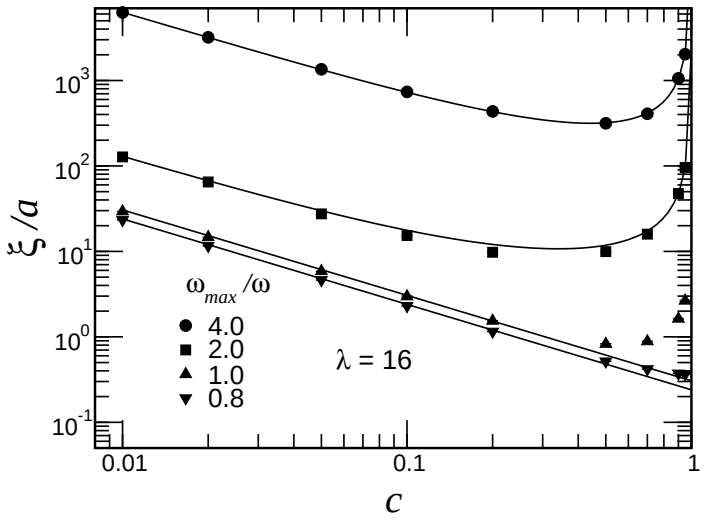

Figure 2.9: Localization length ξ as a function of concentration c for constant wavelength λ and varying m_+ to control ω_{max}.

From Eq. (2.26a), there exists a maximum frequency ω_{max}:

$$\omega_{max} = 2\sqrt{\frac{K}{m_\circ + m_+}} \tag{2.28}$$

Frequencies above ω_{max} should not propagate, and the localization length should be a monotonic function of concentration. As a check, the localization length for $\lambda = 16$ systems was calculated for various frequencies ω, with ω_{max} set by m_+. The results are given in Fig. 2.9 as a function of the impurity concentration. Although the localization length for the $\omega_{max}/\omega = 1$ system was not purely monotonic, the results for $\omega_{max}/\omega = 0.8$ suggest that the conceptual model is reasonably close to reality.

Another test was performed, this time maintaining m_+ constant and varying the wavelength. The value of m_+ was 15.509, the value that corresponds to $\sigma = 0.7$ for $\lambda = 32$, which behaves very much like a continuum wave. The results

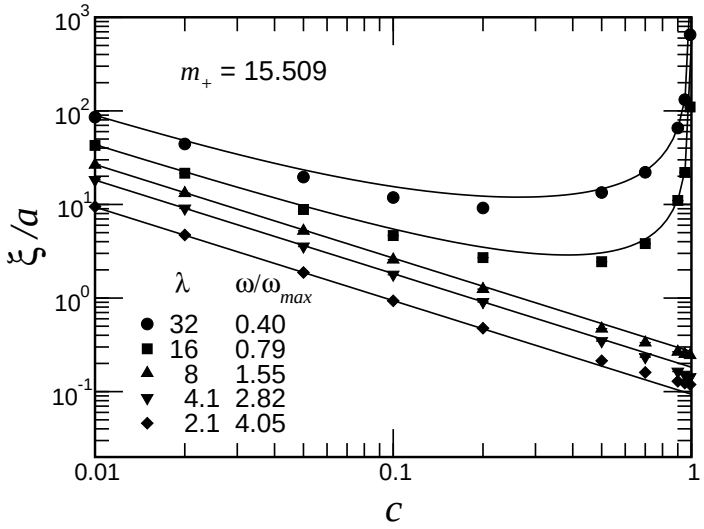

Figure 2.10: Localization length ξ as a function of concentration c for constant m_+ and varying wavelength λ.

are given in Fig. 2.10 as a function of impurity concentration. These results seem to confirm the validity of the conceptual model.

2.5.4 Azbel and Soven Comparison

To further assess the conceptual model, Eq. 2.27 is compared to the more rigorous result of Azbel and Soven [89] (AS). The AS model contains quantum particles interacting with delta function potentials that have strength V and are located at random integer values of x. For the AS systems, the value of V is equal to -1, and the scattering cross section $\sigma_{\rm AS}$ of each scatterer is a function of the particle wave number k:

$$\sigma_{\rm AS} = \frac{1}{1 + 16\sin^2(k/2)} \tag{2.29}$$

This is sufficient to duplicate the AS numerical calculation.

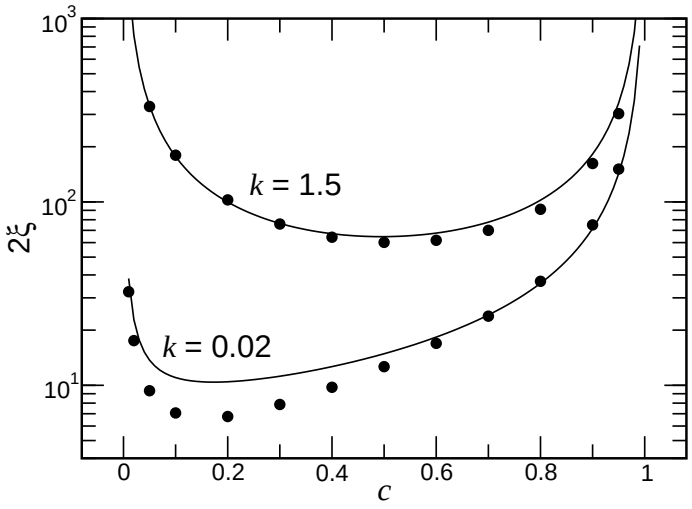

Figure 2.11: Localization length ξ as a function of impurity concentration c for two systems with different wavenumber k. Filled symbols are calculations using the MK method, and solid lines are Eq. (2.27). The figure can be compared directly to Figure 1 of Azbel and Soven.

Figure 1 of Azbel and Soven[89] shows results from calculations made for three values of wavenumber k: 0.02, 1.5, 3.13. The MK method is used here to duplicate the numerical results for the two smaller values of k, and the results are shown as filled symbols in Fig. 2.11. The solid lines in Fig. 2.11 are the corresponding estimate of Eq. (2.27). Two things should be noted explicitly: The AS definition of localization length corresponds to twice the localization length defined here. The definition of localization length in Azbel and Soven[89] uses the Landauer [21] scaling parameter, while subsequent work [95, 96] use the scaling of Anderson et al. [22] The results shown in Fig. 2.11 use the latter scaling definitions.

The two systems shown in Fig. 2.11 are demanding tests of Eq. (2.27). The system k=0.02 requires m_+=2498, corresponding to a cross section of 0.99840. This contrast in mass means that $\xi_{c\to 1}$ dominates the sum in Eqn. 2.27, and the localization length minimum occurs at a relatively low impurity concentration. The system k=1.5 has an impurity cross section of 0.119 and a displacement wavelength of 4.19 lattice spacings. Because m_+=0.394, both components of ξ in Eqn. 2.27 contribute nearly equally, and the shape of the curve is nearly symmetric.

2.5.5 $c\lambda$ Effect

As can be seen in Figs. 2.7 and 2.8, the behavior of the total localization length diverges from the dilute limit $\xi_\circ$. In Fig. 2.7, the point at which ξ begins to differ from $\xi_\circ$ is a function of the displacement wavelength. To more clearly demonstrate this effect, the ratio $\xi/\xi_\circ$ is shown in Fig. 2.12 as a function of the product $c\lambda$. The data shown are those appearing in Fig. 2.7, with the addition of data for $\lambda = 512$. Also shown in the figure is a dotted line denoting the long

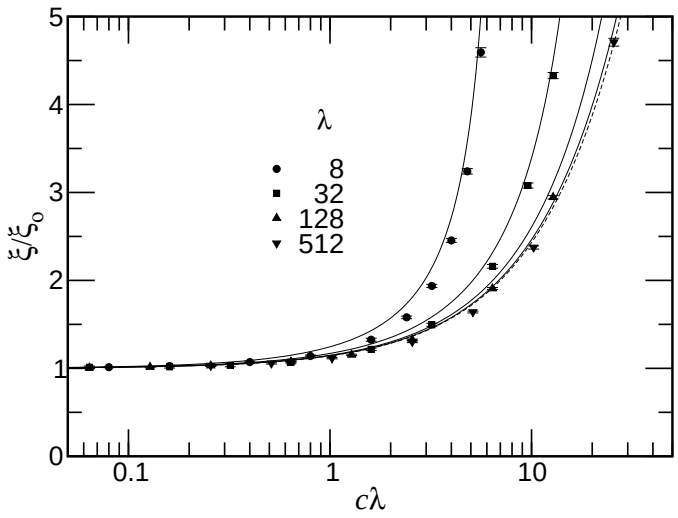

Figure 2.12: The ratio of the measured localization ξ to the dilute concentration value $\xi_\circ$ as a function of the product of impurity concentration c and wavelength λ. Filled symbols are calculated solutions for systems having impurity cross section 0.2. The dotted line is the limiting curve for $\lambda \to \infty$.

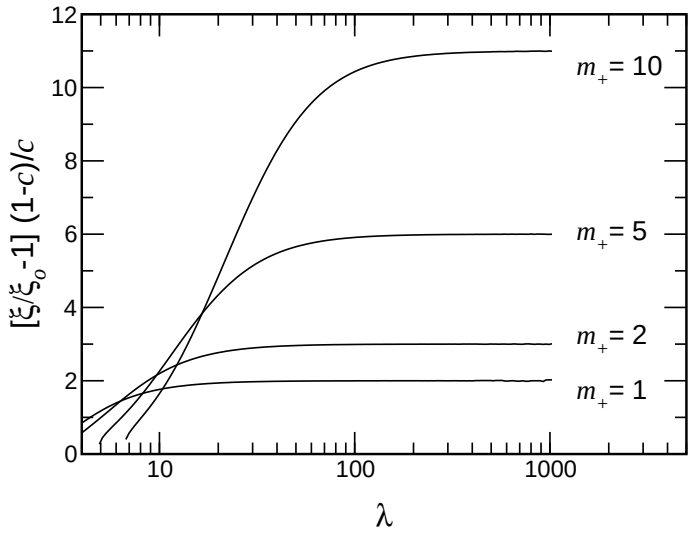

Figure 2.13: The ratio of the measured localization ξ to the dilute limit localization length $\xi_\circ$, normalized by the impurity concentration c, as a function of displacement wavelength λ.

wavelength limiting behavior for $\lambda \to \infty$. For values of $c\lambda$ greater than 1, the dilute limit approximation does not hold, and the observed localization length is greater than the dilute limit estimation. Therefore, even though the effect is less dramatic for increasing λ, there is a minimum effect, regardless of the wavelength.

2.6 Anharmonic Chains

In an anharmonic system, mode interactions will lead to the creation of displacements with varying wavelength. In time, very long wavelength displacements will be created. Because the impurity masses are fixed in time, the scattering cross section for the displacement waves will decrease as λ^{-2}. In addition, because the impurities are fixed in space, the product $c\lambda$ will increase over time. Based on the

results from the last Section, one would expect that the ratio $\xi/\xi_\circ$ will diverge to infinity with increasing wavelength.

Using Eq. (2.27), the ratio $\xi/\xi_\circ$ was calculated as a function of displacement wavelength for systems having constant impurity mass and concentration. The results are shown in Fig. 2.13 for different values for m_+. For all values of impurity concentration c, the ratio $\xi/\xi_\circ$ asymptotes to a constant at long wavelength:

$$\lim_{\lambda\to\infty} \frac{\xi}{\xi_\circ} = 1 + \frac{c}{1-c}\,(m_\circ + m_+) \tag{2.30}$$

Therefore, for anharmonic systems, the localization length is characterized, to within a constant, by the dilute limit expression for $\xi_\circ$ given in Eq. (2.21).

The same relationship applies to both positive and negative values for m_+. For negative values of m_+, in fact, in the limit $m_+ \to -1$, the behavior of the system is accurately characterized by $\xi_\circ$ at long wavelengths.

2.7 Conclusion

The localization length for harmonic chains having binary disorder can be predicted accurately over a wide range of wavelengths, impurity cross section, and impurity concentration. The ingredient needed for this prediction is the cross section of a single scatterer, corrected for short wavelength displacements via the relative pulse propagation speed. The localization length over the entire impurity concentration range can then be estimated by approximating the system as a sum of two independent systems, each accounting for the behavior of the system at the two limits of impurity concentration.

The general result applies to systems in which the impurity mass is either larger or smaller that the original mass. Although the scattering cross section

is symmetric about zero, with respect to the mass added to the background value, the localization length behavior differs for negative and positive changes in mass having the same scattering cross section. This difference in behavior with respect to localization length, along with previous results showing differences in the rate of phonon-phonon interactions, are discussed in the context of numerical experiments on anharmonic systems.

The general results also suggest that the localization length of long displacement wavelengths created by phonon-phonon interactions can be approximated, to within a constant, from dilute limit calculations results. For increasing concentration and constant impurity concentration, the localization length, with respect to the dilute limit prediction, will eventually diverge toward infinity. This deviation occurs for all wavelengths, and is a universal function of the impurity concentration and the displacement wavelength, for a constant cross section. By contrast, in a numerical experiment on an anharmonic system composed of fixed scatterers, the scattering cross section decreases with increasing wavelength. For these systems, the long wavelength behavior is, to within a constant, accurately predicted by dilute limit predictions.

Chapter 3

Mode Decay Experiment

This Chapter is an investigation of mode transitions in disordered nonlinear systems. By analogy to Chapter 2 that isolated and investigated the harmonic properties of disordered chains, this Chapter will attempt to isolate the role of mass impurities on the rate of mode decay in nonlinear systems. For this study, the system is a linear chain with periodic boundary conditions. The initial condition is a single eigenmode of the pure chain.

A one-dimensional system of masses with nearest-neighbor interactions and periodic boundary conditions is used to study mode decay and ergodicity in nonlinear, disordered systems. The system is given an initial periodic displacement, and the total system energy within a specific frequency channel is measured as a function of time. Results indicate that the rate of mode decay at early times increases when impurities are added. However, for long times the rate of mode decay decreases with increasing impurity mass and impurity concentration. This behavior at long times can be explained by Anderson localization effects and the nonergodic response of the system.

3.1 Introduction

The transition from quasi-periodic to ergodic behavior in nonlinear systems has been an active field of research since the seminal work of Fermi, Pasta, and Ulam (FPU) [35]. The behavior of the FPU system has been discussed in great detail [97, 98], and given the degree of nonlinearity and initial energy density, one can estimate the time required before the system becomes ergodic [99]. However, little is known about the effects that impurities have upon the transition dynamics to ergodic behavior in nonlinear systems. Since mode coupling in nonlinear systems occurs through interactions, one expects that the presence of impurities will hasten the transition to ergodic behavior. This expectation, however, is generally not correct due to Anderson localization effects [2, 5, 100].

Reported here are the results from a numerical experiment using a one-dimensional system of masses with nonlinear nearest neighbor forces and periodic boundary conditions. The displacement of each mass is sampled over a finite interval of time and the energy within all frequencies is calculated for each mass. The total energy in a single mode is conserved in harmonic systems both with and without impurities. Therefore, for the nonlinear systems, the effects of the impurities upon the mode decay can be compared directly to the systems without impurities.

3.2 Numerical Experiment

The system used in this experiment is the FPU-β chain composed of N masses with periodic boundary conditions, and with unit equilibrium spacing ($a = 1$). The masses undergo a displacement $u(t)$, and the i-th mass m_i interacts through

nearest neighbor forces:

$$m_i\ddot{u}_i = -K\left[(u_{i+1}-u_i)-(u_i-u_{i-1})\right]-\beta\left[(u_{i+1}-u_i)^3-(u_i-u_{i-1})^3\right] \quad (3.1)$$

For this experiment, the coupling constants $K = \beta = 1$. A pure system is composed of masses $m_\circ = 1$, and disorder is achieved by randomly changing a number N_I of the masses to a second value m_I. The time integration is performed using a 4-th order predictor-corrector algorithm [36, 37].

The initial condition is a unit amplitude, zero-velocity sinusoidal displacement with wavelength $\lambda = 32$. Time is scaled by the harmonic frequency $\omega_o = 2\sqrt{K/m_\circ}\cos ka/2$. At certain intervals, the time-dependent displacement of each mass is transformed to reciprocal space, and these data $u_k(x_i)$ are used to calculate the modal energy $E_\omega = E(\omega_o)$ and mass energy $E_i = E(x_i)$ by summing over masses and frequencies, respectively.

3.3 Results

The hoop consists of $N = 256$ masses, which is a size consistent with systems used elsewhere [98]. Time is expressed as the dimensionless quantity $\omega_o t/2\pi$ which is equivalent to the number of harmonic cycles, and the modal energy is scaled to $E(\omega_o, t = 0)$. Error bars are used to represent the standard error (SE) [92], which is the population standard deviation divided by the square root of the number of systems in the ensemble.

3.3.1 Clean Systems

As a point of reference, it is useful to study the behavior of the systems in the absence of impurities. This way, the role of anharmonicity, frequency, and am-

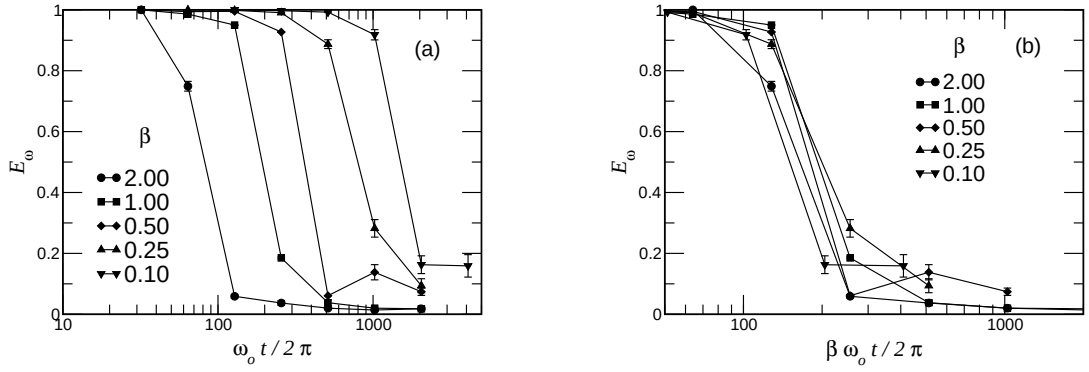

Figure 3.1: Energy in the initial mode E_ω as a function of the number of natural cycles $\omega/2\pi$: (a) raw data for different valus of the anharmonic parameter β; (b) scaled time using the anharmonic parameter β.

plitude can be assessed in the absence of disorder. (Randomness was introduced by adding very small perturbations to the initial displacements.)

The effect of anharmonicity β on the rate that energy leaves the initial mode is summarized in Fig. 3.1. The time required for the energy to leave the initial mode increases with decreasing β, as one would expect [101]. Figure 3.1(b) shows the same data, but with time scaled by the anharmonicity β. For these systems, the time required for the energy in the initial mode to decay from its original value is inversely proportional to β.

A similar experiment was performed with frequency ω as the independent parameter. The frequency varied by changing the number of cycles N_{cyc} within the hoop: $\lambda = 256/N_{cyc}$. The results are shown in Fig. 3.2 for three different values of ω. Figure 3.2(b) shows that the time required for energy to decay away from the initial mode increases as ω^{-3}, as would be expected for a quartic nonlinear term [101].

The last experiment varied the amplitude of the initial condition. The results

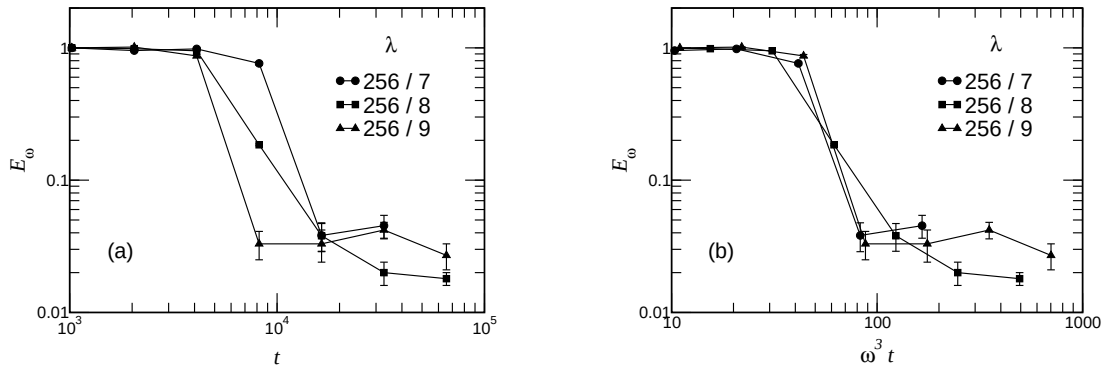

Figure 3.2: Energy in the initial mode E_ω as a function of time t: (a) raw data for different wavelengths; (b) scaled time using the natural period ω.

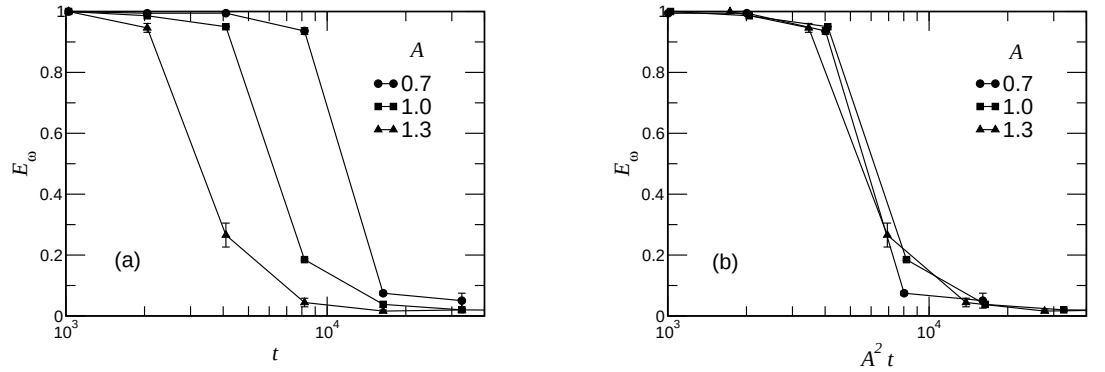

Figure 3.3: Energy in the initial mode E_ω as a function of time t: (a) raw data for different amplitudes; (b) scaled time using the initial amplitude A.

are shown in Fig. 3.3 for three values of amplitude A. As expected, the rate of energy decay decreases with decreasing amplitude because the fraction of anharmonic energy is proportional to the amplitude. Figure 3.3(b) shows that rate of energy decay is proportional to A^2.

3.3.2 Disordered Systems

The disordered systems investigated contained impurity masses $m_I > m_\circ$. Comparisons of the effects upon modal decay as a function of either impurity mass m_I or number of impurities N_I are shown in Figs. 3.4 (a) and (b); the pure nonlinear system is denoted by open circles. As expected, the addition of impurities increases the initial rate at which the harmonic mode ω_o decays. However, for all the combinations of impurity mass and concentration shown, the long time decay is *slower* than for the system without impurities. Further, increases in impurity mass and impurity concentration retard the long time decay.

The long time behavior of the systems containing heavy impurities can be explained by the nonergodic behavior within the system. Systems containing impurities undergo an Anderson transition. The resulting excited modes are localized, concentrating energy near the impurities. Since the impurities are heavier than $m_\circ$ for a given amount of energy, their oscillation amplitudes are smaller, resulting in a smaller nonlinear contribution to the energy at the impurity. This would retard the rate of mode transitions in nonlinear disordered systems.

As a demonstration of the localization of energy at the impurities, the mass energy E_i is calculated at each impurity. The average energy at an impurity $\langle E_i \rangle_I$ is compared to the average energy at all the masses $\langle E_i \rangle_N$. The ratio $\alpha = \langle E_i \rangle_I / \langle E_i \rangle_N$, which is interpreted as a measure of the extent to which ergodicity

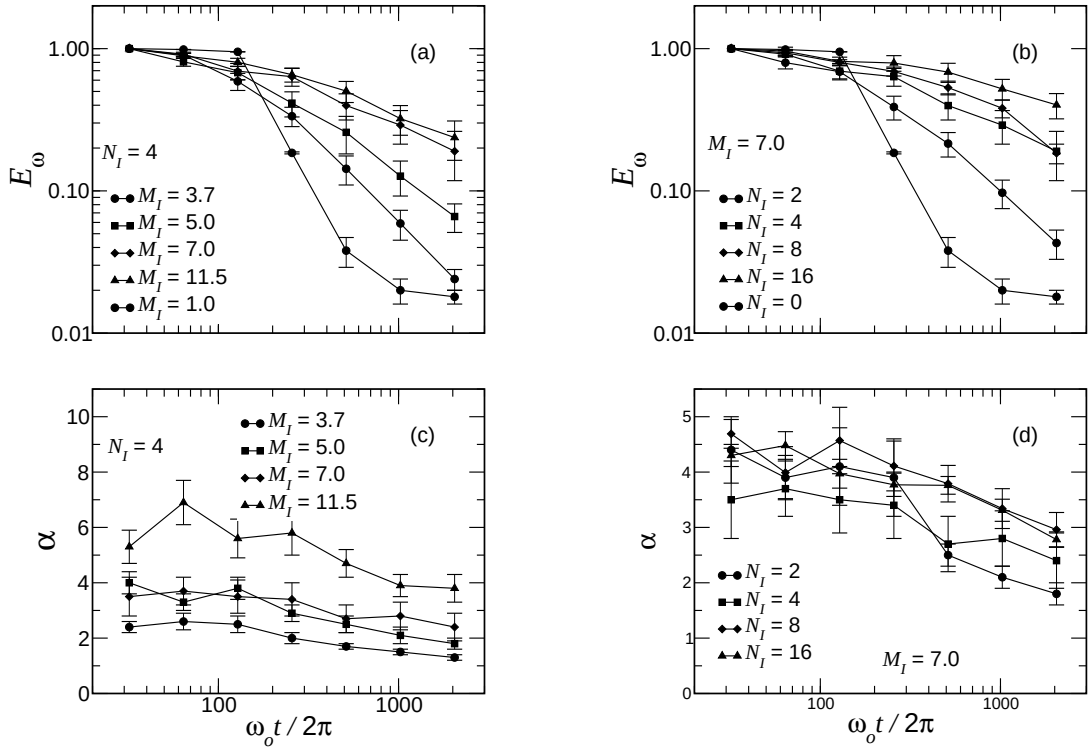

Figure 3.4: Effect of impurity mass M_I and number of impurities N_I on the mode energy E_ω and relative energy α at an impurity. In (a) and (c) the number of impurities N_I is 4. In (b) and (d) the impurity mass M_I is 7. The open circles are for the nonlinear system without impurities. Error bars represent the estimated standard deviation of the mean.

has been achieved, is shown in Figs. 3.4(c) and (d). A value of $\alpha \neq 1$ indicates that energy is distributed uniformly among all the masses.

Figures 3.4(c) and (d) show that the relative energy at an impurity increases with increasing impurity mass, and is somewhat insensitive to changes in the impurity concentration, respectively. Therefore, the total energy located at impurities is proportional to the mass and the number of impurities. This explains why the modal decay rate decreases as either the impurity mass or the impurity

concentration increases.

Based upon the arguments given above, impurities with masses that are lighter than $m_\circ$ should have a different effect upon mode decay. Since the impurities are lighter, the localized energy will create large oscillations, which should enhance nonlinear interactions and, hence, enhance the rate of mode decay. The results of that experiment for impurity mass $M_I = 0.1$ are shown in Fig. 3.5. For low

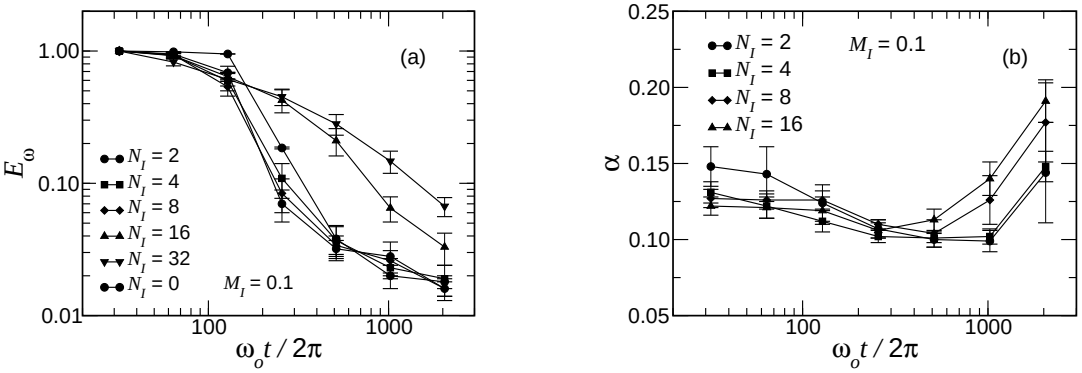

Figure 3.5: Mode decay in systems have impurity mass $M_I = 0.1$: (a) modal energy E_ω and (b) relative energy at the impurities α.

concentrations, the mode decay shown in Fig. 3.5(a) is faster than for the pure system, as expected. However, at sufficiently high concentration, the mode decays slower than the pure system when the average spacing between impurities is one half the initial wavelength. The change in behavior occurs when the impurity concentration $c = N_I/256$ satisfies $c\lambda > 1$.

The relative energy α located at a light impurity shown in Fig. 3.5(b) is less than unity. The light impurities expel energy due to the large oscillation amplitudes, hastening mode decay. Interestingly, although the mode decay rate at the higher impurity concentrations is slower, these high concentration systems have $\alpha \to 1$ faster than that for the lower impurity concentration.

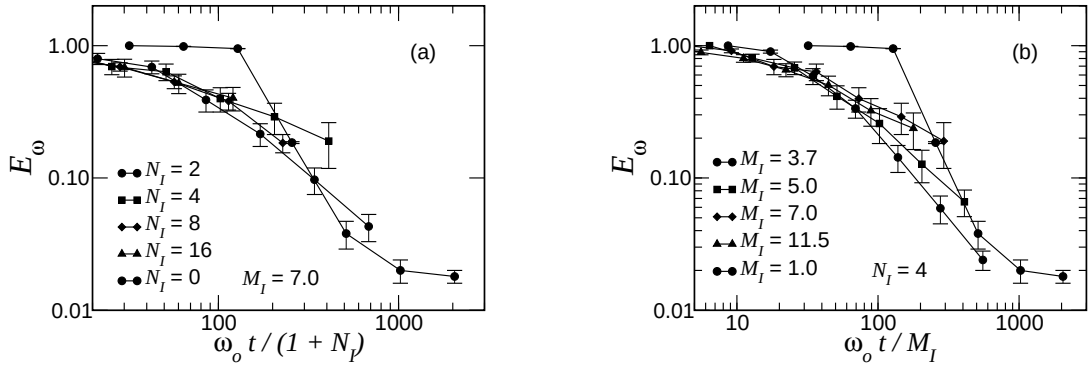

Figure 3.6: The modal energy E_ω as a function of time scaled by (a) the number of impurities N_I, and (b) the impurity mass M_I.

Scaling relations for the number of impurities N_I and the impurity mass M_I can be estimated from combining much of the data already presented. The results are shown in Fig. 3.6. By scaling the time by $(1 + N_I)^{-1}$ and M_I^{-1}, the data appear to lie upon one another. This inverse proportionality is consistent with the concept that the quantity of energy localized at impurities is proportional to both the impurity mass and the number of impurities.

3.4 Conclusion

For the simulation times studied here, the long time mode decay in disordered nonlinear systems seems to be controlled by disorder and Anderson localization effects. For either heavy or light impurities, the energy becomes localized and the assumption of ergodic behavior is not valid. Further, the response of the system depends upon whether the impurities are heavier or lighter than the pure system. Impurities consume energy and heavier impurities, because of the smaller oscillation amplitudes, release their energy through nonlinear interactions very

slowly, thereby retarding mode decay. Lighter impurities appear to expel energy through large oscillation amplitudes, hastening nonlinear interactions and mode decay at low concentrations, but behave in a manner similar to heavy impurities at high concentrations. At impurity concentration c such that $c\lambda > 1$, the lighter impurities delay mode decay, possibly due to some cooperative effect among the impurities.

Chapter 4

Energy Transport

Having established the effects of impurities on both harmonic (Chapter 2) and anharmonic (Chapter 3) chains, one is now able to address energy transport in disordered nonlinear chains. An initial condition is chosen to reduce computational effort, and energy transport is characterized by the second moment of the site energy.

Dissipation from harmonic energy eigenstates is used to characterize energy transport in binary isotopically disordered (BID) Fermi-Pasta-Ulam (FPU-β) chains. Using a continuum analog for the corresponding harmonic portion of the Hamiltonian, the time-independent wave amplitude is calculated for a plane wave that is incident upon the disorder, and the solution is mapped onto the discrete chain. Due to Anderson localization, energy is initially localized near the incident end of the chain, and in the absence of anharmonicity the wave amplitude is stationary in time. For sufficient anharmonicity, however, mode transitions lead to dissipation. Energy transport along the chain is quantified using both the second moment of the site energy and the number of masses contributing to transport, which was estimated from the localization parameter. Over the time scales studied, the second moment increased linearly in time, yielding an effective

diffusive transport coefficient. At low and intermediate impurity concentrations, the transport coefficient can be characterized by a competition between impurity scattering and diffusion over a distance equal to the localization length. At the highest concentrations, there is significant mode transition suppression in BID systems, and the transport coefficient becomes proportional to initial localization length. This result suggests that vibrational energy transfers in strongly localized modes retain the spatial extent of the interacting modes.

4.1 Introduction

Nonlinear binary disordered chains are useful systems for studying the essential characteristics of energy dissipation and transport in materials. Although binary disorder is an idealized model, it has practical application to a number of fields: isotopic disorder effects line width broadening in spectroscopy; [102–104] the glass transition has been considered in terms of binary changes in elasticity parameters;[75] and isolated mechanical defects can lead to a variety of nonlinear effects [105, 106].

An interesting behavior of binary isotopic disorder (BID) occurs in discrete lattices, where the system undergoes a pure-disordered-pure transition as the impurity concentration varies from zero to one. For harmonic one-dimensional chains, finite disorder destroys spatial invariance and gives rise to Anderson [5] localization, characterized by spatially localized eigenstates. Given a discrete system in a localized energy eigenstate, the addition of anharmonicity will lead to interactions that create new modes that can propagate through the system. These propagating modes either will become localized or will undergo further mode transitions.

We are interested in the rate of energy dissipation from localized disturbances along a discrete chain. Previous studies have used either a singular (one or very few elements) pulse or a Gaussian envelope for the initial displacement [66, 73, 74, 76, 77]. Because neither is an eigenstate of the system, both will begin to propagate ballistically and will exhibit some measure of dissipation in both anharmonic and harmonic systems. In time, scattering and localization slow the rates of propagation and dispersion.

To eliminate the initial ballistic motion, a system starting from an energy eigenstate of the corresponding harmonic chain would remain localized until mode transitions occurred. The initial condition can be calculated for a system in which the middle section contains disorder and there are 'pure' sections at both ends. Given the location of each impurity in the disordered section of the chain, a solution could be found for the continuum analog, with the boundary condition of an incident plane wave with frequency ω; there is a reflective wave and a transmitted transmitted wave. Because the continuum calculation is performed for the harmonic system, the solution is separable into spatial and temporal components. The time dependence is sinusoidal, and the entire system has a constant temporal phase. The continuum solution for the wave amplitude everywhere is mapped onto the discrete chain, and becomes the initial displacement for the study of energy transport.

The advantage of this approach is that in the absence of anharmonicity the wave amplitude is stationary. For the harmonic chain, the wave remains localized indefinitely, and there is no energy transport. The addition of anharmonicity will give rise to mode transitions that will de-localize the wave and lead to energy transport through the chain. Instead of having a ballistic-diffusive transition,

this initial condition leads to a localized-diffusive transition. This is important for reducing the integration times required to distinguish between localization and mode transition behavior.

There is reason to believe that nonlinear disordered systems will behave diffusively. A recent study of a disordered FPU-β chain observed a constant thermal conductivity for both large L and low temperature [71]. This is consistent with the assertion that Fourier's law is satisfied when there are phonon-lattice interactions in addition to the phonon-phonon interactions [72].

To study this energy transport, the following numerical experiment will use the binary disordered Fermi-Pasta-Ulam [35] chain with quartic spring potentials (FPU-β). Starting from the initial energy eigenstate, numerical integration will be used to calculate the spatial distribution of energy as a function of time. Based on a local concept of thermal transport [75], an effective transport coefficient will be sought [107] from the second moment of the site energy, and the method is compared to the Helfand [83] moments for thermal conductivity. The second moment will exhibit diffusive behavior, a fact that will be corroborated qualitatively from the number of masses over which energy is distributed, which is estimated from the localization parameter [52, 108].

The effective transport coefficient will be studied as a function of impurity concentration. The mode transfer behavior will change as the concentration varies from dilute (a wavelength far smaller than the mean free path) to very dense (a wavelength spanning many impurities). Energy transfer in dilute systems will be characterized by impurity scattering. As the impurity concentration increases, transport dominated by interacting localized modes [109, 110] will become apparent. For the most concentrated systems, energy transfer will occur among

strongly localized modes. As a result, the spatial extent of these interacting modes will persist and the original localization length will remain the dominant length scale over which transport occurs.

4.2 Numerical Experiment

4.2.1 FPU-β Chain

The FPU-β chain is composed of masses interacting with nearest neighbors through springs. The Hamiltonian H of a chain having N masses is a function of the mass momenta p_i and the mass displacements u_i about their equilibrium position:

$$H = \sum_{i}^{N} \frac{p_i^2}{2\,m_i} + \frac{K}{2}(u_i - u_{i-1})^2 + \frac{\beta}{4}(u_i - u_{i-1})^4 \tag{4.1}$$

The harmonic spring force coefficient K is set equal to one, and in the absence of impurities, each mass has the same value $m_\circ$=1. The site energy e_i is the sum of the kinetic energy plus one-half of the neighboring spring potential energies.

Whenever possible, the results are expressed in dimensionless units through the use of appropriate scaling factors. Time is scaled by the natural frequency ω_o of a single harmonic oscillator:

$$\omega_o = \left(\frac{K}{m_\circ}\right)^{1/2} \tag{4.2}$$

Lengths are scaled by the equilibrium mass separation distance a, which is set equal to one for this experiment.

The time-dependent behavior was determined by numerical integration using the sixth-order Yoshida [40] symplectic integration algorithm. Specifically, best results were obtained from the "Solution A" coefficients (see Table 1 in Ref. [40]).

For the systems studied here, the time step Δt was approximately 1/200 the period of the initial mode. This time step was consistent with that used elsewhere [56, 73], was chosen as a compromise between speed and accuracy, and the results were insensitive to two-fold changes in Δt. Using this time step, the energy fluctuations were always less than 0.2 % (See Appendix F).

4.2.2 Semi-Infinite Approximation

For these systems, the localization length of the very low frequency waves will be longer than the system length. As a result, these waves will propagate down the chain and reach the far end. If the wave is reflected, it could affect the accuracy of the transport calculation. To mitigate this effect, 10 % of the masses at the far end were given a viscous force F_{vis}:

$$F_{vis} = -\eta \, \dot{u} \tag{4.3}$$

This approach has been used elsewhere to achieve a similar effect [46]. For these calculations, a viscosity η of 0.2 was sufficient to eliminate the effects of reflection.

The viscous damping, combined with the accurate time integration, simplified the task of identifying finite size effects. As the system length decreased and the localization length increased, the likelihood of a considerable amount of energy reaching the far end of the system increased. Fortunately, this occurrence was easily identified by changes in the system total energy.

4.2.3 Initial Displacement

The initial condition was a stationary state exhibiting Anderson localization for the harmonic component of the Hamiltonian. This initial condition was chosen

so that for β=0 there is no net energy transport, and these systems could be used as a test to confirm the accuracy of the model and the numerical integration.

The continuum Kronig-Penney liquid model [24, 47] is used to estimate the initial displacement. For the harmonic FPU chain, the analogous continuum system is an elastic medium having mass density $\mu = m_\circ/a$ and Youngs modulus $Y = Ka$. Between the impurities, a longitudinal displacement wave $\psi(x,t|\omega)$ with frequency ω will propagate with phase velocity $v_p = \sqrt{Y/\mu}$. A harmonic oscillator impurity, approximated by a point defect, located at x' will give rise to a reactive force that is proportional to the impurity impedance $Z(\omega)$ [43]:

$$\left[\mu\frac{\partial^2}{\partial t^2} - Y\frac{\partial^2}{\partial x^2} = -Z(\omega)\,\delta(x-x')\frac{\partial}{\partial t}\right]\,\psi(x,t|\omega) \tag{4.4}$$

For a harmonic system, one can assume a sinusoidal solution with frequency ω ($\psi = \phi(x|\omega)\,\mathrm{e}^{-\mathrm{i}\omega t}$):

$$\left[\frac{\partial^2}{\partial x^2} + \zeta^2 = \frac{-\mathrm{i}\omega}{Y}\,Z(\omega)\,\delta(x-x')\right]\phi(x|\omega) \tag{4.5}$$

where $\zeta = \omega/v_p$.

Equation (4.5) is solved for a system having impurities at integer locations with probability c. The boundary conditions are a unit amplitude incident wave and a reflected wave at the incident end and only a transmitted wave at the opposite end. The initial displacement for the FPU system is taken from the real component of the solution $\phi(x|\omega)$. Additional discussion of the initial condition calculation is given in Appendix E.

4.2.4 Impurity Cross Section

To put some of the results in a familiar context, it will be useful to characterize an impurity by its cross section to the original wave. The cross section σ of an

individual impurity can be expressed as a function of the impurity impedance Z: [43]

$$\sigma = \frac{|Z(\omega)|^2}{|Z(\omega)|^2 + 4Km_\circ} \tag{4.6}$$

Here, the isotopic impurities consist of a constant mass m_+ added to the existing mass $m_\circ$; m_+ may be either positive or negative and the impurity mass m_I is $(m_\circ + m_+)$. It has been determined that for a discrete system, the impedance Z of a mass impurity in a continuum system [43] must be modified by c_s, which is the ratio of the group velocity ($v_g = \partial\omega/\partial k$) to the phase velocity v_p [111]:

$$Z(\omega) = -\mathrm{i}\omega m_+/c_s \tag{4.7}$$

For the discrete chain, $c_s = \cos(ka/2)$, where k is the wavenumber $(2\pi/\lambda)$ and λ is the displacement wavelength.

4.2.5 Continuum-Discrete Mapping

The boundary condition for the chain is zero displacement at each end. Because the continuum solution $\phi(x = 0, L|\omega)$ will almost certainty not equal zero at $x = 0, L$, a method is needed for adjusting the continuum solution to accommodate the constraints of zero displacement at both ends. The continuum solution is first mapped to the discrete chain with no modification, and then, starting at one end and moving along the chain, the end is relocated to the mass having the smallest oscillation amplitude, and its displacement is fixed at zero. The process is repeated at the opposite end of the chain.

To facilitate this task, a suitable initial displacement wavelength λ is needed to ensure that some mass has an equilibrium displacement acceptably close to zero. If the displacement wavelength is an integer multiple of the equilibrium mass

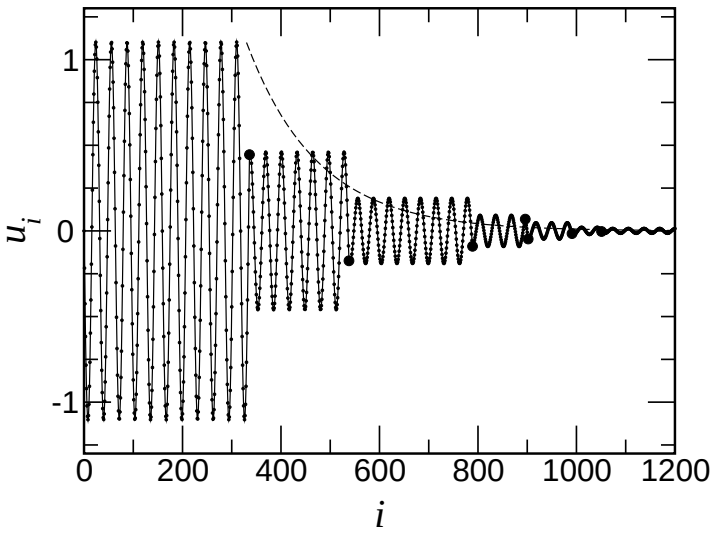

Figure 4.1: Initial displacements u_i for a particular system having wavelength 31.8, impurity concentration 0.01, and impurity scattering cross section 0.5. Mass displacement are denoted by small circles and the impurity locations are denoted by large circles. The first impurity is located at $i = x_o$, and the dashed line is proportional to $\mathrm{e}^{-(i-x_o)/\xi}$.

displacement a, the oscillation amplitude of masses repeats with each successive wavelength, until the next impurity changes the phase.

For this experiment, a nominal displacement (equal to an integer multiple of the unit spacing) was chosen first. The working wavelength is the nominal wavelength minus 0.2 unit spacings. With this wavelength, the displacement amplitudes repeat every 5 wavelengths, with 9 nodal points occurring at different fractions of the spacing a. Probabilistically, it is more likely to find a minimum mass oscillation amplitude that is nearly an order of magnitude smaller than that for an integer wavelength.

An example input displacement is shown in Fig. 4.1 for a system with length

10 000, displacement wavelength 31.8, impurity cross section 0.5, and impurity concentration 0.01. The small dots in the figure represent the initial displacement of the masses. The larger filled circles denote the location and displacement of the impurities. The effect of the impurities is to change both the displacement amplitude and the phase. Also shown in the figure is a dashed line that is proportional to $e^{-(i-x_o)/\xi}$, where x_o is the location of the first impurity, and ξ is the localization length (to be discussed subsequently). Although this particular initial condition would suggest that displacement amplitudes decrease monotonically, that is not always the case.

4.2.6 Dense Systems

For BID systems, the localization length is not a monotonic function of impurity concentration. Rather, the localization length has a minimum with respect to impurity concentration; at higher concentrations, the system returns to a "pure" system. The localization length ξ of BID systems at dilute impurity concentrations, such that $c\lambda \ll 1$, can be calculated from the resistivity scaling law [22]:

$$\xi_{c\to 0}^{-1} = c \ln(1+\rho) \tag{4.8}$$

The single impurity resistivity ρ is related to the single impurity cross section σ:[21]

$$\rho = \frac{\sigma}{1-\sigma} \tag{4.9}$$

As the impurity concentration increases beyond a value of $1/2$, the system approaches a homogeneous system. In the limit $c \to 1$, the system is again ordered, and the localization length diverges:

$$\xi_{c\to 1}^{-1} = (1-c)\ln(1+\rho') \tag{4.10}$$

The quantity ρ' characterizes a system having an equilibrium mass $(m_\circ + m_+)$, an impurity mass $m_\circ$, and oscillations at the same frequency ω: [111]

$$k' = \frac{2}{a}\,\mathrm{Sin}^{-1}\left[\frac{\omega}{2}\sqrt{\frac{m_\circ + m_+}{K}}\right] \tag{4.11a}$$

$$c'_s = \cos\left(k'a/2\right) \tag{4.11b}$$

$$\rho' = \frac{(-m_+\omega/c'_s)^2}{4K(m_\circ + m_+)} \tag{4.11c}$$

Because the localization length of a system is analogous to its conductivity, and the systems described by $\xi_{c\to 0}$ and $\xi_{c\to 1}$ occur independently and in parallel, the localization length over all values of impurity concentration can, by analogy to electrical conductors, be approximated by a sum of the two:[111]

$$\xi = \xi_{c\to 0} + \xi_{c\to 1} \tag{4.12}$$

When the concentration of the impurities increases to $c\lambda > 1$, the energy eigenstate becomes more complicated than the dilute impurity example shown in Fig. 4.1. Example initial conditions for the highest impurity concentration considered in this experiment ($c = 0.5$) are shown in Fig. 4.2 for three scattering cross sections. At these high concentrations, although the frequency remains constant everywhere, the wave structure in the disordered region is considerably more complex than that shown in Fig. 4.1 for a dilute system.

4.2.7 Parameter Space

For the nonlinear systems considered, the incident wave has wavelength λ =31.8, and the anharmonicity parameter β =1. For all the systems from which energy transport is measured, the added mass m_+ will have one of three values: 6.605, 10.089, and 15.412. With respect to a $\lambda = 31.8$ displacement in a harmonic

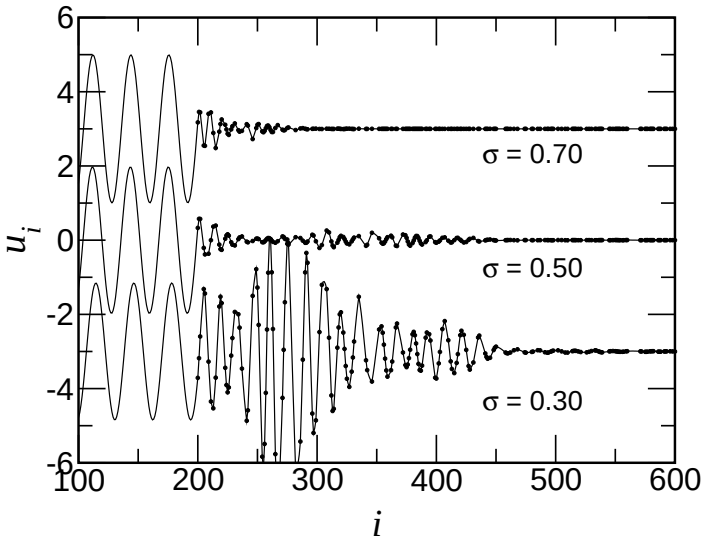

Figure 4.2: Initial displacements u_i for a particular system having wavelength 31.8, impurity concentration 0.50, and all three impurity scattering cross sections. Mass displacement are denoted by line, and the impurity locations are denoted by circles. The systems were shifted horizontally so that the first impurity is located at i =200.

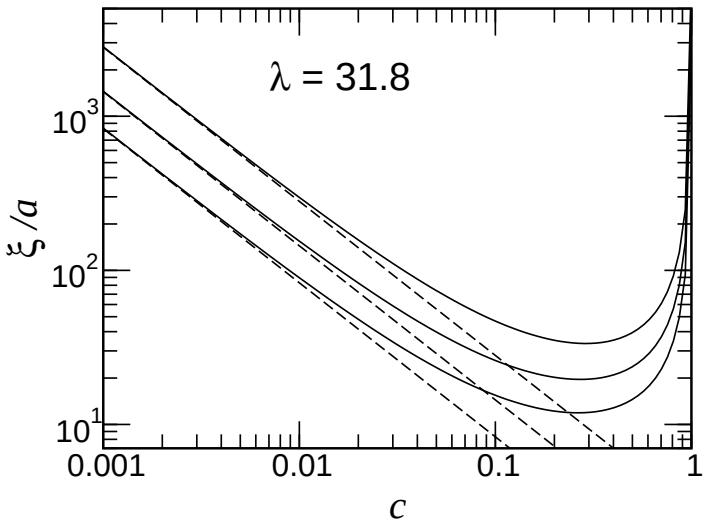

Figure 4.3: Localization length ξ as a function of impurity concentration c for systems having displacement wavelength $\lambda = 31.8$. The three solid curves, from upper to lower, are for $\sigma = 0.30$, 0.50, and 0.70, and were calculated from Eq. (4.12). The dashed lines are the dilute limit localization length $\xi_{c\to 0}$.

system, these impurity masses have scattering cross sections 0.30, 0.50, and 0.70, respectively.

The primary experimental parameter was impurity concentration c. The impurity concentration lower limit was constrained by computing resources. A previous study of these systems revealed that approximately 32 impurities and a system length $L/\xi > 10$ are required in a chain to ensure reliable ensemble statistics [111]. The upper concentration limit was 0.5. Above this concentration, the behavior is analogous to a study of the pure system having mass m_I and impurity mass $m_\circ$.

The initial displacement is a localized mode with localization length ξ. To better understand the length scale over which the energy is initially distributed, the aforementioned impurity masses are used to calculate the localization length, using Eq. (4.12), for a wave having displacement 31.8, and the results are shown in Fig. 4.3. The dilute limit result $\xi_{c\to 0}$ is shown as a dashed line, and begins to depart from ξ at concentrations for which $c\lambda \approx 1$.

Figure 4.3 also reveals the utility of choosing a nominal displacement wavelength $\lambda = 32$. For $c\lambda > 1$, the addition of impurities has a nonlinear effect on localization length. Naturally, one would like to see whether this nonlinear behavior has any effect on energy transport. For shorter displacement wavelengths, the deviation between ξ and $\xi_{c\to 0}$ would not occur until proportionately higher impurity concentrations. Alternatively, using a longer wavelength would reduce the rate of mode transitions considerably, requiring excessively long computational times.

4.3 Thermal Conduction

There are a number of formal methods for calculating thermal conductivity. Thermostats at the boundaries can generate a steady-state flux from which the thermal conductivity is calculated using Fourier's law [69]. The Green-Kubo method [84] is based on time integrals of thermal fluxes for a system in thermal equilibrium. The Evans NEMD thermal conductivity algorithm [84, 87] applies a heat field and calculates an averaged heat flux. The Helfand [83] moments of the excess energy fluctuations are calculated for systems in thermal equilibrium. In each case, the system is either at steady-state or in thermal equilibrium, which does not apply here.

For zero temperature systems, the propagation rate and the second moment of the site energies have been used to characterize pulse dissipation in zero temperature systems [66, 73, 74, 76, 77]. These approaches are reminiscent of the method of Helfand moments [83], so a brief summary of Helfand moments is warranted.

The Helfand moment for thermal conductivity is applied to a system in thermal equilibrium with a temperature reservoir. By application of the Onsager regression hypothesis [78, 79], the transport coefficient related to dissipation of fluctuations are the same as the non-equilibrium transport coefficient. For a system in thermal equilibrium, there is a time-dependent site energy e_i that differs from the ensemble averaged value $\langle e_i \rangle$. The energy fluctuation $\widetilde{E}$ is the difference between the two:

$$\widetilde{E} = e_i - \langle e_i \rangle \tag{4.13}$$

For a system having an initial fluctuation over sites x_{j0}, the thermal conductivity

κ can be estimated from a double sum over particle positions [83]:

$$H^p = \left\langle \sum_{i,j} (x_i - x_{j0})^2 \, \widetilde{E}_i(x,t) \, \widetilde{E}_j(x,0) \right\rangle \sim 2\kappa t \tag{4.14}$$

Replacing conservation of momentum with conservation of energy yields an equivalent alternative expression: [83]

$$H^e = \left\langle \left[\sum_i (x_i \widetilde{E}_i - x_{i0} \widetilde{E}_{i0}) \right]^2 \right\rangle \sim 2\kappa t \tag{4.15}$$

Equations (4.14) and (4.15) are the Helfand moments for calculating the thermal conductivity of a bath of particles.

There are a number of differences between fluctuations in a bath of particles and energy propagation along a discrete chain. Equations (4.14) and (4.15) characterize a bath of freely moving particles. By contrast, in the FPU chain energy moves, but the masses are, more or less, stationary. This is not entirely problematic, however, because one can still evaluate the energy that is at x_i, and the problem can be changed to one in which the energy is evaluated at specific points. In this way, the role of energy is analogous to concentration in the evaluation of self-diffusion.

Another important distinction is that Eqs. (4.14) and (4.15) are functions of the energy fluctuations in an equilibrated system at temperature T. By contrast, a pulse moving through an FPU chain is a system that is not in equilibrium, and the portion of the chain farthest from the initial disturbance is initially at zero temperature. In principle, after very long times, the chain would eventually reach equilibrium, with the energy distributed over all the masses. Because the conceptual problem of interest is a semi-infinite chain, the equilibrium energy $\langle e_i \rangle$ would approach zero. Under the assumption $\langle e_i \rangle = 0$, the fluctuation energy

$\widetilde{E}$ of the bath problem becomes the site energy e_i of the non-equilibrium chain problem.

By analogy to Eqs. (4.14) and (4.15), the energy transport in the FPU-β chain will be characterized by the second moment of the energy. Assuming that the initial pulse occupies a small portion of the entire system, a useful measure is the second moment M about zero:

$$M = \frac{\sum_i r_i^2 e_i}{\sum e_i} \sim 2Gt \tag{4.16}$$

The position $r_i = ia$ is the equilibrium location of the i-th mass. The quantity G is an effective transport coefficient that is neither self-diffusion nor thermal conductivity. To eliminate the effects of fluctuations, the initial value is subtracted from the subsequent values. In addition, the equation is generalized to allow for arbitrary powers of e_i:

$$M_n(t) = \left\langle \frac{\sum_i r_i^2 e_i^n}{\sum e_i^n} - M_n(0) \right\rangle \sim 2G_n t^{\delta_n} \tag{4.17}$$

These definitions are similar to those used by Fröhlich et al.,[112] and are consistent with the local concept of thermal transport of Wagner et al.[75]

A comparison among M_1, M_2, H^p, and H^e is made from the early response of a system of length 8000 that is initially in a localized mode. The wavelength is 31.8, the impurity mass is 11.089, the impurity concentration is 0.010, and $\beta = 1$. The displacement u along the system is shown in Fig. 4.4 at time intervals of $\omega_o \Delta t = 2000$. (The curves are offset vertically from one another, by a distance a, for comparison purposes.) The data in the figure show that long wavelength displacements move virtually ballistically along the chain (parallel to dashed arrow) while the higher frequency displacements propagate a considerably shorter distance over the same time interval.

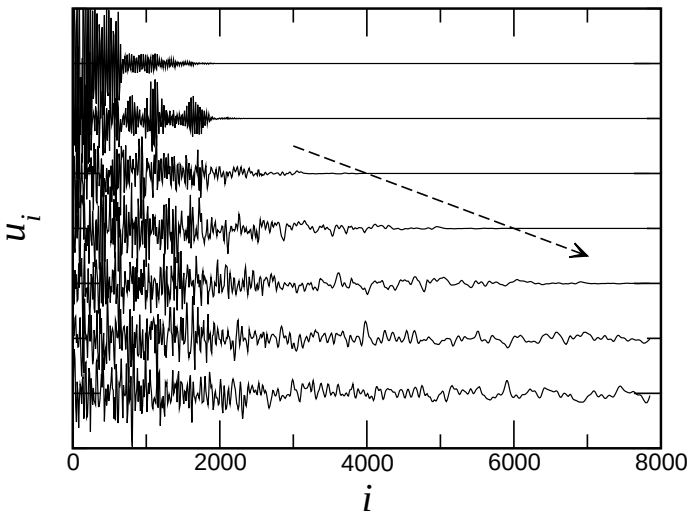

Figure 4.4: Wave displacement u_i along a chain at various times. Chain length is 8000, added mass m_+ is 10.089, and impurity concentration is 0.010. Each curve represents a time difference of 2000, and is offset by a value of one for demonstration purposes. Dashed arrow denotes ballistic propagation.

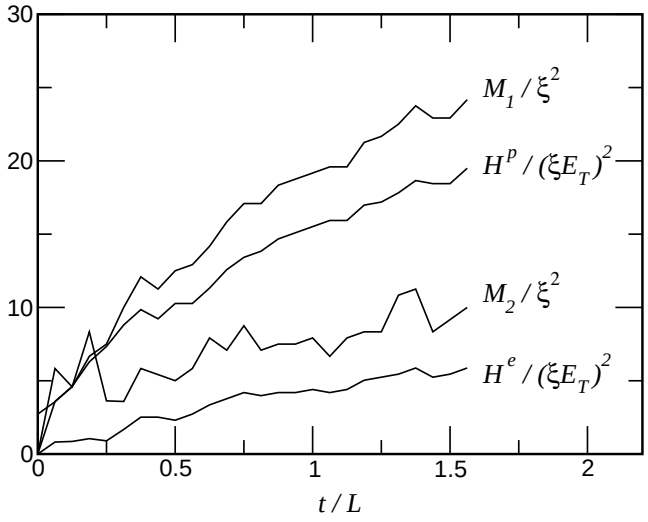

Figure 4.5: Moments M_1, M_2, H^p, H^e as a function of time for the system shown in Fig. 4.4. Quantities are normalized, using localization length ξ and total energy E, to make the values dimensionless.

At regular time intervals, M_1 and M_2 are calculated, along with H^p and H^e (assuming that $\widetilde{E} = E_i$ and $\langle e_i \rangle = 0$). The results of the calculations are shown in Fig. 4.5. All values are normalized by the initial localization length ($\xi \approx 155$). H^p and H^e are also normalized by the total energy E to be on the same scale as M_1 and M_2. The two pairs of equations, (M_1, H^p) and (M_2, H^e), generally agree with one another, but M_1 and M_2 are greater in value than the corresponding H^p and H^e. At the shortest times, M_1 and H^p give the nearly the same value.

H^p and H^e are equivalent descriptions of thermal conductivity. Therefore, the difference between H^p and H^e for the case of an initially localized pulse demonstrates that thermal conductivity for these systems is not well-defined. As a result, the second moments M_n characterize some effective, yet undefined, transport coefficient.

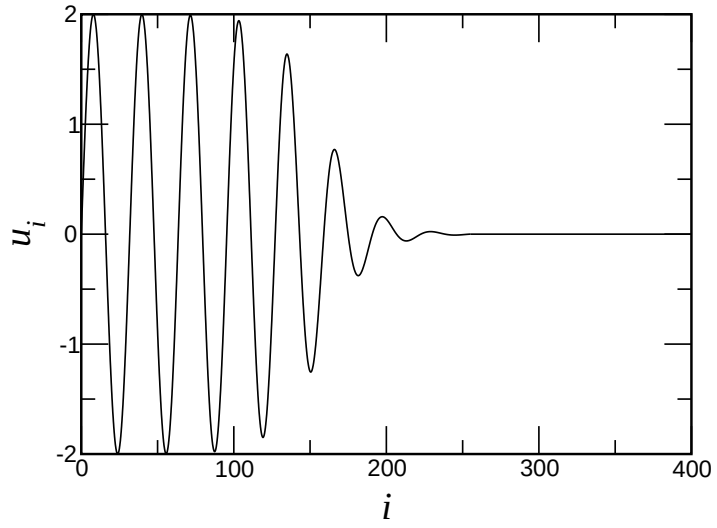

Figure 4.6: Displacement u_i for sinusoidal initial condition with $\lambda = 31.8$.

These curves are also instructive in pointing out the distinction between pulse propagation and energy propagation. From Fig. 4.4 it is clear that low frequency waves propagate ballistically through these systems, starting from near $t = 0$. By contrast, Fig. 4.5 shows no ballistic behavior, suggesting that the vast majority of the energy is in the higher frequency modes located within the initially localized region. Moreover, the moments shown in Fig. 4.5 all continue to increase after there has been sufficient time for the low frequency ballistic modes to reach the far end.

4.4 Alternate Initial Condition

As an alternative, this experiment could have been performed using either an instantaneous impulse or a short sinusoidal pulse like that shown in Fig. 4.6. Both of these initial conditions, however, have drawbacks. Impulses will impart

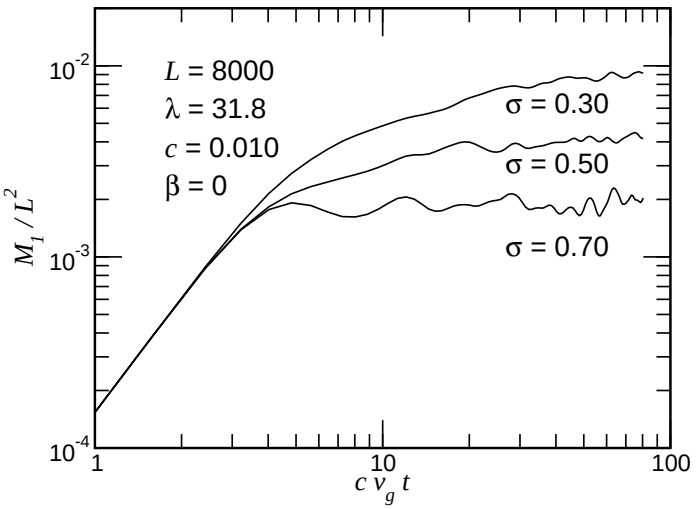

Figure 4.7: Moment M_1 as a function of time t for systems with anharmonic parameter $\beta = 0$ and impurity concentration $c = 0.010$ for systems having length $L = 8000$. The initial condition is that shown in Fig. 4.6.

relatively little energy to the system unless the impulse is large. The sinusoidal wave, not being localized by the impurities, will immediately begin propagating ballistically along the chain. If the chain had only harmonic interactions, the wave would eventually become localized. In a nonlinear chain, there would be immediate competition between localization and anharmonic effects that would lead to mode transitions.

The time required for the sinusoidal pulse to become localized in a harmonic chain is shown in Fig. 4.7 for the $\lambda = 31.8$ pulse shown in Fig. 4.6. The pulse is located at one end of the system, the envelope is the hyperbolic tangent function, and the initial velocity is zero. The harmonic chains have mass impurities located at a site with probability c. The three aforementioned values for m_I are used, corresponding to $\sigma = 0.30$, 0.50, and 0.70. The data in Fig. 4.7 suggest that

between 10 and 100 impurities, depending on the impurity cross section, must be encountered before the sinusoidal wave becomes localized. The localization length for these three cross sections are 298, 155, and 90, respectively, so the transient period is approximately ten times the localization length. For the lowest impurity concentrations considered in this experiment, this transition length would have created overwhelming demands on computing resources. In effect, a large portion of the calculation would be expended on getting the system to some sort of equilibrium condition.

4.5 Equipartition

The dynamics of both mode transitions and spatial energy equipartition will influence the response of the systems. A previous experiment to study the mode transition rate for similar chains configured as small hoops initially excited in a single wavenumber eigenmode suggested that impurities initially hasten the decay of energy in the excited mode [113]. Over long times, however, the rate diminished because the energy became localized at the impurities. Because the impurities were heavier than the background, the oscillations at the impurities were smaller, reducing the rate of energy loss because of the quadratic dependence of amplitude [101].

The systems studied here, however, have energy initially localized at one end, with the energy already localized at the impurities. Once transitions start to occur, the new modes, which are not localized over the same length scale, will propagate and either spontaneously decay or scatter from impurities.

4.5.1 Localization Parameter

As the mode transitions occur, energy will propagate along the chain, redistributing energy. As the energy becomes more evenly distributed among the masses, the energy becomes less localized. A measure of how uniformly the energy is distributed among N masses is the localization parameter Γ [52, 108]:

$$\Gamma = N \left\langle \frac{\sum^N E_i^2}{\left(\sum^N E_i\right)^2} \right\rangle \tag{4.18}$$

The value of Γ is a minimum for ergodic behavior and increases as the degree of localization increases.

The localization parameter can be used to estimate the number of masses over which energy is distributed. The maximum value of Γ is N, which occurs when all the energy is localized at one mass. At long time, Γ approaches a constant, $\Gamma_\infty = \Gamma(t \to \infty)$, that only depends on the value of β [53]. For the FPU-β system, with $\beta = 1$, the equilibrium value Γ_∞ is approximately 1.8. Thus, Γ_∞/Γ is approximately equal to the fraction of the chain over which energy is distributed.

4.5.2 Participating Modes

Another useful measure of ergodicity is the number of harmonic modes contributing to the energy located at a particular mass. The systems to be studied are initially excited in one mode (in frequency space). The time required for the system to excite the maximum number of modes should correspond to the time required for the system to become ergodic.

The energy E_ω in mode ω is estimated from the harmonic approximation involving the Fourier transformed (FT) displacement $Q_i(\omega)$ and momentum $P_i(\omega)$

of mass m_i:

$$E_{i,\omega} = \frac{1}{2}\left(m_i\omega^2 Q_i^2 + \frac{P_i^2}{m_i}\right) \tag{4.19}$$

The energy is then normalized using the total number of frequency modes N_ω considered in the FT:

$$e_{i,\omega} = E_{i,\omega} / \sum_{\omega}^{N_\omega} E_{i,\omega} \tag{4.20}$$

These normalized energies are a measure of energy entropy S_i at mass m_i [52, 56, 59, 99]:

$$S_i = -\sum_{\omega} e_{i,\omega} \ln(e_{i,\omega}) \tag{4.21}$$

If all the energy is in a single frequency mode, S equals 0. If the energy is distributed evenly among all frequency modes, S equals $\ln N_\omega$.

The equivalent number of modes contributing to the overall entropy if the energy is uniformly distributed among those modes is $\exp(S)$. To make comparisons among results using different values for N_ω, results are expressed as the fraction of possible modes n_ω at mass m_i:

$$n_\omega^{(i)} = \frac{\exp(S_i)}{N_\omega} \tag{4.22}$$

Periodically, $n_\omega^{(i)}$ is calculated at various masses and the reported value, $n_\omega(t)$, is the average of these values.

4.5.3 Hoop Example

The localization parameter Γ and the fraction of participating modes n_ω were developed to study systems in which the energy is initially distributed throughout the entire system. For the systems studied here, the initial energy is intentionally localized at one end of the system. If such a system was divided into two equal halves, the values for Γ and n_ω in one half would be very different from the ones

calculated for the other half of the system. Nonetheless, the parameters do have utility for these systems.

One application is the study of behavior within a short section of chain. If the section of chain is quasi-localized (very few modes are present, oscillating with nearly constant amplitude), mode transitions are the primary mechanism for inducing energy transport. A hoop (periodic boundary conditions), initially excited in one wave number mode, could be used to study the behavior of a similar section within a much longer section that is itself quasi-localized. The time-dependent behavior of the localization parameter Γ and the relative number of participating modes n_ω would characterize energy redistribution, with respect to both space and mode frequency.

A brief numerical calculation of Γ and n_ω is made to study the effect of impurity concentration on mode transitions. The initial condition is a BID hoop having length 636, wavelength 31.8, and $\beta = 1$. This initial condition differs, in an important way, from a localized initial state described in Section 4.2.3. In a disordered system, a single k mode will excite multiple ω modes, accelerating the initial rate of mode transitions. Nevertheless, the results illuminate general behavior for nonlinear BID systems.

The effects of impurity concentration on the spatial distribution of energy and on the mode transition rate are shown in Figs. 4.8 and 4.9. The energy distribution data in Fig. 4.8 shows that the time for energy to become distributed among all the masses is relatively constant in systems for which $c\lambda < 1$. At higher concentrations, the initial rate of energy redistribution is nearly the same as for the dilute systems, but the energy is not distributed among all the masses over the same time scale. This suggests that at concentrations for which $c\lambda > 1$, the

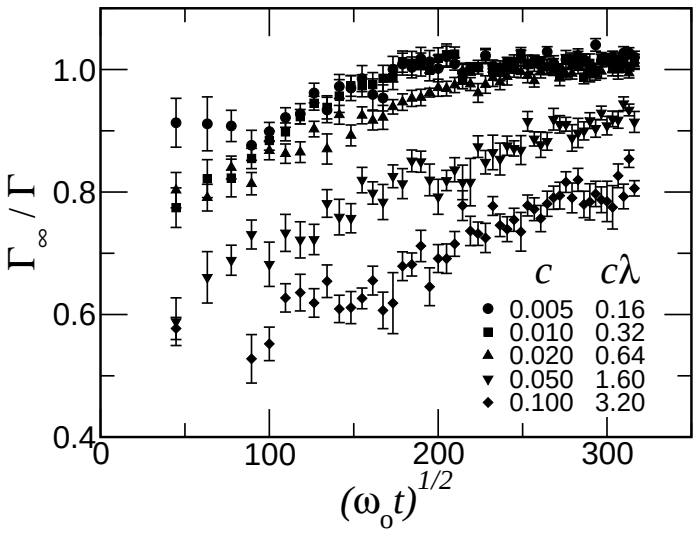

Figure 4.8: Localization parameter Γ as a function of time t for a periodic system with length 636, initial wavelength 31.8, impurity cross section 0.5, and anharmonicity 1.0.

systems behave differently from dilute systems in a fundamental way.

This assessment is consistent with the data for n_ω in Fig. 4.9. The rate that new modes are produced in dilute systems is a constant, until n_ω approaches its asymptotic value. At concentrations for which $c\lambda > 1$, however, the initial rate of mode production does not reach the common initial rate. Furthermore, the asymptotic value for n_ω decreases with increasing impurity concentration. Therefore, concentrated systems produce fewer modes at a slower rate than less concentrated systems.

The decreasing asymptotic value for n_ω with increasing impurity concentration indicates that modes are suppressed significantly in concentrated systems. This is consistent with the effect of impurities on the spectral density D of BID systems. The presence of impurities forces zeroes in $D(\omega)$ [114, 115], thereby

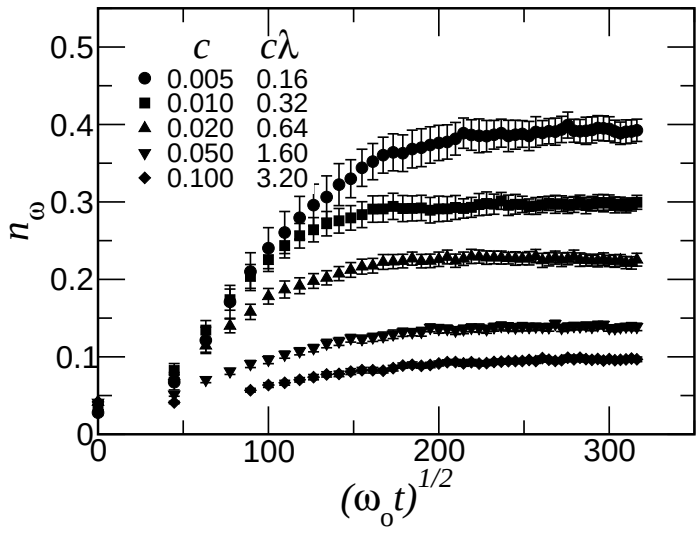

Figure 4.9: Fraction of participating modes n_ω as a function of time t for a periodic system with length 636, initial wavelength 31.8, impurity cross section 0.5, and anharmonicity 1.0.

constraining mode transitions. Moreover, as impurity concentration increases, the spectral density in the interval $[4K/m_I \leq \omega^2 \leq 4K/m_\circ]$ (assuming $m_I > m_\circ$) becomes increasingly suppressed, eventually containing isolated delta functions [48, 116, 117]. If the frequency of the initial displacement is in the interval $[0 \leq \omega^2 \leq 4K/m_I]$, the mode will be in a continuous portion of $D(\omega)$ for all values of impurity concentration. Therefore, at higher impurity concentrations, new modes will be generated more slowly.

Although low frequency modes will be generated, it has already been demonstrated that these modes have no measurable effect on bulk energy transport. Frequencies above $\sqrt{4K/m_I}$ will exist in a portion of the density of states that, with increasing impurity concentration, will inhibit mode transitions. Therefore, in concentrated systems, new modes of any significance will likely have a

frequency in proximity to the initial frequency, particularly for larger values of m_I.

4.6 Results

Some of the results include estimates of uncertainty for quantities calculated from ensemble averages. For a calculation performed on an ensemble of W systems, there is a population standard deviation s and an average value. For this study, the average value is the meaningful quantity that is reported. The uncertainty in the reported mean values is $s/\sqrt{W}$, which estimates the standard deviation of the sample mean, and is referred to as the standard error (SE) of the sample mean [92]. All error bars appearing in figures represent the SE, unless explicitly stated otherwise.

There are two special cases within the parameter space that require special consideration. The M_n data for the nonlinear systems are only meaningful when the M_n data for the corresponding harmonic system are constant. This is true for all cases, especially at concentrations for which $c\lambda \gg 1$. In theory, M_n for harmonic systems would be a constant for all time. In practice, the mapping of the continuum system onto the discrete lattice, and the relocation of the ends, can introduce a small amount of randomness that led to small fluctuations in M_n. These fluctuations, however, were far smaller than the changes for the anharmonic systems.

As a brief example, Fig. 4.10 is a plot of M_1 as a function of time for systems having having impurity concentration 0.500 and length 16 000. In the figure, the $\beta = 1$ data appear as lines having positive slope. The harmonic $\beta = 0$ data for all three impurity masses lie upon one another near $M_1 = 0$. Figure 4.10 is doubly

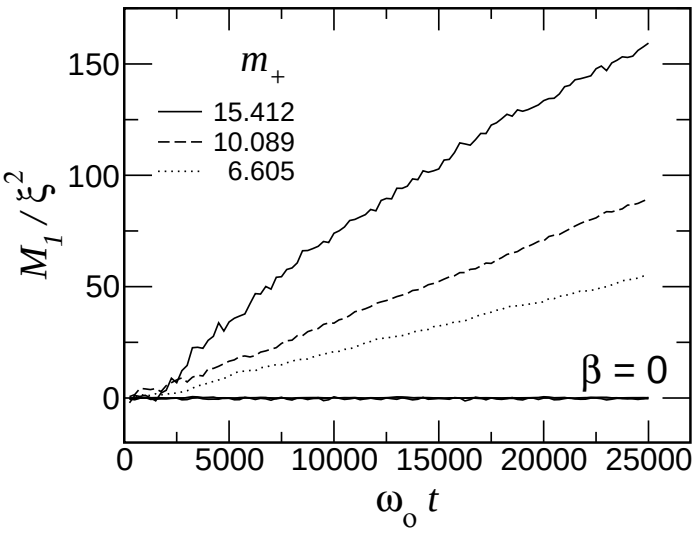

Figure 4.10: The ratio M_1/ξ^2 as a function of time for the systems having impurity concentration 0.500 and length 16 000. The $\beta = 1$ data have positive slopes and all the $\beta = 0$ data fall on top of one another at $M_1 = 0$.

instructive. It demonstrates that M_1 for the $\beta = 0$ data are negligible, even for the systems for which the second moment has the smallest value. Moreover, the harmonic data remain stable in concentrated systems: $c\lambda \gg 1$.

4.6.1 Time Exponent

A quantitative characterization of M_n is made by assuming a power-law dependence on time t:

$$M_n = 2G_n t^{\delta_n} \tag{4.23}$$

The first task is to determine the value of the exponent so as to distinguish among ballistic, diffusive, or sub-diffusive transport. The calculation of δ_n is affected by initial transients, and the details of the analysis are given in Appendix F. The

Table 4.1: Interval from which δ_n was calculated for systems having length L.

L	Interval
16000	$5000 < \omega_o t < 20000$
32000	$10000 < \omega_o t < 25000$
64000	$20000 < \omega_o t < 50000$
96000	$20000 < \omega_o t < 80000$

time interval from which the values of δ_n were calculated were constrained by the initial transients at small times and total energy conservation at long times. The specific intervals are shown in Table 4.1 for each system length used.

The results of the analyses for δ_1 are summarized in Fig. 4.11 for all the systems. In this figure, the symbols at a particular concentration are displaced horizontally to distinguish individual error bars representing the SE. Half the estimated values for δ_1 were within one SE of 1, and three-quarters were within 2 SE of 1. It is apparent from the data in the graph that, over the time scales studied, weakly disordered systems behave diffusively, and that strong disorder introduces variability into the results. Overall, the results suggest that energy transport along the chain is nearly diffusive, and so subsequent analysis of M_1 assumes a linear dependence upon time.

Results of the analysis for δ_2 are shown in Fig. 4.12. Although the values of δ_2 are near 1 for most systems, there is considerably more variability than for δ_1. Moreover, it was difficult to establish a precise value for δ_2 at higher concentrations. As a result, subsequent analysis is confined to M_1.

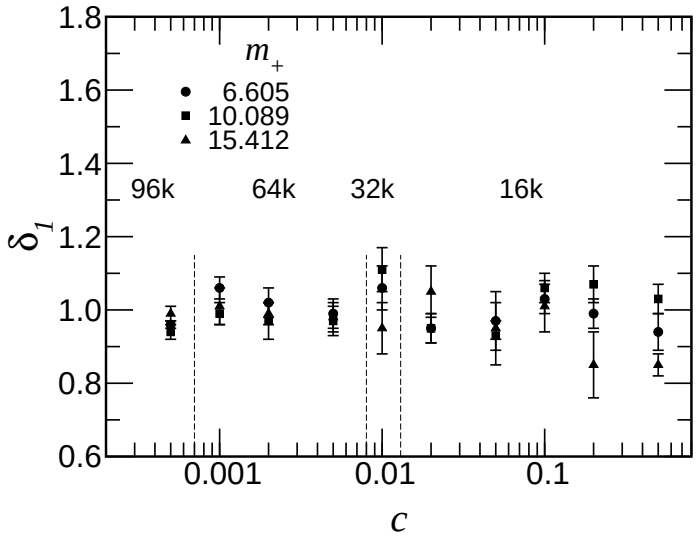

Figure 4.11: The time exponent δ_1 for G_1 as a function of impurity concentration c for impurity cross sections $\sigma = 0.30,\ 0.50,\ 0.70$. Numbers between vertical dashed lines denote system length (k=1000).

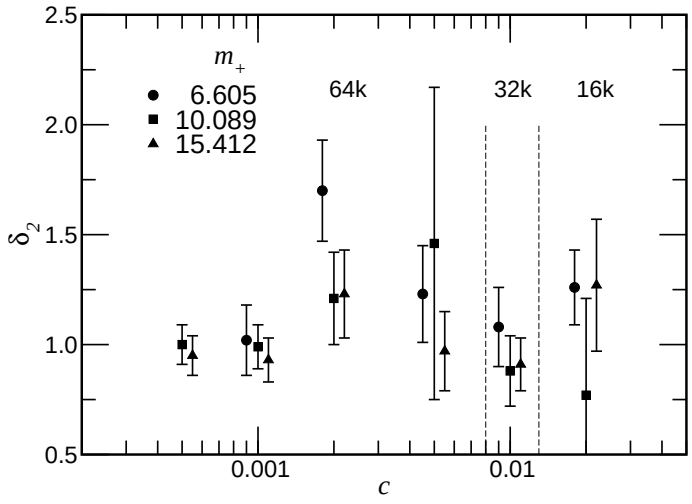

Figure 4.12: The time exponent δ_2 for G_2 as a function of impurity concentration c for impurity cross sections $\sigma = 0.30,\ 0.50,\ 0.70$. Numbers between vertical dashed lines denote system length (k=1000).

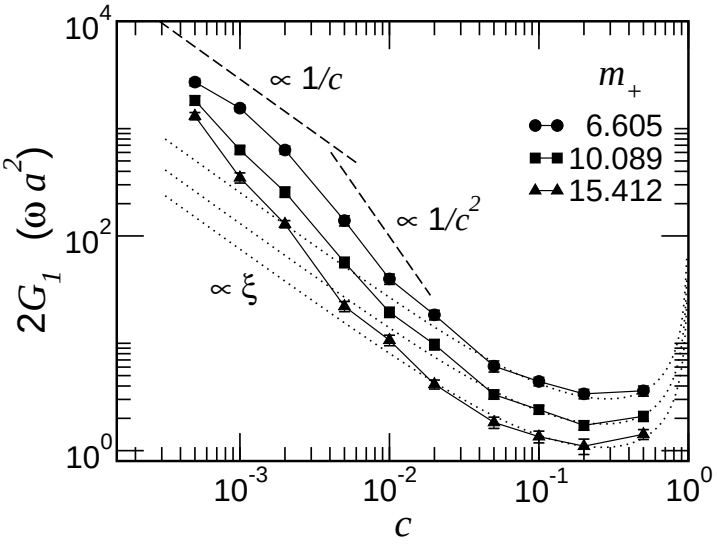

Figure 4.13: Transport coefficient G_1 as a function of impurity concentration c for impurity cross sections $\sigma = 0.30,\ 0.50,\ 0.70$. Dashed line is proportional to c^{-1} and c^{-2}. The dotted lines are proportional to ξ.

4.6.2 Transport Coefficient

Based on the results for δ_1, estimates for $2G_1$ assume a linear relationship between M_1 and t over the same intervals shown in Table 4.1. Although M_1 was determined by linear regression, calculating the uncertainty in M_1 required a slightly more involved analysis; details are give in the Appendix F.

Estimates of $2G_1$ for all the systems considered are plotted in Fig. 4.13 as a function of the impurity concentration c. The calculated values appear as filled symbols having error bars that represent the SE. The solid lines connecting the symbols are only to guide the eye. The two dashed line segments appearing above the data indicate slopes that are proportional to $1/c$ and $1/c^2$.

Data for $2G_1$ in Fig. 4.13 exhibit different behavior in three regions. At the lowest concentrations, $2G_1$ is nearly proportional to c^{-1} for the two smaller

impurity masses. At higher concentration, the coefficient $2G_1$ is proportional to c^{-2} for all three impurity masses. This transition is not apparent in the results of Payton *et al.* [69] on a similar system having thermostats because their computing resources prevented them from resolving the smaller concentrations required to see the effect.

The interesting behavior occurred at the highest concentrations. For all three impurity masses, the transport coefficient is proportional to the initial localization length ξ. This effect was also observed by Payton *et al.*,[69] but was not discussed in the context of a localization length. The three dotted curves labeled $\propto \xi$ are proportional to the localization lengths that appear in Fig. 4.3 for $\lambda = 31.8$. The value of ξ for each impurity mass is multiplied by the same coefficient (approximately 0.09) to make the curves overlay the measured transport coefficients.

4.6.3 Localization Parameter

The localization parameter can also be used as a measure of energy propagation. Although systems of different lengths were used, energy transport, starting from a localized state, should be independent of total system length. Based on the previous discussion of the localization parameter, the ratio L/Γ is proportional to the number of masses over which the total energy is distributed. For a given m_I and c, and assuming that $L \gg \xi$, the time-dependent number of masses over which energy is distributed should be independent of total system length. Therefore, the ratio L/Γ will serve as a means for comparing results from systems of different lengths.

If the linear time dependence of the second moment M_1 indicates diffusive

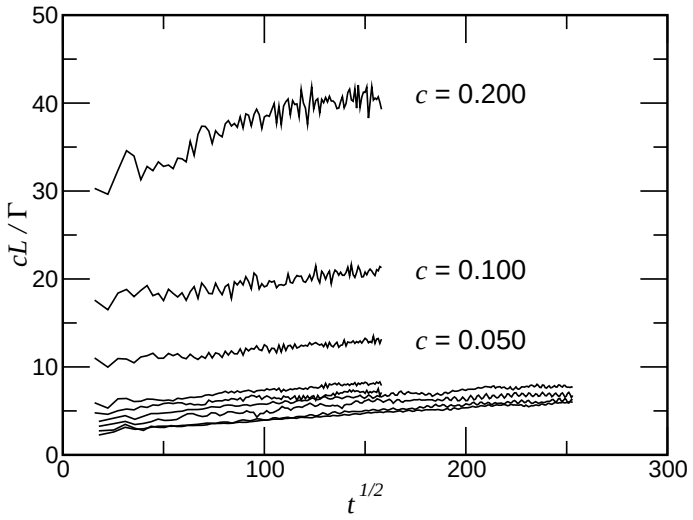

Figure 4.14: Localization parameter Γ as a function of time $t^{1/2}$ for systems having $m_+ = 6.605$.

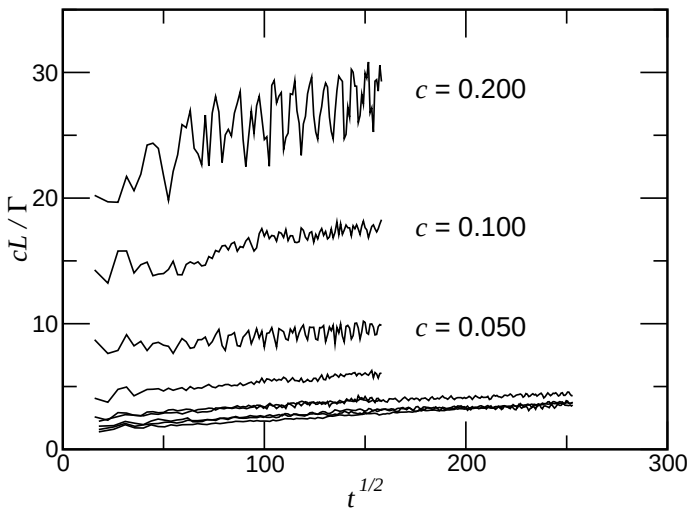

Figure 4.15: Localization parameter Γ as a function of time $t^{1/2}$ for systems having $m_+ = 10.089$.

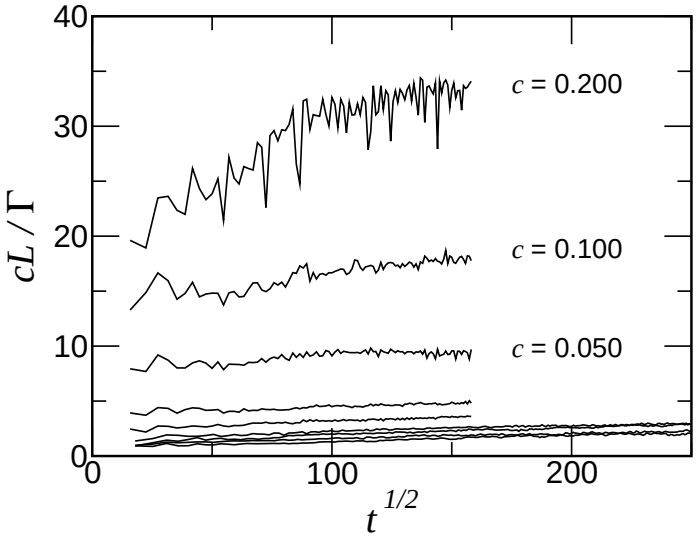

Figure 4.16: Localization parameter Γ as a function of time $t^{1/2}$ for systems having $m_+ = 15.412$.

behavior, the number of masses involved in energy transport should increase in proportion to $t^{1/2}$. In addition, because transport in dilute systems is proportional to c^{-1}, the quantity cL/Γ should approach a constant for systems with low impurity concentrations. The quantity cL/Γ, as a function of $t^{1/2}$, is plotted in Figs. 4.14–4.16 for most of the systems studied. In the figures, curves for decreasing impurity concentration appear consecutively lower in each graph.

There are two noteworthy features in Figs. 4.14–4.16. The number of masses participating appears to be proportional to $t^{1/2}$ over the time intervals considered, particularly for the dilute impurity systems. This is consistent with the expectation of a diffusive energy transport coefficient G_1. Also, as expected, the curves for the most dilute impurity concentrations appear to approach an asymptote, supporting the c^{-1} dependence for the number of masses participating in energy transport, even for the $m_+ = 15.412$ systems. For $c\lambda > 1$, the linearity

of the curves appears to break down. A more precise statement cannot be made because of the variability in cL/Γ with increasing impurity concentration.

4.7 Discussion

4.7.1 Concentration Dependence

The transition from $1/c$ to $1/c^2$ dependence in G_1 can be explained, in part, using arguments based on the relevant length and time scales. At the lowest impurity concentrations, the chain is composed of long segments of homogeneous nonlinear chain between adjacent impurities. Scattering generates new modes that are not localized and begin to propagate ballistically along the chain. These waves will continue to propagate until they scatter from an impurity or undergo a spontaneous transition. A spontaneous transition along the homogeneous portion of the chain is unlikely to occur in the time required to span the distance between impurities. It is more likely that the impurities will initiate scattering. The time τ between these scattering events can be characterized by some relevant length scale ℓ and the group velocity v_g:

$$\tau = \frac{\ell}{v_g} \tag{4.24}$$

This scattering will give rise to an effective transport coefficient that is proportional to the group velocity:

$$G \approx v_g \ell \tag{4.25}$$

It is common to assume that the mean free path (MFP) $(c\sigma)^{-1}$ is the relevant length scale. In dilute concentration BID systems, however, the localization length is slightly shorter than the mean free path. Regardless, the dissipation

mechanism is due to plane waves scattering over a length scale that is proportional to $1/c$ at low concentration.

As the impurity concentration increases, the localization length decreases and the wave experiences considerably more wave interference. As a result, transport becomes dominated by interactions between and among localized modes [109, 110]. The relevant time scale is the time t_ξ required for energy to diffuse a distance comparable to the localization length ξ:

$$G \approx \frac{\xi^2}{t_\xi} \tag{4.26}$$

For this type of behavior, the transport coefficient G is proportional to $1/c^2$, and t_ξ is a weak function of concentration.

In the dense systems for which $c\lambda > 1$, the transport coefficient is proportional to ξ. For these concentrations, both G_1 and ξ are relatively weak functions of concentration. Moreover, the transport coefficient is proportional to the original localization length, and not some averaged value. Although energy transfer in these dense systems occurs from interactions among overlapping localized modes (as in the slightly lower concentration range), the spatial extent of the interacting modes in strongly disordered systems persists for all subsequent interactions. As a result, the transport coefficient reflects this dependence on the initial spatial extent of the energy.

4.7.2 β-Dependence

It was argued that the results given for β=1 are indicative of results for 'large' values of β that are above the critical threshold that leads to ergodic behavior. As a check, the value of G_1 for two systems are calculated for different values of β. The two systems are $(c = 0.005, \sigma = 0.70)$ and $(c = 0.100, \sigma = 0.70)$, and the

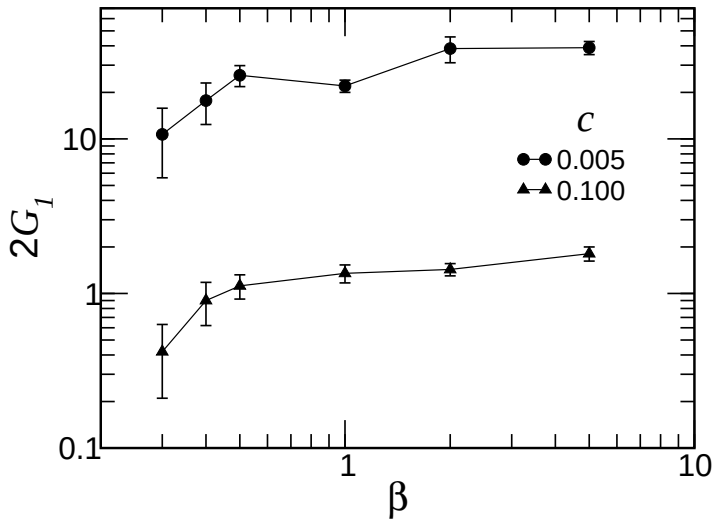

Figure 4.17: Transport coefficient G as a function of β for two impurity concentrations: $c = 0.100$, 0.005, and $\sigma = 0.70$.

analysis for these systems was carried out in a manner identical to that for the $\beta = 1$ data.

The values for G_1 are shown in Fig. 4.17 as a function of β. For $0.5 \leq \beta \leq 5.0$, the transport coefficient has a sub-linear dependence on the anharmonicity. The transport coefficient decreased markedly as β fell below 0.5, decreasing to nearly zero at $\beta = 0.2$. This result is consistent with numerical experiments on finite temperature nonlinear BID systems [69], and with numerical measurements for anharmonic silicon chains [109]. Therefore, although G_1 increases slowly for β greater than 0.5, there does not appear to be any significance to any particular value for β that is greater than 0.5.

Table 4.2: Comparison of $2G_1$ and δ_1 for systems having $L = 16\ 000$ and $L = 96\ 000$. All systems have impurity concentration $c = 0.5$.

	G_1		δ_1	
m_+	16 000	96 000	16 000	96 000
6.605	3.61±0.39	3.22±0.24	0.87±0.05	0.97±0.01
10.089	2.09±0.22	2.15±0.29	1.03±0.04	0.99±0.02
15.412	1.42±0.15	1.15±0.22	0.85±0.03	0.85±0.02

4.7.3 Length Dependence

To verify that the results are independent of system length, the $c = 0.5$ system is repeated with a system length of 96 000. Among all the systems, this system is the most likely to have length dependent properties because of the strong disorder.

The values of G_1 and δ_1 for the two different systems are shown in Table 4.2. The major distinction between the two systems is the system length. As a result, the total time integration, as shown in Table 4.1, differs by a factor of four. The data in the table show that increasing the integration time by a factor of four does not yield a significantly different transport coefficient. The data do suggest that the time exponent δ_1 for the ($m_+ = 6.605$, $L = 16\ 000$) system may be the result of a finite-size effect, but the exponent of 0.85 for the $m_+ = 15.412$ is likely to be accurate.

4.7.4 Time Scale

The significance of the reported results presented depends, in part, on the relative duration of the calculation. One measure of duration, to gauge whether long

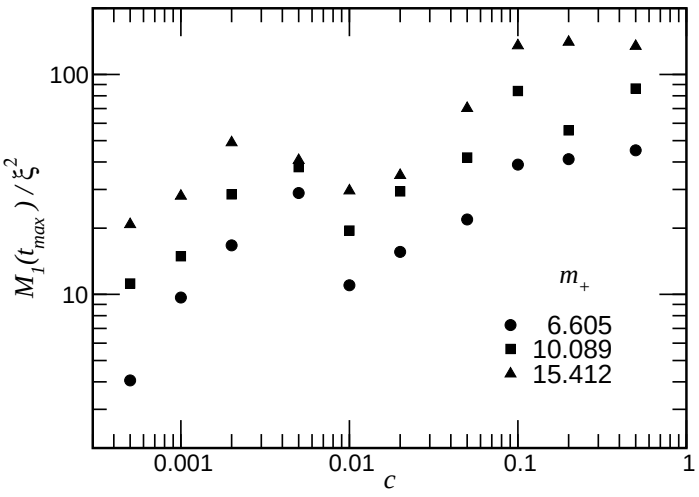

Figure 4.18: The ratio $M_1(t_{max})/\xi^2$ as a function of impurity concentration c.

enough times have been probed to capture meaningful behavior, is the ratio of the distance energy propagates along the system to the distance over which energy was distributed initially. The maximum energy propagation length is proportional to $M_1(t_{max})$, and the initial span is proportional to the initial localization length ξ.

The ratio $M_1(t_{max})/\xi^2$ for each system is plotted in Fig. 4.18. The ratio varied from 5 to 100, increasing with impurity concentration. The square root of this ratio is a measure of the depth to which energy propagated. Therefore, the energy penetration depth varied from 3 to 10 times the initial localization length.

4.8 Conclusion

There is evidence for diffusive energy dissipation from energy eigenstates in binary isotopically disordered nonlinear FPU chains at zero temperature. Given suffi-

cient anharmonicity, the second moment of the site energies increased linearly. Over the time scale studied, the square root of the second moment increased to a value that was approximately 10 times the initial localization length. The evidence for diffusive behavior was corroborated by $t^{1/2}$ dependence for the number of masses over which energy was distributed, estimated from the localization parameter.

The most interesting aspect of the transport coefficient was the concentration dependence. At low impurity concentration c, the transport coefficient was proportional to c^{-1}. At higher impurity concentrations, the transport coefficient developed a c^{-2} dependence. This concentration dependence was consistent with a transition from transport dominated by impurity scattering to one in which interactions among overlapped localized modes dominated transport.

At the highest impurity concentrations, the concentration dependence of the transport coefficient was proportional to the original localization length. In strongly disordered systems for which $c\lambda > 1$, far fewer modes are produced, and at a lower rate. In addition, the character of the spectral density at these concentrations constrains mode production. The dynamics of the mode transition in combination with the fact that the localization length is a weak function of concentration for strongly disordered systems suggests that vibrational energy transfer among strongly localized modes yields new modes that retain the spatial extent of the interacting modes. As a result, the initial spatial extent of interacting modes is retained as the dominant length scale characterizing transport in strongly disordered binary isotopic systems.

Chapter 5

Conclusion

The results from the three experiments of the preceding chapters forms a continuous study of the role of localization and nonlinearity in energy transport in Fermi-Pasta-Ulam chains. The summary begins with the unique concentration dependent localization properties of harmonic BID chains. This property ultimately appears again in the concentration dependence of an effective thermal transport coefficient in the nonlinear disordered chain. Explanations for this behavior are based on the studies of mode transition and ergodicity in the nonlinear BID chains. The quantitative measure of participating modes suggested that the number of new modes generated in a BID chain decreases with increasing impurity concentration. This constrained mode generation is the primary argument for why the spatial extent over which energy was initially distributed remained the dominant length scale for transport at these high impurity concentrations.

5.1 Harmonic Chains

Harmonic BID chains contain interesting behavior that can be explained with straightforward physical arguments. The starting point is the impurity scattering

cross section. A continuum model explains the majority of the behavior, with the quadratic dependence of scattering cross section on the impurity impedance. This was true for long wavelength displacements and impurity masses that were either larger or smaller than the equilibrium mass. As the wavelength decreased, effects of the discrete lattice required a correction to the cross section. The correction, which was proportional to the group velocity, was attributed to a correction of impurity impedance in a discrete chain.

From the precise formulation of scattering cross section, the experiment to investigate localization length in harmonic BID chains could be studied on a strong foundation. At low impurity concentration c, the localization length of BID systems agrees with dilute scattering theory. As the impurity concentration increases beyond $1/2$ the system approaches a homogeneous system with an infinite localization length. The behavior of the system at intermediate concentrations was explained by assuming that, as a harmonic system, the system is composed simultaneously of two disordered sub-systems that were independent of one another. One sub-system is the homogeneous chain in the limit $c \to 0$, and the second is the homogeneous chain in the limit $c \to 1$. At intermediate impurity concentration, the localization length is the sum of the two disordered sub-systems. This physical interpretation can predict the localization at any concentration to within a few percent, a performance that was comparable to more involved published calculations.

The physical model also predicted the existence of a cut-off frequency for the $c \to 1$ sub-system. By assuming that the driving frequency is constant for both sub-systems, and that the impurity mass is heavier than the homogeneous mass, this frequency could be in the forbidden band of the $c \to 1$ sub-system.

Oscillations with frequencies beyond the allowable band have a zero wave speed, and so the sub-system does not contribute to localization. In these cases, the localization length is a monotonic function of impurity concentration, as was observed by numerical simulation.

The aforementioned results were calculated from very long systems. To reduce computational demands on subsequent studies of energy transport, a quantitative measure of the minimum allowable system length was needed. Because the statistics of the Lyapunov exponent are knowable, a comparison of these predictions to measurements made on systems of varying length revealed that approximately 32 impurities and a system length ten times greater than the localization length are required in the system. These criteria, along with available computational resources, established a lower limit for impurity concentration in the subsequent numerical experiments.

5.2 Mode Decay in Disordered Systems

Having established the behavior of linear BID systems, the next objective was to quantify the role of impurities on mode transitions in nonlinear chains. The experiment to study mode decay in hoops with nonlinear interactions revealed that BID systems do not undergo ergodic behavior. The systems start with all the energy initially in a single wavelength mode. For systems where the impurity mass was greater than the equilibrium value, the energy became localized at the impurities, as one might expect from Anderson localization. The interesting part was that the energy remained localized at the impurities in the nonlinear systems that were capable of mode transitions. The explanation for this was that the heavier impurities, for a given amount of energy, oscillate at a lower amplitude

than the other masses. This lower oscillation amplitude leads to a much slower subsequent mode-mode interactions.

The theory was corroborated for BID systems in which the impurity mass was smaller than the equilibrium values. By logical extension of the argument for heavy impurity masses, lighter impurity masses should oscillate at large amplitudes, thereby expelling energy more quickly. Calculations of the fraction of energy at the impurities confirmed this. Interestingly, however, for $c\lambda > 1$ the rate of mode decay for the lighter impurities slowed dramatically, which may be a source of study for future work.

5.3 Energy Transport

Further mode transitions studies were performed on disordered hoops to quantify the degree of ergodicity via the localization parameter Γ and the number of participating modes n_ω. The localization parameter was used to estimate the number of masses over which energy is distributed, and n_ω was the fraction of possible harmonic modes over which energy is distributed. Although the initial effect of impurities is to hasten mode transitions, the long time response suggests an overall suppression of mode transitions. Both the localization parameter and the number of participating modes revealed that BID chains severely suppress the mode generation in nonlinear systems. The reduction of the localization parameter was consistent with the previous study of mode transitions, particularly the behavior for $c\lambda > 1$. The reduction in the number of participating modes indicates that the impurities not only suppress energy release, they also limit the total number of modes generated.

The energy transport experiment was designed to be reminiscent of a labo-

ratory experiment in which a macroscopic specimen is struck at one end, and the elastic waves propagate along the specimen. As the magnitude of the impact displacement was to be far greater than the amplitude of thermal oscillations, the system was approximated by a localized disturbance at one end of a chain that is otherwise at zero temperature. For an arbitrary impulse, a wave propagating through a disordered nonlinear system will undergo competition between localization and mode transitions. To avoid this competition, the initial condition for this study was a frequency eigenstate for the harmonic component of the Hamiltonian. The initial condition was calculated from the continuum solution of the Kronig-Penney liquid model and then mapped onto the chain. In the presence of sufficient nonlinearity, numerical integration of the equation of motion leads to energy transport along the chain.

Because the systems studied were at zero temperature, the usual measures of thermal conductivity could not be used. Instead, the second moment of the site energy was used to characterize the rate that energy was transported along the chain. By analogy to studies of mean squared displacement, the time exponent was found to be near 1 for all the systems studied, with the variability increasing with increasing impurity concentration. Having established a linear relationship between the second moment and time, an effective thermal conductivity was determined from the ratio of the two.

The effective thermal conductivity was calculated as a function of impurity concentration, using a moderate wavelength: $\lambda = 31.8$ At the lowest impurity concentration, the thermal conductivity decreased as c^{-1}. At the highest concentrations, the effective localization length was proportional to the original localization length. This seemed surprising because the systems were sufficiently long

to ensure considerable mode interactions. As a check, longer systems were used to verify the independence between the effective thermal conductivity and system length. Moreover, experiments done at different values of the anharmonicity parameter showed that the results were a weak function of anharmonicity parameter, above a minimum value.

The interesting result was that at the highest impurity concentrations studied the effective transport coefficient had the same concentration dependence as the localization length of the $\lambda = 31.8$ displacement wave. Ostensibly, this length scale only had meaning for the initial displacement wave. Therefore, one would have expected that mode transitions would have destroyed any significance that the initial spatial extent of the energy might possibly have.

A possible explanation for the behavior of the most concentrated systems is based on the spectral properties of these systems. Although new modes were created, the high impurity concentration severely restricted the spectrum of these new modes. Moreover, direct observation showed that very low frequency waves propagated nearly ballistically through the system, with no observable effect on the effective thermal conductivity. Given all this, it would appear that the initial spatial extent of the initial disturbance remains an important factor in subsequent transport through the system.

Appendix A

Green's Functions

The most important reference on Green's Functions for the study of disordered systems is Economou's book, *Green's Functions in Quantum Physics* [30]. Most of these notes are taken directly from his book.

A.1 Formalism

A Green's function (GF) $G(\mathbf{r}, \mathbf{r}'; z)$ is the solution to an inhomogeneous equation of the following type:

$$[z - \mathcal{L}(\mathbf{r})]\, G(\mathbf{r}, \mathbf{r}'; z) = \delta(\mathbf{r} - \mathbf{r}') \tag{A.1}$$

$G(\mathbf{r}, \mathbf{r}'; z)$ is subject to some boundary conditions on $\mathbf{r}$ and $\mathbf{r}'$ at the boundary. The quantity z is a complex variable with the following components:

$$\lambda = \Re\{z\} \qquad\qquad s = \Im\{z\} \tag{A.2}$$

$\mathcal{L}(\mathbf{r})$ is a linear Hermitian differential operator having a complete set of eigenfunctions $\{\phi_n(\mathbf{r})\}$:

$$\mathcal{L}(\mathbf{r})\, \phi_n(\mathbf{r}) = \lambda_n\, \phi_n(\mathbf{r}) \tag{A.3}$$

The eigenfunction ϕ_n are those that satisfy the same boundary conditions as $G(\mathbf{r}, \mathbf{r}'; z)$. The eigenfunctions are orthogonal,

$$\int_\Omega \mathrm{d}\mathbf{r}\, \phi_n^* \, \phi_m = \delta_{nm} \tag{A.4}$$

and they form a complete set:

$$\sum_n \phi_n(\mathbf{r})\ \phi_n^*(\mathbf{r}') = \delta(\mathbf{r} - \mathbf{r}') \tag{A.5}$$

The summation is used here to denote both summation over the discrete portion of the spectrum and integration over the continuous portion of the spectrum.

The algebra of GF manipulation is facilitated by working in an abstract vector space, where the previous representation was only a particular case. The representation uses the Dirac bra-ket notation, which has the following equivalences to the previous notation:

$$\begin{aligned}
\phi_n(\mathbf{r}) &= \langle \mathbf{r} \,|\, \phi_n \rangle && \text{(A.6)} \\
\delta(\mathbf{r} - \mathbf{r}')\mathcal{L}(\mathbf{r}) &= \langle \mathbf{r}| \, \mathcal{L} \, |\mathbf{r}'\rangle && \text{(A.7)} \\
G(\mathbf{r}, \mathbf{r}'; z) &= \langle \mathbf{r}| \, G(z) \, |\mathbf{r}'\rangle && \text{(A.8)} \\
\delta(\mathbf{r} - \mathbf{r}') &= \langle \mathbf{r} \,|\, \mathbf{r}' \rangle && \text{(A.9)} \\
1 &= \int \mathrm{d}\mathbf{r}\ |\mathbf{r}\rangle \langle \mathbf{r}| && \text{(A.10)}
\end{aligned}$$

In the new notation, we can write

$$\begin{aligned}
(z - \mathcal{L})\, G(z) &= 1 && \text{(A.11)} \\
\mathcal{L}\, |\phi_n\rangle &= \lambda_n \, |\phi_n\rangle && \text{(A.12)} \\
\langle \phi_n \,|\, \phi_m \rangle &= \delta_{nm} && \text{(A.13)} \\
\sum_n |\phi_n\rangle \langle \phi_n| &= 1 && \text{(A.14)}
\end{aligned}$$

The immediate advantage of the bra-ket notation is that algebra is simplified. The practical advantage is that one is not committed to either the $\mathbf{r}$ or the $\mathbf{k}$ representation.

The following representations for G will be useful. If all the eigenvalues of $z - \mathcal{L}$ are not equal to zero, which is equivalent to $z \neq \{\lambda_n\}$, G can be expressed formally as

$$G(z) = \frac{1}{z - L} \tag{A.15}$$

Multiplying by Eq. (A.14) yields and equivalent representation using an orthogonal basis set:

$$G(z) = \sum_n \frac{1}{z - \mathcal{L}} \left|\phi_n\right\rangle \left\langle\phi_n\right| = \sum_n \frac{\left|\phi_n\right\rangle \left\langle\phi_n\right|}{z - \lambda_n} \tag{A.16}$$

The final result uses the general relation $F(\mathcal{L}) \left|\phi_n\right\rangle = F(\lambda_n) \left|\phi_n\right\rangle$, for any function F. The above summation is a generalization for both a summation and an integral:

$$G(z) = \sum_n{}' \frac{\left|\phi_n\right\rangle \left\langle\phi_n\right|}{z - \lambda_n} + \int \mathrm{d}n \, \frac{\left|\phi_n\right\rangle \left\langle\phi_n\right|}{z - \lambda_n} \tag{A.17}$$

We can project this into $\mathbf{r}$ representation using Eq. (A.8):

$$G(\mathbf{r}, \mathbf{r}'; z) = \sum_n{}' \frac{\phi_n(\mathbf{r}) \, \phi_n^*(\mathbf{r}')}{z - \lambda_n} + \int \mathrm{d}n \, \frac{\phi_n(\mathbf{r}) \, \phi_n^*(\mathbf{r}'}{z - \lambda_n} \tag{A.18}$$

Because $\mathcal{L}$ is Hermitian, each λ_n is real. Therefore, if $\Im\{z\} \neq 0$, z cannot equal any of the λ_n and $G(z)$ is an analytic function in the complex plane, except for those parts of the real axis corresponding to eigenvalues of $\mathcal{L}$.

The behavior of $G(z)$ along the real axis is important. For a discrete eigenvalue spectrum, $G(z)$ exhibits simple poles at the eigenvalues of $\mathcal{L}$. For the continuous spectrum where $z = \lambda$, the behavior of $G(\mathbf{r}, \mathbf{r}'; \lambda)$ is not well defined. Alternatively, one can use a limiting procedure $G(\mathbf{r}, \mathbf{r}'; \lambda \pm \mathrm{i}s)$. If the eigenstates

associated with the continuous spectrum are propagating or extended, the side limits as $s \to 0^+$ will exist, but will be different from one another. This results in a branch cut in $G(z)$ along the real axis.

It is possible to have a localized eigenfunction in the continuum spectra of disordered systems. Even for these systems, the side limits do not exist. The line of singularity for such a spectrum is called a natural boundary.

Returning to extended states, there is an advanced and retarded GF:

$$G^+(\mathbf{r}, \mathbf{r}'; \lambda) = \lim_{s \to 0^+} G(\mathbf{r}, \mathbf{r}'; \lambda + \mathrm{i}s) \tag{A.19}$$

$$G^-(\mathbf{r}, \mathbf{r}'; \lambda) = \lim_{s \to 0^+} G(\mathbf{r}, \mathbf{r}'; \lambda - \mathrm{i}s) \tag{A.20}$$

$$\tag{A.21}$$

From Eq. (A.18) it is easy to verify

$$G^*(\mathbf{r}, \mathbf{r}'; z) = G(\mathbf{r}', \mathbf{r}; z^*) \tag{A.22}$$

If z is real ($z = \lambda$) and $\lambda \neq \{\lambda_n\}$, it follows from Eq. (A.22) that $G(\mathbf{r}, \mathbf{r}'; \lambda)$ is Hermitian, and that $G(\mathbf{r}, \mathbf{r}; \lambda)$ is real. If the eigenvalue spectrum is continuous, the Eq. (A.22) gives

$$G^-(\mathbf{r}, \mathbf{r}'; \lambda) = \left[G^+(\mathbf{r}', \mathbf{r}; \lambda)\right]^* \tag{A.23}$$

From this relationship, it is clear that

$$\Re\{G^-(\mathbf{r}, \mathbf{r}; \lambda)\} = \Re\{G^+(\mathbf{r}, \mathbf{r}; \lambda)\} \tag{A.24}$$

and

$$\Im\{G^-(\mathbf{r}, \mathbf{r}; \lambda)\} = -\Im\{G^+(\mathbf{r}, \mathbf{r}; \lambda)\} \tag{A.25}$$

We seek to characterize the discontinuity

$$\widetilde{G}(\lambda) = G^+(\lambda) - G^-(\lambda) \tag{A.26}$$

using the identity

$$\lim_{y\to 0^+} \frac{1}{x \pm \mathrm{i}y} = \mathrm{P}\left(\frac{1}{x}\right) \mp \mathrm{i}\pi\, \delta(x) \tag{A.27}$$

where P represents the principle value. From Eq. (A.18) we have the discontinuity in $\mathbf{r}$ representation:

$$\widetilde{G}(\mathbf{r}, \mathbf{r}'; \lambda) = -2\pi\mathrm{i} \sum_n \delta(\lambda - \lambda_n)\, \phi_n(\mathbf{r})\, \phi_n^*(\mathbf{r}') \tag{A.28}$$

where the summation is meant to represent both summation over the discrete spectrum and integration over the continuous spectrum.

A.2 Density of States

Using Eq. (A.27), the diagonal elements of the advanced and retarded GF are

$$G^{\pm}(\mathbf{r}, \mathbf{r}; \lambda) = \mathrm{P} \sum_n \frac{\phi_n(\mathbf{r})\, \phi_n^*(\mathbf{r})}{\lambda - \lambda_n} \mp \mathrm{i}\pi \sum_n \delta(\lambda - \lambda_n)\, \phi_n(\mathbf{r})\, \phi_n^*(\mathbf{r}) \tag{A.29}$$

Integerating over $\mathbf{r}$ gives the trace:

$$\mathrm{Tr}\, G^{\pm}(\lambda) = \mathrm{P} \sum_n \frac{1}{\lambda - \lambda_n} \mp \mathrm{i}\pi \sum_n \delta(\lambda - \lambda_n) \tag{A.30}$$

The quantity $\sum_n \delta(\lambda - \lambda_n)$ is the density of states ($N(\lambda)$) at λ. Given that the first term is real:

$$N(\lambda) = \mp \frac{1}{\pi} \Im\{\mathrm{Tr}\, G^{\pm}(\lambda)\} \tag{A.31}$$

The quantity

$$\rho(\mathbf{r}; \lambda) = \sum_n \delta(\lambda - \lambda_n)\, \phi_n(\mathbf{r})\, \phi_n^*(\mathbf{r}) \tag{A.32}$$

is the density of states per unit volume:

$$N(\lambda) = \int \mathrm{d}\mathbf{r}\ \rho(\mathbf{r}; \lambda) \tag{A.33}$$

Using the above relationships,

$$\rho(\mathbf{r};\lambda) = \mp\frac{1}{\pi}\,\Im\{G^{\pm}(\mathbf{r},\mathbf{r};\lambda)\} = \frac{-1}{2\pi\mathrm{i}}\,\widetilde{G}(\mathbf{r},\mathbf{r};\lambda) \tag{A.34}$$

It can be shown that

$$G(\mathbf{r},\mathbf{r};z) = \int_{-\infty}^{+\infty} \mathrm{d}\lambda \frac{\rho(\mathbf{r};\lambda)}{z-\lambda} \tag{A.35}$$

Therefore, finding the density of states and finding the Green's function are synonomous.

Appendix B

Numerical Time Integrators

x^n : position at $n\Delta t$

v^n : velocity at $n\Delta t$

a^n : acceleration at $n\Delta t$

B.1 ABM Predictor-Corrector

A predictor-corrector integrator of order m starts by predicting the new position x^{n+1} based on the present and previous $m-1$ velocities. It uses the new positions x^{n+1} to evaluate new acceleration a^{n+1}, which are then used to correct the new velocities v^{n+1} and positions x^{n+1}.

A shorthand notation for the predictor-corrector steps are the following:

P(x) - predict x^{n+1}

E(a) - evaluate a^{n+1} from x^{n+1}

C(v) - correct v^{n+1}

C(x) - correct x^{n+1}

The most general algorithm for a predictor-corrector integrator can be expressed more formally [37]:

$$\mathrm{P}(x)[\mathrm{E}(a)\ \mathrm{C}(v)\ \mathrm{C}(r)\ \mathrm{E}(a)]^p \tag{B.1}$$

The exponent p signifies repeating the steps within the square brackets. For a small step size, there is negligible benefit from implimenting a predictor-corrector algorithm with $p > 2$, and there is only a small advantage to $p = 2$ over $p = 1$ [36].

The particular predictor-corrector approach used here is the Adams-Bashforth/Adams-Moulton (ABM) method. The ABM method represents the predictor step $P()$ with Adams-Bashforth coefficients γ^{AB}:

$$P(x): \qquad x^{n+1} = x^n + \Delta t \sum_{k=-m+1}^{0} \gamma^{AB} v^{n+k} \tag{B.2}$$

Correspondingly, the corrector step $C()$ uses the Adams-Moulton coefficients γ^{AM}:

$$C(v): \qquad v^{n+1} = v^n + \Delta t \sum_{k=-m+2}^{1} \gamma^{AM} a^{n+k} \tag{B.3}$$

Similarly for $C(r)$.

Table B.1: Adams-Bashford predictor coefficients γ^{AB} up to order $m = 5$.

			k		
m	0	-1	-2	-3	-4
1	+1				
2	+3/2	-1/2			
3	+23/12	-16/12	+5/12		
4	+55/24	-59/24	+37/24	-9/24	
5	+1901/720	-2774/720	+2616/720	-1274/720	+251/720

Table B.2: Adams-Moulton corrector coefficients γ^{AM} up to order $m = 5$.

	k				
m	+1	0	-1	-2	-3
1	+1				
2	+1/2	+1/2			
3	+5/12	+8/12	-1/12		
4	+9/24	+19/24	-5/24	+1/24	
5	+251/720	+646/720	-264/720	+106/720	-19/720

B.2 Symplectic

Let there be N bodies in motion. The i-th mass has cannonical position q_i and momentum p_i. It is assumed that the entire system can be described by a Each cannonical variable can be expressed as a column vector $\mathbf{q}$ and $\mathbf{p}$. It is assumed that the entire system can be characterized by a Hamiltonian $H(\mathbf{q}, \mathbf{p})$. The equations of motion for the system can be expressed in a compact notation:

$$\frac{d\mathbf{q}}{dt} = \nabla_p H(\mathbf{q}, \mathbf{p}) \qquad \frac{d\mathbf{p}}{dt} = -\nabla_q H(\mathbf{q}, \mathbf{p}) \tag{B.4}$$

The cannonical variables can be expressed using a shorthand notation using the time-dependent phase space column vector $\mathbf{z}$:

$$\mathbf{z} = \begin{pmatrix} \mathbf{q} \\ \mathbf{p} \end{pmatrix} \tag{B.5}$$

The equations of motion (cannonical transform) for $\mathbf{z}$ can be expressed succinctly:

$$\frac{d\mathbf{z}}{dt} = \mathsf{J}\nabla_z H(\mathbf{z}) \tag{B.6}$$

The matrix J is the symplectic matrix composed of the indentity matrix I of rank N:

$$\mathsf{J} = \begin{pmatrix} 0 & +\mathsf{I} \\ -\mathsf{I} & 0 \end{pmatrix} \tag{B.7}$$

In general, a cannonical transformation $s(\mathbf{z}_1, \mathbf{z}_2)$ between phase space vectors $\mathbf{z}_1$ and $\mathbf{z}_2$ leaves the symplectic form unchanged if it satisfies the following:

$$s(\mathbf{z}_1, \mathbf{z}_2) = \mathbf{z}_1^T \mathsf{J}\, \mathbf{z}_2 \tag{B.8}$$

The objective of a symplectic integrator is to find a transform s in time that preserves the symplectic form.

Assume that the time trajectory of phase point $\mathbf{z}$ can be expressed using a matrix operator A:

$$\mathbf{z}(t) = \mathsf{A}\, \mathbf{z}(t_o) \tag{B.9}$$

Therefore, two phase points $\mathbf{z}_1$ and $\mathbf{z}_2$ that satisfy the cannonical transform

$$s(\mathbf{z}_1(t_o), \mathbf{z}_2(t_o)) = \mathbf{z}_1 \mathsf{J}\, \mathbf{z}_2 \tag{B.10}$$

will have the follwing time-dependence:

$$\begin{aligned} s(\mathbf{z}_1(t), \mathbf{z}_2(t)) &= \mathbf{z}_1^T \mathsf{J}\, \mathbf{z}_2 && \text{(B.11)} \\ &= \mathbf{z}_1^T(t_o) \mathsf{A}^T \mathsf{J}, \mathsf{A}\, \mathbf{z}_2(t_o) && \text{(B.12)} \end{aligned}$$

The symplectic form is preserved if

$$\mathsf{A}^T \mathsf{J}\, \mathsf{A} = \mathsf{J}$$

B.2.1 SHO Example

Consider a simple harmonic oscillator (SHO) composed of a mass m coupled to a fixed wall via a linear spring with force constant K. The mass is described by

its cannonical coordinate q and momentum p:

$$\mathbf{z} = \begin{pmatrix} q \\ p \end{pmatrix} \tag{B.13}$$

The time dependent behavior can be approximated by a cannonical transform:

$$\mathbf{z}(t+h) = \begin{pmatrix} 1 & h/m \\ -hK & 1 \end{pmatrix} \mathbf{z}(t) = \mathsf{B}\mathbf{z}(t) \tag{B.14}$$

To make this cannonical transform symplectic, we must determine what, if any, modifications are needed to matrix B to preserve the symplectic form:

$$\mathsf{B}^T \mathsf{J} \mathsf{B} = \begin{pmatrix} 0 & 1 + h^2K/m \\ -(1 + h^2K/m) & 0 \end{pmatrix} \tag{B.15}$$

$$= \left[1 + (\omega h)^2\right] \mathsf{J} \tag{B.16}$$

The angular frequency $\omega = K/m$ is the natural frequency of the SHO. The symplectic transform A is

$$\mathsf{A} = \frac{1}{\sqrt{1 + (\omega h)^2}} \mathsf{B}$$

B.2.2 Implimentation

The general form of an s-stage symplectic integrator is [118]:

$$\mathbf{y}^n = \mathbf{y}^{n-1} + A_n \mathbf{v}^{n-1} \Delta t \tag{B.17}$$

$$\mathbf{v}^n = \mathbf{v}^{n-1} + B_n \mathbf{F}^n \Delta t / \mathbf{m} \tag{B.18}$$

$$1 \leq n \leq s \tag{B.19}$$

Different implimentations sometimes reverse the position and velocity evalution, but the general form remains the same. What makes the method symplectic is the choice of the coefficients A_n and B_n.

Table B.3: Coefficients for a 4-th order symplectic integrator.

n	A_n	B_n
1	$(2 + 2^{+1/3} + 2^{-1/3})/6$	0
2	$(1 - 2^{+1/3} - 2^{-1/3})/6$	$1/(2 - 2^{1/3})$
3	$(1 - 2^{+1/3} - 2^{-1/3})/6$	$1/(1 - 2^{2/3})$
4	$(2 + 2^{+1/3} + 2^{-1/3})/6$	$1/(2 - 2^{1/3})$

The coefficients used for the 4-th order symplectic integrator were taken from Candy and Rozmus [39], and are shown here in Table B.3. These coefficients are solved for algebraically, but 4-th order is the highest order integrator that can be solved for using this method.

The coefficients for the 6-th order symplectic integrator are from Yoshida [40] and are shown here in Table B.4. These coefficients were calculated using Lie algebra, which can be extended to 10-th order and beyond; above 10-th order, the number of coefficients required becomes far greater than the order of the integrator. For the 6-th order integrator, three solutions are given for the intermediate coefficients (W, X, Y, Z). The coefficients used here were those from Table 1 in Ref. [40].

Table B.4: Coefficients for a 6-th order symplectic integrator.

$$X = -1.17767998417887$$

$$Y = +0.235573213359357$$

$$Z = +0.784513610477560$$

$$W = 1 - 2(X + Y + Z)$$

n	A_n	B_n
1	$Z/2$	Z
2	$(Z+Y)/2$	Y
3	$(Y+X)/2$	X
4	$(X+W)/2$	W
5	$(X+W)/2$	X
6	$(Y+X)/2$	Y
7	$(Z+Y)/2$	Z
8	$Z/2$	0

Appendix C

Harmonic Systems

C.1 Longitudinal Waves in a Rod

The equations of motion for the displacement **u** within a crystal come from a balance between the inernal stress force $\partial\sigma_{ik}/\partial x_k$ to the product of the acceleration $\ddot{u}_i$ and the mass density μ [119]:

$$\mu\ddot{u}_i = \frac{\partial\sigma_{ik}}{\partial x_k} \tag{C.1}$$

Here we assume adiabatic (slow thermal transport) motion.

The free energy F is [119, Eq. 5.10]:

$$F = \frac{Y}{2(1+\sigma)}\left(u_{ik}^2 + \frac{\sigma}{1-2\sigma}\,u_{ll}^2\right) \tag{C.2}$$

The notation u_{ll} implies an internal summation on l (Einstein notation).

For isothermal deformations, the stress tensor σ_{ik} is the gradient in the free energy:

$$\sigma_{ik} = \left(\frac{\partial F}{\partial u_{ik}}\right)_T \tag{C.3}$$

Substitution gives,

$$\sigma_{ik} = \frac{Y}{1+\sigma}\left(u_{ik} + \frac{\sigma}{1-2\sigma}\,u_{ll}\delta_{ik}\right) \tag{C.4}$$

As a check,

$$\sigma_{xx} = \frac{Y}{(1+\sigma)(1-2\sigma)} \left[(1-\sigma)u_{xx} + \sigma(u_{yy} + u_{zz})\right] \tag{C.5}$$

At equilibrium (assuming gravitational acceleration $\mathbf{g}$):

$$\frac{\partial \sigma_{ik}}{\partial x_k} + \mu g_i = 0 \tag{C.6}$$

Substitution gives the following equation of motion:

$$\mu \ddot{\mathbf{u}} = \frac{Y}{2(1+\sigma)} \nabla^2 \mathbf{u} + \frac{Y}{2(1+\sigma)(1-2\sigma)} \nabla(\nabla \cdot \mathbf{u}) \tag{C.7}$$

As a reminder:

$$\nabla^2 \mathbf{u} = \hat{i} \nabla^2 u_x + \hat{j} \nabla^2 u_y + \hat{k} \nabla^2 u_z \tag{C.8}$$

For longitudinal waves in a finite rod, the $\hat{k}$ component is:

$$\frac{\partial^2 u_z}{\partial t^2} = \left[\frac{Y(1-\sigma)}{\mu(1+\sigma)(1-2\sigma)}\right] \frac{\partial^2 u_z}{\partial z^2} \tag{C.9}$$

The transverse $\hat{x}$ component is

$$\frac{\partial^2 u_x}{\partial t^2} = \frac{Y}{2\mu(1+\sigma)} \frac{\partial^2 u_x}{\partial x^2} \tag{C.10}$$

For the case of a longitudinal wave in an infinite medium, there is no Poisson's effect: $\sigma = 0$. The equations simplify:

$$\frac{\partial^2 u_z}{\partial t^2} = \frac{Y}{\mu} \frac{\partial^2 u_z}{\partial z^2} \tag{C.11}$$

This gives the analogous wave propagation speed $\sqrt{Y/\mu}$ to the FPU chain through the substitution $Y = Ka$ and $\mu = m_\circ/a$.

If one assumes longitudinal waves in a infinite medium such that $u_x = u_y = 0$ and $u_z(x, y) = 0$, the Poisson's ratio $\sigma = 0$. For longitudinal waves ($\hat{z}$-direction)

in a rod, the only contribution to the stress tensor is σ_{zz} [119, Section 25]. The relationship between displacement u_k and the stress tensor is

$$\rho \ddot{u}_z = \frac{\partial \sigma_{zz}}{\partial z} \tag{C.12}$$

Since $\sigma_{zz} = E u_{zz}$ [119, Section 5], the equation for a rod becomes the Helmholtz equation:

$$\frac{\partial^2 u_z}{\partial t^2} = \frac{E}{\rho} \frac{\partial^2 u_z}{\partial z^2} \tag{C.13}$$

Therefore, the sound speed c for longitudinal waves in a rod is a function of the Youngs modulus and the mass density:

$$c^2 = \frac{E}{\rho} \tag{C.14}$$

Appendix D

Harmonic Many Body

D.1 Many-Body GF: Scattering Theory

The scattering theory used here is from Chapter 5 in Joachain's two-volume book [120]. The objective is to find the function $\psi(r)$ that satisfies an inhomogeneous Helmholtz equation:

$$\left[\nabla_r^2 + k^2\right] \psi(r) = U(r)\psi(r) \tag{D.1}$$

The integral equation for $\psi(r)$ is the Lippmann-Schwinger equation:

$$\psi(r) = \Phi(r) + \int G_\circ(r|r')\, U(r')\, \psi(r')\, \mathrm{d}r' \tag{D.2}$$

where

$$\left[\nabla_r^2 + k^2\right] \Phi(r) \;=\; 0 \tag{D.3}$$

$$\tag{D.4}$$

$$\left[\nabla_r^2 + k^2\right] G_\circ(r|r') \;=\; \delta(r - r') \tag{D.5}$$

The function $\psi(r)$ is a sum of the homogeneous solution $\Phi(r)$ and a scattering function $\psi_{sc}(r)$:

$$\psi(r) = \Phi(r) + \psi_{sc}(r) \tag{D.6}$$

Given that

$$\left[\nabla_r^2 + k^2 - U(r)\right]\psi(r) = 0$$

we wish to solve the following equation:

$$\left[\nabla_r^2 + k^2 - U(r)\right]\Phi(r) + \left[\nabla_r^2 + k^2 - U(r)\right]\psi_{sc}(r) = 0 \tag{D.7}$$

Substituting for $\Phi(r)$ from Eqn. D.3 gives the inhomogeneous equation for the scattering function $\psi(r)$:

$$\left[\nabla_r^2 + k^2 - U(r)\right]\psi_{sc}(r) = U(r)\,\Phi(r) \tag{D.8}$$

This is the inhomogeneous equation we need to solve. This is also why Shankar [121, Section 19.4] refers to $\Phi(r)$ as the source of the scattering.

Given a *total* GF$G(r|r')$ that satisfies

$$\left[\nabla_r^2 + k^2 - U(r)\right]G(r|r') = \delta(r - r') \tag{D.9}$$

the integral equation for $\psi_{sc}(r)$ is

$$\psi_{sc}(r) = \int G(r|r')\,U(r')\,\Phi(r')\,\mathrm{d}r' \tag{D.10}$$

The solution for $\psi(r)$ adds the homogeneous function $\Phi(r)$:

$$\psi(r) = \Phi(r) + \int G(r|r')\,U(r')\,\Phi(r')\,\mathrm{d}r' \tag{D.11}$$

The solution continues by solving for the total GF$G(r|r')$.

Rearranging Eqn. D.9 give the PDE for $G(r|r')$:

$$\left[\nabla_r^2 + k^2\right]G(r|r') = \delta(r - r') + U(r)\,G(r|r') \tag{D.12}$$

This is an inhomogeneous PDE for $G(r|r')$, where the homogeneous solution is $G_\circ(r|r')$. The integral equation for $G(r|r')$ is

$$G(r|r') = G_\circ(r|r') + \int G_\circ(r|r'')\,U(r'')\,G(r''|r')\,\mathrm{d}r'' \tag{D.13}$$

The solution for $\psi(r)$ is now one of solving for total GF$G(r|r')$ and substituting into Eqn. D.11

D.2 Cross Section

The development of the previous section can be used to calculate the 1-D scattering cross section of a single scatterer. Consider a single mass impurity located at x_i. The total GFin Eqn. D.13 is calculated using 1-D Helmholtz GF$G_\circ(x|x')$ [60] and a delta function for the potential $U(x)$:

$$G_\circ(x|x') = \frac{\mathrm{i}}{2k}\mathrm{e}^{\mathrm{i}k|x-x'|} \qquad\qquad U(x) = \alpha\,\delta(x-x_i) \tag{D.14}$$

The GFis expanded

$$\begin{aligned} G(x|x') &= G_\circ(x|x') + \int \mathrm{d}x'' G_\circ(x|x'')U(x'')G_\circ(x''|x') \\ &\quad + \int \mathrm{d}x'' G_\circ(x|x'')U(x'') \int \mathrm{d}x''' G_\circ(x''|x''')U(x''')G_\circ(x'''|x') \\ &\quad + \cdots \\ \\ &= \left(\frac{\mathrm{i}}{2k}\right), \mathrm{e}^{\mathrm{i}k|x-x'|} + \alpha\left(\frac{\mathrm{i}}{2k}\right)^2 \mathrm{e}^{\mathrm{i}k|x-x_i|}\mathrm{e}^{\mathrm{i}k|x_i-x'|} \\ &\quad + \alpha^2\left(\frac{\mathrm{i}}{2k}\right)^3 \mathrm{e}^{\mathrm{i}k|x-x_i|}\mathrm{e}^{\mathrm{i}k|x_i-x\prime|} + \cdots \\ \\ &= \frac{1}{\alpha}\left[\left(\frac{\mathrm{i}\alpha}{2k}\right)\mathrm{e}^{\mathrm{i}k|x-x'|} + \mathrm{e}^{\mathrm{i}k|x-x_i|}\mathrm{e}^{\mathrm{i}k|x_i-x\prime|}\sum_{n=2}^{\infty}\left(\frac{\mathrm{i}\alpha}{2k}\right)^n\right] \end{aligned}$$

This result is the total GFused to solve for the scattering function ψ_{sc}:

$$\begin{aligned}
\psi_{sc} &= \int \mathrm{d}x' G(x|x') U(x') \Phi(x') \\
&= \mathrm{e}^{\mathrm{i}kx_i} \left[\left(\frac{\mathrm{i}\alpha}{2k} \right) \mathrm{e}^{\mathrm{i}k|x-x_i|} + \mathrm{e}^{\mathrm{i}k|x-x_i|} \sum_{n=2}^{\infty} \left(\frac{\mathrm{i}\alpha}{2k} \right)^n \right] \\
&= \left(\frac{\mathrm{i}\alpha}{2k - \mathrm{i}\alpha} \right) \mathrm{e}^{\mathrm{i}kx_i} \mathrm{e}^{\mathrm{i}k|x-x_i|}
\end{aligned}$$

The complete function $\psi(x)$ adds to this the homogeneous solution:

$$\psi(x) = \mathrm{e}^{\mathrm{i}kx} + \left(\frac{\mathrm{i}\alpha}{2k - \mathrm{i}\alpha} \right) \mathrm{e}^{\mathrm{i}kx_i} \mathrm{e}^{\mathrm{i}k|x-x_i|} \tag{D.15}$$

The function ψ can be separated into the "upstream" ($x_<$) and "downstream" ($x_>$) solutions:

$$\begin{aligned}
\psi(x_<) &= \mathrm{e}^{\mathrm{i}kx} + \left(\frac{\mathrm{i}\alpha \mathrm{e}^{2\mathrm{i}kx_i}}{2k - \mathrm{i}\alpha} \right) \mathrm{e}^{-\mathrm{i}kx} \\
\psi(x_>) &= \left(\frac{2k}{2k - \mathrm{i}\alpha} \right) \mathrm{e}^{\mathrm{i}kx}
\end{aligned}$$

In this form, the reflection amplitude r and transmission amplitude t are immediately apparent:

$$r = \left(\frac{\mathrm{i}\alpha \mathrm{e}^{2\mathrm{i}kx_i}}{2k - \mathrm{i}\alpha} \right) \tag{D.16}$$

$$t = \left(\frac{2k}{2k - \mathrm{i}\alpha} \right) \tag{D.17}$$

It is interesting to note that the phase $Ph\{\}$ of the reflected wave depends on the location of the impurity, but the phase of the transmitted wave is independent of its position:

$$Ph\{t\} = \mathrm{Tan}^{-1} \frac{\alpha}{2k} \tag{D.18}$$

Finally, the scattering cross section σ in 1-D is the reflection probability $|r|^2$.

$$\sigma = \frac{\alpha^2}{4k^2 + \alpha^2}$$

Appendix E

Harmonic Disorder Initial Condition

The initial steady state condition for the harmonic disordered system can be estimated from the continuum solution. The general solution is represented by the complex displacement function $\psi(x,t)$, from which the displacements of the physical system are calculated from the real component of ψ. Since we are interested in the single frequency ω solution, the displacement function can be decomposed into separate displacement and temporal components:

$$\psi(x,t) = \phi(x)\,\mathrm{e}^{-i\omega t} \tag{E.1}$$

E.1 Constitutive Equation

Table E.1: Mechanical impedance of impurities: mass, spring, and resistor.

Impurity	$Z(\omega)$
Mass	$-i\omega m_+$
Spring	$+iK/\omega$
Resistor	R

The difference between the kinetic and potential components of the string equation is the reactance [43] from the impurities located at x'_n:

$$\rho \frac{\partial^2 \psi}{\partial t^2} - Y \frac{\partial^\psi}{\partial x^2} = - \sum_n Z(\omega)\, \delta(x - x'_n) \frac{\partial \psi}{\partial t} \tag{E.2}$$

The quantities ρ and Y are the mass density and Young's modulus of the pure string. The quantity $Z(\omega)$ is the impedance of the impurity. The impedance of three types of impurity are shown in Table E.1. Upon substituting from both Eqn. E.1 and Table E.1 yields the governing equation for the spatial displacement function $\phi(x)$:

$$\left[\nabla^2 + k^2\right]\ \phi(x) = -m_+ \omega^2 \delta\left(x - x'_n\right) \phi(x) \tag{E.3}$$

This equation can be used to describe the behavior of the function ϕ at each impurity. Using physical arguments, the function ϕ must be continuous across an impurity. The derrivative of ϕ will not be continuous. Integrating Eqn. E.3 across the n-th impurity,

$$\int_{x'_n - \epsilon}^{x'_n + \epsilon} \left[\nabla^2 + k^2 = -m_+ \omega^2 \delta(x - x'_n)\right]\ \phi(x)\ \mathrm{d}x \tag{E.4}$$

reveals that the change in derrivative across an mass impurity is proportional to the impurity mass:

$$\left.\frac{d\phi}{dx}\right|_{x'_n + \epsilon} - \left.\frac{d\phi}{dx}\right|_{x'_n - \epsilon} = -m_+ \omega^2\ \phi(x'_n) \tag{E.5}$$

E.2 Matrix Solution

Between impurities, the spatial function ϕ satisfies the Helmholtz equation:

$$\left[\nabla^2 + k^2\right]\ \phi = 0 \tag{E.6}$$

Therefore, in the n-th interval, between the impurities labelled n and $n+1$, the function $\phi_n(x)$ can be represented by counter propagating waves, each with arbitrary complex amplitude:

$$\phi_n(x) = A_n \mathrm{e}^{+ikx} + B_n \mathrm{e}^{-ikx} \tag{E.7}$$

Assuming N impurities, there are $N-1$ intervals with a total of $2(N-1)$ unknown amplitudes A_n and B_n. The amplitude A_0 is the boundary condition, and one assumes there is no reflected wave after the last impurity ($B_N = 0$). The result is a system of $2N$ unknowns and $2N$ constraints, the solution of which can be found using exising linear algebra computer program libraries.

E.2.1 First Impurity

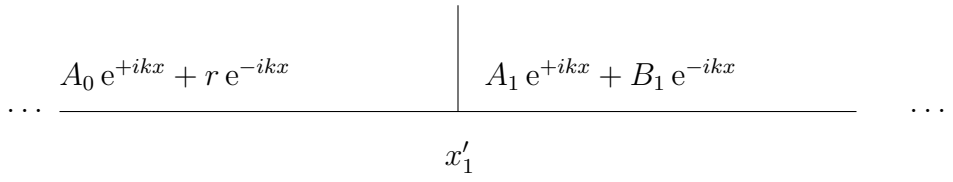

Figure E.1: Schematic for the first impurity.

$$A_0\mathrm{e}^{+ikx_1'} + r\mathrm{e}^{-ikx_1'} = A_1\mathrm{e}^{+ikx_1'} + B_1\mathrm{e}^{-ikx_1'}$$

$$+ikA_1\mathrm{e}^{+ikx_1'} - ikB_1\mathrm{e}^{-ikx_1'} - ikA_0\mathrm{e}^{+ikx_1'} + ikr\mathrm{e}^{-ikx_1'} \tag{E.8}$$

$$= -m_+\omega^2(A_0\mathrm{e}^{+ikx_1'} + r\mathrm{e}^{-ikx_1'}) \tag{E.9}$$

These equations can be expressed in matrix form:

$$\begin{bmatrix} \mathrm{e}^{-2ikx'_1} & -1 & -\mathrm{e}^{-2ikx'_1} \\ (ik+m_+\omega^2)\mathrm{e}^{-2ikx'_1} & +ik & -ik\mathrm{e}^{-2ikx'_1} \end{bmatrix} \begin{bmatrix} r \\ A_1 \\ B_1 \end{bmatrix} = \begin{bmatrix} -A_0 \\ A_0(ik-m_+\omega^2) \end{bmatrix} \tag{E.10}$$

E.2.2 Middle Impurity

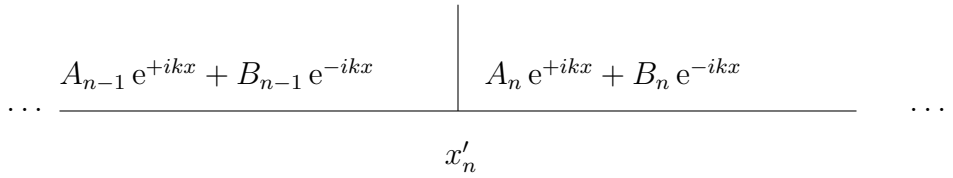

Figure E.2: Schematic for the n-th impurity.

The middle matrix elements, corresponding to intervals 1 through N-1, all have the same form, regardless of the boundary condition. The constraint that the displacement be continuous, and that its derivative obey Eqn. E.5, yields the following two constraint equations at the n-th impurity:

$$A_{n-1}\mathrm{e}^{+ikx'_n} + B_{n-1}\mathrm{e}^{-ikx'_n} = A_n\mathrm{e}^{+ikx'_n} + B_n\mathrm{e}^{-ikx'_n}$$

$$+ikA_n\mathrm{e}^{+ikx'_n} - ikB_n\mathrm{e}^{-ikx'_n} - ikA_{n-1}\mathrm{e}^{+ikx'_n} + ikB_{n-1}\mathrm{e}^{-ikx'_n} \tag{E.11}$$

$$= -m_+\omega^2(A_n\mathrm{e}^{+ikx'_n} + B_n\mathrm{e}^{-ikx'_n}) \tag{E.12}$$

These equations can be expressed in matrix form:

$$\begin{bmatrix} +1 & \mathrm{e}^{-2ikx'_n} & -1 & -\mathrm{e}^{-2ikx'_n} \\ ik - m_+\omega^2 & (-ik - m_+\omega^2)\mathrm{e}^{-2ikx'_n} & -ik & +ik\mathrm{e}^{-2ikx'_n} \end{bmatrix} \begin{bmatrix} A_{n-1} \\ B_{n-1} \\ A_n \\ B_n \end{bmatrix} = 0 \tag{E.13}$$

E.2.3 Last Impurity

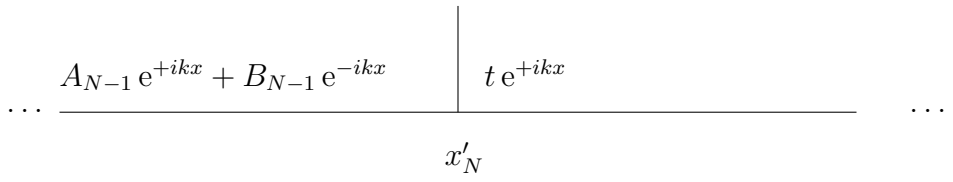

Figure E.3: Schematic for the last impurity.

$$A_{N-1}\mathrm{e}^{+ikx'_N} + B_{N-1}\mathrm{e}^{-ikx'_N} = t\mathrm{e}^{+ikx'_N}$$

$$+ikt\mathrm{e}^{+ikx'_N} - ikA_{N-1}\mathrm{e}^{+ikx'_N} + ikB_{N-1}\mathrm{e}^{-ikx'_N} \tag{E.14}$$

$$= -m_+\omega^2 t\mathrm{e}^{+ikx'_N} \tag{E.15}$$

These equations can be expressed in matrix form:

$$\begin{bmatrix} +1 & \mathrm{e}^{-2ikx'_N} & -1 \\ ik & -ik\mathrm{e}^{-2ikx'_N} & -(ik + m_+\omega^2) \end{bmatrix} \begin{bmatrix} A_{N-1} \\ B_{N-1} \\ t \end{bmatrix} = 0 \tag{E.16}$$

E.3 Projection to Physical Space

The coefficients A_n and B_n determine the continuum analytical solution for the functions $\phi_n(x)$ in Eqn. E.7. Each ϕ_n determines the wave amplitude between consecutive impurities. The displacement of the β-FPU chain is taken from the real component $\Re\{\ \}$ of the amplitude ϕ_n:

$$u(x) = \Re\{\phi_n\}(x) \qquad\qquad x'_n \leq x \leq x'_{n+1} \tag{E.17}$$

E.4 Boundary Adjustment for Zero Displacement

The calculations will, for the most part, be performed using fixed ends: the displacement at both ends is zero. In general, the projected physical displacement function $u(x)$ is not zero at either physical boundary. Therefore, a method is needed to ensure zero displacement at the ends of the FPU chain.

Unfortunately, one cannot simply assert $u(0) = 0$ and $u(L) = 0$ because the solution $u(x)$ may be near a maximum at either end, and so forcing values to zero would initiate a wave that having a different natural frequency from the eigenwave. This disturbance would then propagate through the disordered system, and the energy R^2 would not be a constant.

The solution used here was to project the continuum solution onto $u(x)$ as described above, and then remove masses at both ends until one findes the mass having a displacement closest to zero. In principle, one should only have to remove, at most, a small number of wavelengths of the eigenmode. Once this mass is found, it is assigned a displacement of zero, and becomes the end of the chain.

To improve upon this technique, a specific wavelength is chosen to ensure

finding a displacement near zero. If the wavelength is an integer multiple of the unit displacement a, as one moves into the chain searching for the displacement closest to zero, the value closest to zero will repeat itself with each consecutive wavelength number of masses. In fact, the minimum will repeat itself every $\lambda/2$ masses.

At each end of the chain, the spatial dependence of the displacement field $u(x)$ can be expressed as a sinusoid with amplitude C, wavenumber k and arbitrary phase ϑ:

$$u(x) = C\sin(kx + \vartheta) \tag{E.18}$$

For a wavelength that is an even integer multiple of the unit spacing a, the displacement will be represented by a mass with zero displacement one every $\Delta\vartheta = 2\pi a/\lambda$; half this value for odd integer wavelengths.

By contrast, if the wavelength is a non-integer multiple of the unit mass separation a, each consecutive wavelength of masses will give a different displacement closest to zero. In principle, the change in the phase ϑ could be vanishingly small, but the number of masses that must be removed to find that particular near-zero displacement may be large. Although, in principle, an irrational wavelength would be best, there is a practical upper limit to the number of masses that can be removed and the system retain its overall characteristics. Moreover, the concentration of impurities sets the upper limit of the number of masses through which one can pass before the phase is changed by the presence of the impurity. Therefore, by picking this practical upper limit, one can then make a sensible determination for a suitable displacement wavelength.

Alternatively, one can start with a nominal wavelength λ_o that is an integer multiple of the unit spacing a. The working wavelength λ is calculated from the

following relation with integer N:

$$\lambda = \frac{N\lambda_o - 1}{N} \tag{E.19}$$

The displacement starting with zero displacement at $x = 0$ will return to zero displacement after a distance $N\lambda$. In the interval $[0, N\lambda]$, the displacement will intersect zero $2N - 1$ times, but not at integer values of x. Now, the phase angle ϑ separating consecutive intersections of zero at integer values of x has been reduced by a factor of $(2N - 1)$:

$$\Delta\vartheta = \frac{2\pi a}{\lambda(2N - 1)} \tag{E.20}$$

For the purposes of these calculations, a value of $N = 5$ was chosen as a sensible balance between finding a near-zero displacement and removing as few masses as possible.

A typical value for the nominal wavelength λ_o is 32. Using $N = 5$ from above, the working wavelength $\lambda = 31.8$. Therefore, the phase difference between consecutive intersections is approximately

$$\Delta\vartheta = 0.0035 \times 2\pi \tag{E.21}$$

Equivalently, the mass having the displacement closest to zero should be within a distance

$$\Delta x = \frac{a}{2N - 1} \tag{E.22}$$

of the true value.

Given that the magnitude of the amplitudes are of order 1, the slope of a sinusoid near zero displacement is proportional to the wavenumber k. The mass found having a displacement closest to zero will typically have a displacement

differing from zero by an amount

$$\Delta u = \frac{2\pi a}{\lambda(2N-1)} \tag{E.23}$$

A sampling from 19 systems yielded (0.021± 0.015) for the magnitude of the distance to the actual zero displacement point.

Appendix F

Transport Data Analysis

The analyses of the results in Chapter 4 involve some minor subtleties that deserve a clear exposition. Neglecting these subtleties and performing an ordinary least squares (OLS) analysis of the data would lead to misleading results. Specifically, not adjusting for initial transient behavior would lead to a different conclusion regarding the existence of diffusive energy transport.

As mentioned in Section 4.6, the reported uncertainties are the standard error (SE) [92] that was calculated from the ensemble population standard deviation s. For an ensemble of W systems, the SE reported here is $s/\sqrt{W}$. This uncertainty characterizes the reported average value from the population.

F.1 Energy Fluctuation

For each calculation, the total energy $E(t)$ was calculated as a function of time. Due to randomness, the initial total energy fluctuates among the ensembles. To ensure that values of E were on comparable scales, the values were divided by the initial value $E(0)$. The ratio $E_m(t)/E_m(0)$ $(1 \leq m \leq W)$ is calculated as a function of time for each of the W systems composing the ensemble. The averaged

values are calculated at each of the P values of t_i:

$$\overline{E}(t_i) = \frac{1}{W} \sum_{m}^{W} \frac{E_m(t_i)}{E_m(0)} \qquad 1 \leq i \leq P \tag{F.1}$$

These averaged values, along with the population standard deviation, are pooled and stored in the output data file. The population of W values at t_i do not, unfortunately, represent energy fluctuation for a single system. Rather, it characterizes statistical fluctuations among the different systems, evaluated at the same time.

Energy fluctuation can only be approximated from fluctuations in the P average values of $\overline{E}(t_i)$. The standard deviation $s_{\overline{E}}$ of each $\overline{E}(t_i)$ represents a standard deviation in the mean. The population standard deviation is approximated by $s_{\overline{E}}\sqrt{P}$. This population standard deviation was never more than 0.2 %. Spot checks of $E(t)$ in individual systems rarely gave a standard deviation greater than 0.2 %.

F.2 M_1 Data Collection

There were, in principle, a number of methods for collecting the $M(t)$ data. One approach would have been to analyze M_1 versus t for each system. An alternate approach would have been to generate a rolling average of the $M_1(t)$ data. Performing an analysis on each system is problematic because of the large variability that can occur among systems. The challenge with the rolling average is to determine how the collection should be performed.

Here, the values $M_1(t_i)$ were collected at identical regular intervals for each realization. In effect, this is the first moment of $M_1(t_i)$. By also collecting $M_1^2(t_i)$, the second moment about the mean (variance) in M_1 can be calculated to estimate

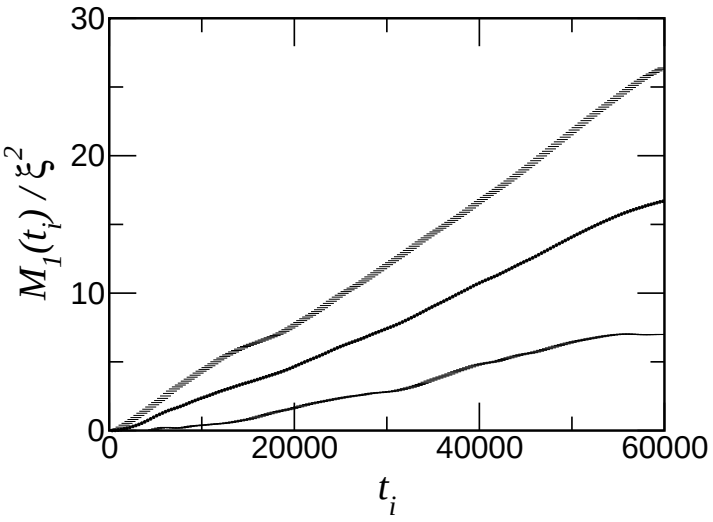

Figure F.1: As collected $M_1(t_i)$ data, scaled by the localization length ξ for convenience. The mean values are represented by the small circles. The short horizontal lines above and below the mean are the population standard deviations for each $M_1(t_i)$.

the population standard deviation for $M_1(t_i)$.

Data were collected for the $L = 64\ 000$, $\sigma = 0.30$, and $c = 0.002$ systems and averaged as explained. The results are shown in Fig. F.1. The mean values are the middle row of small filled circles. The short horizontal lines denote the population standard deviation of $M_1(t_i)$; the error bar risers were omitted for clarity. The significant point to take from Fig. F.1 is that the uncertainties are growing in time. As a result, one cannot apply ordinary least squares analysis on the data without first addressing this fact.

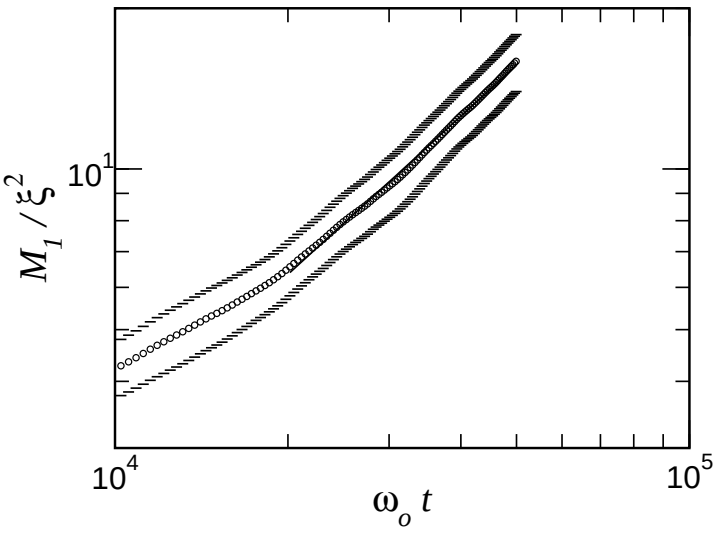

Figure F.2: A log-log plot of data in Fig. F.1, along with horizontal error bars denoting the population standard deviation; the vertical risers are omitted for clarity. The solid line was determined by OLS regression applied to the mean values.

F.3 δ_n Analysis

The straightforward means of determining the time exponent δ_n is from the slope of a log-log plot of M_n versus time t. Unfortunately, some of the systems exhibited an initial transient period. To account for this, the origin is relocated to the last M_1 datum before the time intervals given in Table 4.1. The time exponent δ is calculated from the slope of the mean values in log-log space.

The uncertainty in δ_n is calculated from both the regression residuals and the ensemble population of M_n values. Fortunately, because the population standard deviation in M_n increases in time, the logarithm transform yields uncertainties that are nearly constant over the time intervals of interest. A log-log plot of the

data from Fig. F.1 are shown in Fig. F.2, along with the ensemble population standard deviations that are denoted by horizontal error bars. The ensemble population standard deviation, instead of the SE, is shown in the figure for clarity of the demonstration. For an ensemble of W systems, the SE error bars would be a factor of $\sqrt{W}$ smaller than those shown in the figure. Also shown in Fig. F.2 is the result of the regression analysis of the average values. The error bars denote the ensemble uncertainty, and the residuals represent the regression uncertainty.

The OLS linear regression in log-space will yield an estimated uncertainty (standard deviation) for slope that is a function of the standard error of the residuals. The standard error s can be used to estimate the regression standard deviation s_{reg} for the slope δ_n:

$$s_{reg} = \frac{s}{\sqrt{S_{XX}}} \tag{F.2}$$

where the quantity S_{XX} is the sum of squares:

$$S_{XX} = \sum_i \left(\ln t_i - \overline{\ln t}\right)^2 \tag{F.3}$$

The quantity $\overline{\ln t}$ represents the average value over the specified interval.

The uncertainty in δ_n should also reflect the SE recorded for the ensemble s_{ens}. It is assumed that these two uncertainties are independent of one another, and that they are additive. The uncertainty (estimated standard deviation) in the time exponent is

$$s_{\delta_n}^2 = \frac{s_{res}^2}{S_{XX}} + \frac{s_{ens}^2}{S_{XX}} \tag{F.4}$$

Because s_{ens} is the majority of s_{δ_n}, the uncertainty in δ_n is referred to as a SE, and the coverage factor is approximately equivalent to one standard deviation for a normal distribution.

F.4 M_1 Analysis

Based on the results of the δ_1 analysis, an estimate for G_1 is based on the assumption of a linear relationship between M_1 and time t. The ability to use a linear model simplifies the analysis of M_1. As for the δ analysis, the origin is relocated to the beginning of the appropriate interval in Table 4.1. The transport coefficient $2G_1$ is the slope.

The uncertainty in $2G_1$ cannot be determined from a regression analysis of the M_1 versus t data because the uncertainties in M_1 increase in time, as was shown in Fig. F.1. Fortunately, the data can be transformed into a more suitable format for the purpose of estimating the uncertainty in G.

Assuming diffusive behavior, the values of M_1 are a collection of lines, radiating from the origin. The error model for the observations assumes that there exists an inherent error ϵ and that the total error increases with time:

$$M_n(t_i) = A + 2G_n\, t_i + t_i\epsilon_i \tag{F.5}$$

To use OLS techniques, the error term must be additive and constant. Equation (F.5) can be transformed into a suitable model:

$$\frac{M_n(t_i)}{t_i} = \frac{A}{t_i} + 2G_n + \epsilon_i \tag{F.6}$$

Unfortunately, any initial transient behavior must be accounted for. The error model assumes that the uncertainty grows linearly from $t = 0$. In reality, the increase in M_n occurred after some initial transient time $t_\circ$. To correct for this, linear regression is applied to the M_1 versus t data to determine the value of $t_\circ$. Using $t_\circ$, the data are shifted horizontally so that the linear region of interest points to the origin. These shifted data are then transformed according to Eq. (F.6).

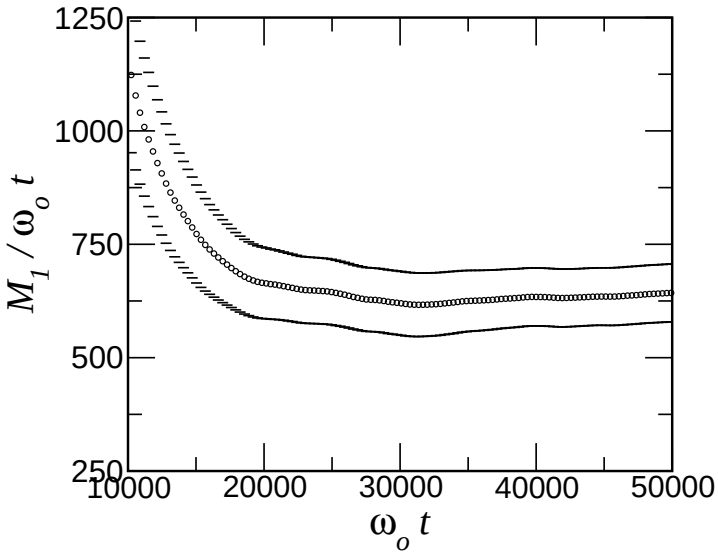

Figure F.3: Transformed M_1 to demonstrate how uncertainty in δ_1 is calculated.

The result of this transform, applied to both the mean and SE, is shown in Fig. F.3 for the data in Fig. F.1. In Fig. F.3, the error bars represent the SE. Over the range of regression (see Table 4.1), the SE is relatively constant, consistent with Eq. (F.6). Because the model in Eqn. (F.6) assumes a constant factor of $2G_1$, the error bars in Fig. F.3 represent the SE for $2G_1$.

Appendix G

Programming Data Structures

A number of individual computer programs were written to perform the calculations required to produce the results presented here. The programs that were used to perform significant calculations were written in the `FORTRAN 90` programming language. The choice to use `FORTRAN 90` was based on availability, utility, and programming structure. Moreover, the `FORTRAN 90` library interface to `LAPACK` required far less effort.

The modular nature of `FORTRAN 90` was exploited to create an `FPUsystem` data structure upon which useful operations were performed. The objective was to create a data structure that was self-contained; it contained enough internal information to perform operations such as initialization and numerical integration.

The `FPUsystem` data structure then led to rapid application development. Generally, differences occurred in the user interface and conversion of parameters into the type required by `FPUsystem`

G.1 FORTRAN 90 Modules

The following is a template for a FORTRAN 90 module. It is meant only to guide the reader through though the general makeup of a FORTRAN 90 module file. These files have a .F90 extension so that the compiler understands that the formatting adheres to FORTRAN 90 conventions, and is compiled into an object file; the compiler automatically makes a module file with a .mod extension.

TEMPLATE

```
MODULE mymodule

  PUBLIC
    ! Define user accessible variables

  PRIVATE
    ! Variables private to mymodule

  CONTAINS
    ! Module SUBROUTINES and FUNCTIONS

END MODULE mymodule
```

G.2 `math` Module

Although rather minor, a `math` module was made to define the single precision and double precision data types. In addition, commonly used numbers are defined. It was originally thought that this module would grow, which is why it is separate from the main `fpu` module that follows.

math

```
!!!!!!!!!!!!!!!!!!!!!!!!!!!!!!!!!!!!!!!!!!!!!!!!!!!!!!!!!!!!
! MODULE math
!
!    Define single and double precision
!    Define pi and other commonly used numbers
!!!!!!!!!!!!!!!!!!!!!!!!!!!!!!!!!!!!!!!!!!!!!!!!!!!!!!!!!!!!

MODULE math
  PUBLIC
    INTEGER, PARAMETER          :: single=SELECTED_REAL_KIND(6,37)
    INTEGER, PARAMETER          :: double=SELECTED_REAL_KIND(15,307)

    !!!!!!!!!!!!!!!!!!!!!!!!!!!!!!!!!!!!!!!!!!!!!!!!!!!!!!!!!!!!
    !  Common numbers
    !!!!!!!!!!!!!!!!!!!!!!!!!!!!!!!!!!!!!!!!!!!!!!!!!!!!!!!!!!!!
    REAL (double), PARAMETER    :: PI = 3.141592653589793_double
    REAL (double), PARAMETER    :: TWO = 2._double
    REAL (double), PARAMETER    :: ONE_HALF = 0.5_double
END MODULE math
```

G.3 `fpu` Module

The `fpu` module contains both the `FPUsystem` data type and all the relevant subroutines and functions associated with the data type. It is the core of all the FPU calculations. It was designed to be general enough to handle tasks such as cross section calculations, energy calculations, localization parameter, Fourier transforms, etc.

The organization of the `fpu` module is similar to that for `C++` classes. The data structure type `FPUsystem` is defined by all the member data. The `CONTAINS` section begins with an `Init()` subroutine that corresponds to a `C++` constructor. The next subroutine is `Clear()` that acts as the class destructor by deleting all the allocated memory that was performed in `Init()`; this function is useful for overwriting an object by first `Clear`-ing the object and then `Init`-ializing the new version.

The subroutines and functions that follow `Clear()` operate on the class type `FPUsystem`. Generally, the first argument of any subroutine or function is an object of type `FPUsystem`. There are routines to initialize the system, integrate the system, and perform post-processing calculations on the present state of the system.

fpu: PUBLIC

```
!!!!!!!!!!!!!!!!!!!!!!!!!!!!!!!!!!!!!!!!!!!!!!!!!!!!!
!
!  MODULE fpu
!
!    This module contains all the necessary
!  subroutines and functions for operating on
!  an Fermi-Pasta-Ulam system of masses and springs.
!
!!!!!!!!!!!!!!!!!!!!!!!!!!!!!!!!!!!!!!!!!!!!!!!!!!!!!
MODULE fpu
  USE math
  IMPLICIT NONE

  PUBLIC
  !!!!!!!!!!!!!!!!!!!!!!!!!!!!!!!!!!!!!!!!!!!!!!!!!!!!
  !  System Configurations
  !!!!!!!!!!!!!!!!!!!!!!!!!!!!!!!!!!!!!!!!!!!!!!!!!!!!
  INTEGER, PARAMETER    :: LINE = 0   ! Zero-displacement ends
  INTEGER, PARAMETER    :: HOOP = 1   ! Periodic boundary conditions
  INTEGER, PARAMETER    :: FREE = 2   ! Free ends
  INTEGER, PARAMETER    :: TAIL = 3   ! Semi-Infinite

  !!!!!!!!!!!!!!!!!!!!!!!!!!!!!!!!!!!!!!!!!!!!!!!!!!!!
  !  Consideration for greater than cubic forces
  !!!!!!!!!!!!!!!!!!!!!!!!!!!!!!!!!!!!!!!!!!!!!!!!!!!!
  INTEGER, PARAMETER    :: MAX_EXPONENT = 5

  !!!!!!!!!!!!!!!!!!!!!!!!!!!!!!!!!!!!!!!!!!!!!!!!!!!!
  !  FPUsystem data structure:
  !     Entirely self-contained so that all one needs to pass
  !     as a parameter is the structure
  !!!!!!!!!!!!!!!!!!!!!!!!!!!!!!!!!!!!!!!!!!!!!!!!!!!!
  TYPE :: FPUsystem
    INTEGER                                  :: Length ! system length
    INTEGER                                  :: Config
                                                    ! = HOOP|LINE|FREE
    LOGICAL                                  :: HasBeenAllocated
    REAL (double), DIMENSION(:), POINTER  :: y    ! mass displacement
    REAL (double), DIMENSION(:), POINTER  :: v    ! mass velocity
    REAL (double), DIMENSION(:), POINTER  :: mass
    REAL (double), DIMENSION(:), POINTER  :: invmass  ! integrator
    REAL (double), DIMENSION(:), POINTER  :: eps,disp ! strain
    REAL (double), DIMENSION(:), POINTER  :: F    ! force on mass
    REAL (double), DIMENSION(:), POINTER  :: alpha  ! force exponents
```

```
42    REAL (double), DIMENSION(:), POINTER  :: alphaTau ! time scale
43    REAL (double), DIMENSION(:), POINTER  :: viscosity  ! damping
44    REAL (double), DIMENSION(:), POINTER  :: Ex     ! energy(x)
45    REAL (double), DIMENSION(:), POINTER  :: ExInit ! initial Ex
46    LOGICAL                               :: FirstEx  ! 1st Ex eval ?
47    REAL (double), DIMENSION(:), POINTER  :: Ec     ! cumulative Ex
48    REAL (double), DIMENSION(:), POINTER  :: AndersonAmp
49                                                ! initial amp.
50    REAL (double), DIMENSION(:), POINTER  :: Psi2! Interval amplitude
51    REAL (double)                         :: dT     ! integrator dt
52    REAL (double)                         :: time   ! age of system
53    REAL (double)                         :: Etime ! last Energy eval
54    REAL (double)                         :: k      ! wave number
55    REAL (double)                         :: omega  ! angular freq.
56    REAL (double)                         :: MaxFreq
57    REAL (double)                         :: Etot,R2E,R2E2,R2Ec,H2
58    INTEGER                               :: MaxExponent
59                                                ! max force exp.
60    INTEGER                               :: IntegrationOrder  ! 4|6
61    INTEGER                               :: Nmasses
62    INTEGER                               :: InitLength
63    INTEGER                               :: InitNmasses
64    INTEGER                               :: Nleft,Nright
65                                                !HOOP neighbors
66    INTEGER                               :: MPI_Buffer  ! MPI info
67    REAL (double)                         :: MPI_Xleft   ! MPI info
68  END TYPE FPUsystem
```

fpu: PRIVATE

```
69  !!!!!!!!!!!!!!!!!!!!!!!!!!!!!!!!!!!!!!!!!!!!!!!!!!!!!!!!!!!!
70  !  Private variables:
71  !!!!!!!!!!!!!!!!!!!!!!!!!!!!!!!!!!!!!!!!!!!!!!!!!!!!!!!!!!!!


72  !!!!!!!!!!!!!!!!!!!!!!!!!!!!!!!!!!!!!!!!!!!!!!!!!!!!!!!!!!!!
73  !     These are various integrator coefficients
74  !!!!!!!!!!!!!!!!!!!!!!!!!!!!!!!!!!!!!!!!!!!!!!!!!!!!!!!!!!!!
75  REAL (double), DIMENSION(20), PRIVATE         :: An, Bn
76  REAL (double), PRIVATE                        :: w0, w1, w2, w3
77  REAL (double), DIMENSION(20), PRIVATE         :: w

78  !!!!!!!!!!!!!!!!!!!!!!!!!!!!!!!!!!!!!!!!!!!!!!!!!!!!!!!!!!!!!
79  ! FORMATting info for writing and reading systems to/from files.
80  ! This facilitates restarting a stopped integration.
81  ! The use of '#' allows one to use the gnuplot 'plot'
82  !     command on the file.
83  !!!!!!!!!!!!!!!!!!!!!!!!!!!!!!!!!!!!!!!!!!!!!!!!!!!!!!!!!!!!!
84  INTEGER, PARAMETER, PRIVATE      :: FILE_VERSION = 1
85                                        ! FPUsystem file type
86  CHARACTER*20, PARAMETER, PRIVATE :: LINE_1_FMT="'# ',I"
87  CHARACTER*20, PARAMETER, PRIVATE :: LINE_2_FMT="'# ',I,I,I"
88  CHARACTER*20, PARAMETER, PRIVATE :: LINE_3_FMT="'# ',F,F,F"
89  CHARACTER*20, PARAMETER, PRIVATE :: LINE_4_FMT="'# ',I"
90  CHARACTER*20, PARAMETER, PRIVATE :: LINE_5_FMT="'# ',6F12.8"
91  CHARACTER*20, PARAMETER, PRIVATE :: LINE_6_FMT="'# ',I6,F"
92  CHARACTER*20, PARAMETER, PRIVATE :: LINE_7_FMT="A"
93  CHARACTER*20, PARAMETER, PRIVATE :: LINE_N_FMT="I5,3E25.14E3"
```

fpu: Init()

```
94  !!!!!!!!!!!!!!!!!!!!!!!!!!!!!!!!!!!!!!!!!!!!!!!!!!!!!!!!!!!!
95  !  FPUsystem module functions and subroutines
96  !      These perform actions on the FPUsystem such
97  !      as initialization and numerical integration.
98  !!!!!!!!!!!!!!!!!!!!!!!!!!!!!!!!!!!!!!!!!!!!!!!!!!!!!!!!!!!!
99  CONTAINS

100 !!!!!!!!!!!!!!!!!!!!!!!!!!!!!!!!!!!!!!!!!!!!!!!!!!!!!!!!!!!!
101 !  Initialize an FPU system
102 !
103 !      Length         (integer)               length of system
104 !      Configuration  (integer)               HOOP|LINE|FREE
105 !      IntOrder       (integer) [OPTIONAL]    Integration Order
106 !                                                 (4,6,10)
107 !!!!!!!!!!!!!!!!!!!!!!!!!!!!!!!!!!!!!!!!!!!!!!!!!!!!!!!!!!!!

108 SUBROUTINE Init(sys,Length,Configuration,IntOrder)
109   TYPE (FPUsystem) , INTENT(INOUT)    :: sys
110   INTEGER, INTENT(IN)                 :: Length, Configuration
111   INTEGER, OPTIONAL, INTENT(IN)       :: IntOrder

112   sys%Length = Length

113   IF ( PRESENT(IntOrder) ) THEN
114     SELECT CASE ( IntOrder)
115         CASE (4)
116           sys%IntegrationOrder = IntOrder
117         CASE (6)
118           sys%IntegrationOrder = IntOrder
119         CASE (10)
120           sys%IntegrationOrder = IntOrder
121         CASE DEFAULT
122           PRINT *,'Unknown IntegrationOrder in Init()!'
123           PRINT *,' '
124     END SELECT
125   ELSE
126     sys%IntegrationOrder = 4
127   END IF


128   !!!!!!!!!!!!!!!!!!!!!!!!!!!!!!!!!!!!!!!!!!!!!!!!!!!!!!!!!!!!
129   ! Calculate number of masses and which mass corresponds to
130   ! end mass.
131   ! The 0-th mass and N+1-th mass have zero displacement
```

```
132     !!!!!!!!!!!!!!!!!!!!!!!!!!!!!!!!!!!!!!!!!!!!!!!!!!!!!!!!!!!!
133     sys%Config = Configuration
134     IF (Configuration.EQ.LINE) THEN
135        sys%Nmasses = Length - 1
136        sys%Nleft = 0
137        sys%Nright = sys%Nmasses + 1
138     ELSE IF (Configuration.EQ.HOOP) THEN
139        sys%Nmasses = Length
140        sys%Nleft = sys%Nmasses
141        sys%Nright = 1
142     ELSE IF (Configuration.EQ.FREE) THEN
143        sys%Nmasses = Length + 1
144        sys%Nleft = 1
145        sys%Nright = sys%Nmasses
146     ELSE IF (Configuration.EQ.TAIL) THEN
147        sys%Nmasses = Length
148        sys%Nleft = 0
149        sys%Nright = sys%Nmasses
150     ELSE
151        PRINT *, 'ERROR: Unknown Configuration in Init()'
152        STOP
153     END IF

154     IF (sys%Nmasses.LT.1) THEN
155        PRINT *, 'ERROR: FPUsystem.Nmasses < 1'
156        PRINT *, ' '
157        STOP
158     END IF

159     !!!!!!!!!!!!!!!!!!!!!!!!!!!!!!!!!!!!!!!!!!!!!!!!!!!!!!!!!!!!
160     !  CHECK IF USER IS TRYING TO RE-ALLOCATE ARRAYS
161     !!!!!!!!!!!!!!!!!!!!!!!!!!!!!!!!!!!!!!!!!!!!!!!!!!!!!!!!!!!!
162     IF (ASSOCIATED(sys%y)) THEN
163       CALL Clear(sys)
164       PRINT *,'WARNING: Clear()-ing FPUsystem!'
165       PRINT *,'WARNING: RE-ALLOCATING ARRAYS!'
166     END IF

167     !!!!!!!!!!!!!!!!!!!!!!!!!!!!!!!!!!!!!!!!!!!!!!!!!!!!!!!!!!!!
168     !  ALLOCATE all arrays
169     !!!!!!!!!!!!!!!!!!!!!!!!!!!!!!!!!!!!!!!!!!!!!!!!!!!!!!!!!!!!
170     ALLOCATE(sys%y(0:sys%Nmasses+1))
171     ALLOCATE(sys%v(0:sys%Nmasses+1))
172     ALLOCATE(sys%mass(0:sys%Nmasses+1))
173     ALLOCATE(sys%invmass(0:sys%Nmasses+1))
```

```
174     ALLOCATE(sys%eps(0:sys%Nmasses+1))
175     ALLOCATE(sys%disp(0:sys%Nmasses+1))
176     ALLOCATE(sys%F(0:sys%Nmasses+1))
177     ALLOCATE(sys%Ex(0:sys%Nmasses+1))
178     ALLOCATE(sys%ExInit(0:sys%Nmasses+1))
179     ALLOCATE(sys%Ec(0:sys%Nmasses+1))
180     ALLOCATE(sys%AndersonAmp(0:sys%Nmasses+1))
181     ALLOCATE(sys%Psi2(0:sys%Nmasses+1))
182     ALLOCATE(sys%viscosity(0:sys%Nmasses+1))

183     sys%HasBeenAllocated = .TRUE.

184     !!!!!!!!!!!!!!!!!!!!!!!!!!!!!!!!!!!!!!!!!!!!!!!!!!!!!!!!!!!!
185     ! Initialize arrays to default values
186     !!!!!!!!!!!!!!!!!!!!!!!!!!!!!!!!!!!!!!!!!!!!!!!!!!!!!!!!!!!!
187     sys%y(:) = 0._double
188     sys%v(:) = 0._double
189     sys%mass(:) = 1._double
190     sys%invmass(:) = 1._double
191     sys%eps(:) = 0._double
192     sys%disp(:) = 0._double
193     sys%F(:) = 0._double
194     sys%Ex(:) = 0._double
195     sys%ExInit(:) = 0._double
196     sys%FirstEx = .TRUE.
197     sys%Ec(:) = 0._double
198     sys%AndersonAmp(:) = 0._double
199     sys%Psi2(:) = 0._double
200     sys%viscosity(:) = 0._double

201     sys%time = 0.
202     sys%Etime = -1.


203     !!!!!!!!!!!!!!!!!!!!!!!!!!!!!!!!!!!!!!!!!!!!!!!!!!!!!!!!!!!!
204     !   alpha() can be changed by the user later
205     !     so you have to initially allocate (MAX_EXPONENTS)
206     !!!!!!!!!!!!!!!!!!!!!!!!!!!!!!!!!!!!!!!!!!!!!!!!!!!!!!!!!!!!
207     ALLOCATE(sys%alpha(MAX_EXPONENT))
208     ALLOCATE(sys%alphaTau(MAX_EXPONENT))

209     sys%MaxExponent = 1
210     sys%alpha(:) = 0._double
211     sys%alpha(1) = 1._double
212     sys%alphaTau(:) = -1._double
```

```
213     sys%MaxFreq = -1.
214     sys%dT = 0.10_double

215     !!!!!!!!!!!!!!!!!!!!!!!!!!!!!!!!!!!!!!!!!!!!!!!!!!!!!!!!!!!!
216     ! Initialize the integrator coefficients
217     !!!!!!!!!!!!!!!!!!!!!!!!!!!!!!!!!!!!!!!!!!!!!!!!!!!!!!!!!!!!
218     SELECT CASE (sys%IntegrationOrder)
219       CASE ( 4 )

220         An = (/ (2.+2.**(+1./3.)+2.**(-1./3.))/6., &
221                 (1.-2.**(+1./3.)-2.**(-1./3.))/6., &
222                 (1.-2.**(+1./3.)-2.**(-1./3.))/6., &
223                 (2.+2.**(+1./3.)+2.**(-1./3.))/6., &
224                 0., 0., 0., 0., 0., 0., &
225                 0., 0., 0., 0., 0., 0., 0., 0., 0., 0. /)

226         Bn = (/ 0., &
227                 1./(2.-2.**(+1./3.)), &
228                 1./(1.-2.**(+2./3.)), &
229                 1./(2.-2.**(+1./3.)), &
230                 0., 0., 0., 0., 0., 0., &
231                 0., 0., 0., 0., 0., 0., 0., 0., 0., 0. /)

232       CASE ( 6 )
233         w1 = -1.17767998417887
234         w2 = +0.235573213359357
235         w3 = +0.784513610477560

236         !!!!!!!!!!!!!!!!!!!!!!!!!!!!!!!!!!!!!!!!!!!!!!!!!!!!!!!!!!!!
237         ! These coefficients are the other two solutions
238         !!!!!!!!!!!!!!!!!!!!!!!!!!!!!!!!!!!!!!!!!!!!!!!!!!!!!!!!!!!!
239         !  w1 = -2.13228522200144
240         !  w2 = +0.00426068187079180
241         !  w3 = +1.43984816797678

242         !  w1 = +0.00152886228424922
243         !  w2 = -2.14403531630539
244         !  w3 = +1.44778256239930

245         w0 = 1._double - TWO * (w1 + w2 + w3)

246         An = (/ ONE_HALF *  w3, &
247                 ONE_HALF * (w3 + w2), &
248                 ONE_HALF * (w2 + w1), &
```

```
249                 ONE_HALF * (w1 + w0), &
250                 ONE_HALF * (w1 + w0), &
251                 ONE_HALF * (w2 + w1), &
252                 ONE_HALF * (w3 + w2), &
253                 ONE_HALF *  w3, &
254                 0._double, 0._double, &
255                 0., 0., 0., 0., 0., 0., 0., 0., 0., 0. /)

256          Bn = (/  w3, &
257                   w2, &
258                   w1, &
259                   w0, &
260                   w1, &
261                   w2, &
262                   w3, &
263                   0._double, &
264                   0._double, 0._double, &
265                   0., 0., 0., 0., 0., 0., 0., 0., 0., 0. /)

266         CASE ( 10 )
267           w(1) = +0.0269001360476896 8968
268           w(2) = +0.9398015671356833 3790
269           w(3) = -0.0080358392038535 8750
270           w(4) = -0.8664851973737613 7280
271           w(5) = +0.1023112911193598 7311
272           w(6) = -0.1970772151393080 1014
273           w(7) = +0.6178777133180693 5734
274           w(8) = +0.1907272896000121 0016
275           w(9) = +0.2072605028852482 5594
276           w(10)= -0.3950061977609206 6739
277           w(11)= -0.5824234473116445 9471
278           w(12)= +0.7426733143573198 6348
279           w(13)= +0.1643375495204672 9102
280           w(14)= -0.6151166390605451 8266
281           w(15)= +0.2017504140367640 3506
282           w(16)= +0.4523871722434672 0618
283           w(0) = 1. - 2.*SUM(w(1:7))

284           An = (/ ONE_HALF *  w(7), &
285                   ONE_HALF * (w(7) + w(6)), &
286                   ONE_HALF * (w(6) + w(5)), &
287                   ONE_HALF * (w(5) + w(4)), &
288                   ONE_HALF * (w(4) + w(3)), &
289                   ONE_HALF * (w(3) + w(2)), &
290                   ONE_HALF * (w(2) + w(1)), &
```

```
                ONE_HALF * (w(1) + w(0)), &
                ONE_HALF * (w(1) + w(0)), &
                ONE_HALF * (w(2) + w(1)), &
                ONE_HALF * (w(3) + w(2)), &
                ONE_HALF * (w(4) + w(3)), &
                ONE_HALF * (w(5) + w(4)), &
                ONE_HALF * (w(6) + w(5)), &
                ONE_HALF * (w(7) + w(6)), &
                ONE_HALF * w(7), &
                0., 0., 0., 0. /)

        Bn = (/ w(7), &
                w(6), &
                w(5), &
                w(4), &
                w(3), &
                w(2), &
                w(1), &
                w(0), &
                w(1), &
                w(2), &
                w(3), &
                w(4), &
                w(5), &
                w(6), &
                w(7), &
                w(0), &
                0., 0., 0., 0. /)

    END SELECT


    !!!!!!!!!!!!!!!!!!!!!!!!!!!!!!!!!!!!!!!!!!!!!!!!!!!!!!!!!!!
    !  MPI variables
    !!!!!!!!!!!!!!!!!!!!!!!!!!!!!!!!!!!!!!!!!!!!!!!!!!!!!!!!!!!
    sys%MPI_Buffer = 0
    sys%MPI_Xleft = 1._double


    !!!!!!!!!!!!!!!!!!!!!!!!!!!!!!!!!!!!!!!!!!!!!!!!!!!!!!!!!!!
    ! Save initial values
    !!!!!!!!!!!!!!!!!!!!!!!!!!!!!!!!!!!!!!!!!!!!!!!!!!!!!!!!!!!
    sys%InitLength = sys%Length
    sys%InitNmasses = sys%Nmasses
```

```
329   END SUBROUTINE Init
```

fpu: Clear()

```
330   !!!!!!!!!!!!!!!!!!!!!!!!!!!!!!!!!!!!!!!!!!!!!!!!!!!!!!!!!!!!
331   !  FPUsystem Destructor
332   !!!!!!!!!!!!!!!!!!!!!!!!!!!!!!!!!!!!!!!!!!!!!!!!!!!!!!!!!!!!
333   SUBROUTINE Clear(sys)
334     TYPE (FPUsystem)    :: sys

335     DEALLOCATE(sys%y)
336     DEALLOCATE(sys%v)
337     DEALLOCATE(sys%alpha)
338     DEALLOCATE(sys%alphaTau)
339     DEALLOCATE(sys%mass)
340     DEALLOCATE(sys%invmass)
341     DEALLOCATE(sys%eps)
342     DEALLOCATE(sys%disp)
343     DEALLOCATE(sys%F)
344     DEALLOCATE(sys%Ex)
345     DEALLOCATE(sys%ExInit)
346     DEALLOCATE(sys%Ec)
347     DEALLOCATE(sys%AndersonAmp)
348     DEALLOCATE(sys%Psi2)
349     DEALLOCATE(sys%viscosity)

350   END SUBROUTINE Clear
```

fpu: COPY()

```
!!!!!!!!!!!!!!!!!!!!!!!!!!!!!!!!!!!!!!!!!!!!!!!!!!!!!!!!!!!!
!  Copy one FPUsystem onto a new FPUsystem
!
!      SrcSys          (FPUsystem)     Source
!      DestSys         (FPUsystem)     Destination
!!!!!!!!!!!!!!!!!!!!!!!!!!!!!!!!!!!!!!!!!!!!!!!!!!!!!!!!!!!!

SUBROUTINE Copy(SrcSys,DestSys)
  TYPE (FPUsystem) , INTENT(IN)       :: SrcSys
  TYPE (FPUsystem) , INTENT(INOUT)    :: DestSys

  !!!!!!!!!!!!!!!!!!!!!!!!!!!!!!!!!!!!!!!!!!!!!!!!!!!!!!!!!!!!
  ! Erase an existing sys
  !!!!!!!!!!!!!!!!!!!!!!!!!!!!!!!!!!!!!!!!!!!!!!!!!!!!!!!!!!!!
  IF ( ASSOCIATED(DestSys%y) ) THEN
     CALL Clear(DestSys)
  END IF

  CALL Init(DestSys,SrcSys%Length,SrcSys%Config, &
                                    SrcSys%IntegrationOrder)
  DestSys%dT = SrcSys%dT
  DestSys%MaxFreq = SrcSys%MaxFreq
  DestSys%time = SrcSys%time
  DestSys%MPI_Buffer = SrcSys%MPI_Buffer
  DestSys%MPI_Xleft = SrcSys%MPI_Xleft
  DestSys%MaxExponent = SrcSys%MaxExponent
  DestSys%alpha(1:SrcSys%MaxExponent) = &
                                SrcSys%alpha(1:SrcSys%MaxExponent)
  DestSys%alphaTau(1:SrcSys%MaxExponent) = &
                                SrcSys%alphaTau(1:SrcSys%MaxExponent)
  DestSys%y(0:DestSys%Nmasses+1) = SrcSys%y(0:SrcSys%Nmasses+1)
  DestSys%v(0:DestSys%Nmasses+1) = SrcSys%v(0:SrcSys%Nmasses+1)
  DestSys%mass(0:DestSys%Nmasses+1) = &
                                SrcSys%mass(0:SrcSys%Nmasses+1)
  DestSys%invmass(0:DestSys%Nmasses+1) = &
                                SrcSys%invmass(0:SrcSys%Nmasses+1)

END SUBROUTINE Copy
```

fpu: SETY() GETY()

```
385   !!!!!!!!!!!!!!!!!!!!!!!!!!!!!!!!!!!!!!!!!!!!!!!!!!!!!!!!!!!!!!!!
386   ! Application interface to Set(ting) and
387   !    Get(ting) the mass displacements
388   ! These routines are usually ignored out of laziness
389   !!!!!!!!!!!!!!!!!!!!!!!!!!!!!!!!!!!!!!!!!!!!!!!!!!!!!!!!!!!!!!!!

390   SUBROUTINE SetY(sys,index,displacement)
391     TYPE (FPUsystem), INTENT(INOUT)     :: sys
392     INTEGER                             :: index
393     REAL (double)                       :: displacement

394     sys%y(index)  = displacement
395   END SUBROUTINE SetY

396   REAL (double) FUNCTION GetY(sys,index) RESULT (displacement)
397     TYPE (FPUsystem), INTENT(INOUT)     :: sys
398     INTEGER                             :: index

399     displacement  = sys%y(index)
400   END FUNCTION GetY
```

fpu: SetExponent()

```
!!!!!!!!!!!!!!!!!!!!!!!!!!!!!!!!!!!!!!!!!!!!!!!!!!!!!!!!!!!!
!  Assign force exponents via an array:
!    Exp              (double)(:)     Exponent array
!    Nexponents       (double)        Maximum force exponent
!!!!!!!!!!!!!!!!!!!!!!!!!!!!!!!!!!!!!!!!!!!!!!!!!!!!!!!!!!!!
SUBROUTINE SetExponent(sys,Exp,Nexponents)
  TYPE (FPUsystem),            INTENT(OUT)    :: sys
  REAL (double), DIMENSION(:), INTENT(IN)     :: Exp
  INTEGER,                     INTENT(IN)     :: Nexponents

  !!!!!!!!!!!!!!!!!!!!!!!!!!!!!!!!!!!!!!!!!!!!!!!!!!!!!!!!!!!!
  !  Check for MAX_EXPONENT violation
  !!!!!!!!!!!!!!!!!!!!!!!!!!!!!!!!!!!!!!!!!!!!!!!!!!!!!!!!!!!!
  IF (Nexponents.GT.MAX_EXPONENT) THEN
    PRINT *,' ERROR: SetExponent() Nexponents too big!'
    PRINT *,' '
    STOP
  ELSE
    sys%MaxExponent = Nexponents
  END IF
  sys%alpha(1:Nexponents) = Exp(1:Nexponents)
END SUBROUTINE SetExponent
```

fpu: SetImpurity()

```
!!!!!!!!!!!!!!!!!!!!!!!!!!!!!!!!!!!!!!!!!!!!!!!!!!!!!!!!!!!!
! Set the impurities:
!   xImpurity         (INTEGER)(:)    array of impurity locations
!   Nx                (INTEGER)       # of impurities
!   ImpurityMass      (double)        impurity mass = m_o + m_+
!!!!!!!!!!!!!!!!!!!!!!!!!!!!!!!!!!!!!!!!!!!!!!!!!!!!!!!!!!!!

SUBROUTINE SetImpurity(sys,xImpurity,Nx,ImpurityMass)
  TYPE (FPUsystem), INTENT(INOUT)     :: sys
  INTEGER, DIMENSION(:), INTENT(IN)   :: xImpurity
  INTEGER, INTENT(IN)                 :: Nx
  REAL (double), INTENT(IN)           :: ImpurityMass

  INTEGER     :: i

  DO i = 1,Nx
    IF (xImpurity(i).GT.0.AND.xImpurity(i).LE.sys%Length) THEN
      sys%mass(xImpurity(i)) = ImpurityMass
      sys%invmass(xImpurity(i)) = 1./ImpurityMass
    ELSE
      PRINT *,'ERROR: xImpurity(i) outside bounds!'
```

```
440         PRINT *,' '
441         STOP
442       END IF
443     END DO
444   END SUBROUTINE SetImpurity
```

fpu: InitHarmonic()

```
445   !!!!!!!!!!!!!!!!!!!!!!!!!!!!!!!!!!!!!!!!!!!!!!!!!!!!!!!!!!!!
446   !  Initialize a harmonic system.  The wavelength is
447   !  determined from the number of "HalfCycles" specified.
448   !  By definition, the displacement at the extrema, for both
449   !  LINE and HOOP is zero.
450   !
451   !  HalfCycles         (INTEGER)               Number of half-cycles
452   !  Amplitude          (double) [OPTIONAL]     wave amplitude
453   !  InitPhase          (double) [OPTIONAL]     wave phase
454   !!!!!!!!!!!!!!!!!!!!!!!!!!!!!!!!!!!!!!!!!!!!!!!!!!!!!!!!!!!!

455   SUBROUTINE InitHarmonic(sys,HalfCycles,Amplitude,InitPhase)
456     TYPE (FPUsystem), INTENT(INOUT)     :: sys
457     INTEGER,          INTENT(IN)        :: HalfCycles
458     REAL (double),    INTENT(IN), OPTIONAL      :: Amplitude
459     REAL (double),    INTENT(IN), OPTIONAL      :: InitPhase

460     REAL (double), DIMENSION(:), ALLOCATABLE            :: index
461     REAL (double)                       :: lambda, A, phase
462     INTEGER                             :: i

463     IF ( PRESENT(Amplitude) ) THEN
464       A = Amplitude
465     ELSE
466       A = 1.
467     END IF

468     IF ( PRESENT(InitPhase) ) THEN
469       phase = InitPhase
470     ELSE
471       phase = 0.
472     END IF

473     ALLOCATE(index(0:sys%Nmasses))

474     lambda = TWO * sys%Length / HalfCycles
475     sys%k = TWO * PI / lambda
476     sys%omega = TWO * SIN(sys%k / TWO)

477     !!!!!!!!!!!!!!!!!!!!!!!!!!!!!!!!!!!!!!!!!!!!!!!!!!!!!!!!!!!!
478     !  Estimate the maximum freq if it hasn't already been
479     !    set by the user.  The MaxFreq is then used to determine
480     !    the appropriate integration interval dT
481     !
```

```
482     !!!!!!!!!!!!!!!!!!!!!!!!!!!!!!!!!!!!!!!!!!!!!!!!!!!!!!!!!!!!
483     IF (sys%MaxFreq.LT.0) THEN
484        sys%MaxFreq = sys%omega / (TWO * PI)
485     END IF
486     sys%dT = MAX(PI/20.,0.005/sys%MaxFreq)

487     index = (/ (i, i=0,sys%Nmasses) /)

488     sys%y(1:sys%Nmasses) = A * SIN(sys%k*index(1:sys%Nmasses)+phase)

489     DEALLOCATE(index)
490   END SUBROUTINE InitHarmonic
```

fpu: PiMode()

```
491   !!!!!!!!!!!!!!!!!!!!!!!!!!!!!!!!!!!!!!!!!!!!!!!!!!!!!!!!!!!!
492   ! Initialize a system in the  k = pi mode  (wavelength = 2)
493   ! A small amount of randomness is added to the displacement
494   !    of each mass.
495   !!!!!!!!!!!!!!!!!!!!!!!!!!!!!!!!!!!!!!!!!!!!!!!!!!!!!!!!!!!!

496   SUBROUTINE InitPiMode(sys,seed)
497     TYPE (FPUsystem), INTENT(INOUT)     :: sys
498     INTEGER, OPTIONAL, INTENT(INOUT)    :: seed

499     REAL (double)                       :: N, a, ran3
500     INTEGER                             :: i, sgn, RAND

501     N = REAL(sys%Nmasses)
502     a = 10. * SIN(PI/N)/SQRT(sys%alpha(3)*(9.*COS(PI/N)**2 - 3.))

503     IF ( PRESENT(seed) ) THEN
504        seed = RAND()
505     END IF

506     sgn = +1
507     DO i = 1, sys%Nmasses
508       sys%y(i) = sgn * a
509       sys%v(i) = 1.E-08 * (2.*ran3(seed) - 1.)
510       sgn = -1 * sgn
511     END DO

512     sys%MaxFreq = 1./PI
513     sys%dT = MAX(1._double/PI/4.,0.005/sys%MaxFreq)

514   END SUBROUTINE InitPiMode
```

fpu: InitSigmoidal()

```
515   !!!!!!!!!!!!!!!!!!!!!!!!!!!!!!!!!!!!!!!!!!!!
516   ! Initialize a sigmoidal pulse
517   !
518   ! For a traveling pulse of length nLambda*Wavelength
519   !   and amplitude Amplitude, the initial zero-velocity
520   !   pulse is nLambda*Wavelength/2 long and has amplitude
521   !   2*Amplitude.
522   !!!!!!!!!!!!!!!!!!!!!!!!!!!!!!!!!!!!!!!!!!!!

523   SUBROUTINE InitSigmoidal(sys,Wavelength,nLambda,Amplitude)
524     TYPE (FPUsystem),   INTENT(INOUT)           :: sys
525     REAL (double),      INTENT(IN)              :: Wavelength
526     INTEGER,            INTENT(IN), OPTIONAL    :: nLambda
527     REAL (double),      INTENT(IN), OPTIONAL    :: Amplitude

528     INTEGER             :: i, nWavelength
529     REAL                :: k, A

530     k = TWO * PI / Wavelength
531     sys%omega = 2. * SIN(k/2.)

532     IF ( PRESENT(nLambda) ) THEN
533       nWavelength = INT(3*nLambda/2. + 0.5)
534     ELSE
535       nWavelength = 12
536     END IF

537     IF ( PRESENT(Amplitude) ) THEN
538       A = Amplitude
539     ELSE
540       A = 1.
541     END IF

542     !!!!!!!!!!!!!!!!!!!!!!!!!!!!!!!!!!!!!!!!!!!!
543     ! Wave 'decays' over 5 * Wavelength
544     !!!!!!!!!!!!!!!!!!!!!!!!!!!!!!!!!!!!!!!!!!!!
545     DO i = 0, INT(8*nWavelength*Wavelength/3. + 0.5) - 1
546       sys%y(i) = 2.*A*SIN(k*i) &
547         * 0.5*(1.+TANH(1.*(nWavelength*Wavelength/2-i)/Wavelength))
548     END DO

549     sys%MaxFreq = sys%omega / (TWO * PI)
550     sys%dT = MAX(PI/20.,0.005/sys%MaxFreq)
```

```
551   END SUBROUTINE InitSigmoidal
```

fpu: InitAnderson()

```
552   !!!!!!!!!!!!!!!!!!!!!!!!!!!!!!!!!!!!!!!!!!!!
553   !  Initialize a system in a localized eigenstate for the harmonic
554   !    component of the Hamiltonian
555   !
556   !  WaveNumber         (double)                2 pi/ lambda
557   !  MassPlus           (double)                m_+
558   !  xImpurity          (INTEGER) (1:nImpurity+1)  impurity locations
559   !  nImpurity          (INTEGER)               # of imurities
560   !  T                  (double) (OUT)          transmission coef.
561   !  Ao                 (COMPLEX*8)             incident wave amp.
562   !!!!!!!!!!!!!!!!!!!!!!!!!!!!!!!!!!!!!!!!!!!!

563   SUBROUTINE InitAnderson(sys,WaveNumber,MassPlus,xImpurity,&
564                                                 nImpurity,T,Ao)
565     TYPE (FPUsystem),           INTENT(INOUT)   :: sys
566     REAL (double),              INTENT(IN)      :: WaveNumber
567     REAL (double),              INTENT(IN)      :: MassPlus
568     INTEGER, DIMENSION(:),      INTENT(INOUT)   :: xImpurity
569     INTEGER,                    INTENT(IN)      :: nImpurity
570     REAL (double),              INTENT(OUT)     :: T  ! trans. coef.
571     COMPLEX*8,                  INTENT(IN)      :: Ao ! init amp.
572     REAL (double)                               :: lambda, eps
573     REAL (double)                               :: xo
574     REAL (double)                               :: AmpMin, AmpMax
575     INTEGER     :: i,j,iTemp
576     TYPE (FPUsystem)                            :: TmpSys
577     INTEGER, DIMENSION(1000)                    :: TmpXimpurity
578     INTEGER                                     :: TmpNimpurity
579     INTEGER                                     :: TmpLength

580     lambda = TWO * PI/WaveNumber
581     sys%k = WaveNumber
582     sys%omega = TWO * SIN(sys%k / TWO)



583     !!!!!!!!!!!!!!!!!!!!!!!!!!!!!!!!!!!!!!!!!!!!
584     !  Estimate the maximum freq if it hasn't already been
585     !    set by the user.  The MaxFreq is then used to determine
586     !    the appropriate integration interval dT
587     !!!!!!!!!!!!!!!!!!!!!!!!!!!!!!!!!!!!!!!!!!!!
588     IF (sys%MaxFreq.LT.0) THEN
589        sys%MaxFreq = sys%omega / (TWO * PI)
590     END IF
591     sys%dT = MAX(PI/20.,0.005/sys%MaxFreq)
```

```
592     !!!!!!!!!!!!!!!!!!!!!!!!!!!!!!!!!!!!!!!!!!!!
593     ! Ensure impurities are in ascending order by
594     !        sorting xImpurity array
595     ! This is important for the Initial() subroutine
596     !!!!!!!!!!!!!!!!!!!!!!!!!!!!!!!!!!!!!!!!!!!!
597     DO i = 1,nImpurity-1
598     DO j = i+1,nImpurity
599       IF (xImpurity(i).GT.xImpurity(j)) THEN
600         iTemp = xImpurity(i)
601         xImpurity(i) = xImpurity(j)
602         xImpurity(j) = iTemp
603       ELSE IF (xImpurity(i).EQ.xImpurity(j)) THEN
604         PRINT *, ' '
605         PRINT *,'WARNING:  xImpurity(i) = xImpurity(j)!'
606         PRINT *, ' '
607       END IF
608     END DO
609     END DO


610     !!!!!!!!!!!!!!!!!!!!!!!!!!!!!!!!!!!!!!!!!!!!
611     !  For systems having MANY impurities, a solution is found for
612     !   the first 400 impurities.   The result is mapped onto the
613     !   larger system, with amplitudes after the 400-th impurity
614     !   set to zero.
615     ! InitLength and InitNmasses are used to map between the
616     !   two systems.
617     !!!!!!!!!!!!!!!!!!!!!!!!!!!!!!!!!!!!!!!!!!!!
618     sys%Length = sys%InitLength
619     sys%Nmasses = sys%InitNmasses


620     !!!!!!!!!!!!!!!!!!!!!!!!!!!!!!!!!!!!!!!!!!!!
621     ! Initial() populates the matrix, solves the equation, and maps
622     !   the continuum solution, making no adjustments, to sys%y
623     !!!!!!!!!!!!!!!!!!!!!!!!!!!!!!!!!!!!!!!!!!!!
624     IF (nImpurity <= 400) THEN
625        CALL Initial(sys%y,WaveNumber,MassPlus,T,xImpurity, &
626                  sys%Nmasses,nImpurity,sys%AndersonAmp,sys%Psi2,Ao)
627     !!!!!!!!!!!!!!!!!!!!!!!!!!!!!!!!!!!!!!!!!!!!
628     !  nImpurity > 400, make a temporary FPUsystem from a copy of the
629     !     original system.  Send the temporary system to Initial()
630     !     and declare only the first 400 impurities.
631     !!!!!!!!!!!!!!!!!!!!!!!!!!!!!!!!!!!!!!!!!!!!
```

```
632     ELSE
633        tmpNimpurity = 400
634        tmpLength = xImpurity(tmpNimpurity+1)
635        tmpXimpurity(1:tmpNimpurity) = xImpurity(1:tmpNimpurity)
636        CALL Init(TmpSys,tmpLength,sys%Config,sys%IntegrationOrder)
637        CALL Initial(TmpSys%y,WaveNumber,MassPlus,T,tmpXimpurity, &
638            TmpSys%Nmasses,TmpNimpurity,sys%AndersonAmp,sys%Psi2,Ao)
639        sys%y(0:TmpSys%Nmasses) = TmpSys%y(0:TmpSys%Nmasses)
640        CALL Clear(TmpSys)
641     ENDIF


642     !!!!!!!!!!!!!!!!!!!!!!!!!!!!!!!!!!!!!!!!!!!
643     !  With almost certainty, the displacement at the ends will not
644     !   be zero.  Relocate the ends to the mass having the smallest
645     !   oscillation amplitude
646     !!!!!!!!!!!!!!!!!!!!!!!!!!!!!!!!!!!!!!!!!!!
647     eps = 1.
648     DO i = 1, INT(5 * lambda + 0.5)
649       IF (ABS(sys%y(i)) .LT. eps) THEN
650          iTemp = i
651          eps = ABS(sys%y(i))
652       END IF
653     END DO
654     xo = (sys%y(iTemp-1)+sys%y(iTemp+1))/ &
655                (sys%y(iTemp-1)-sys%y(iTemp+1))

656     DO i = iTemp + 1, sys%Nmasses
657        sys%y(i-iTemp) = sys%y(i)
658        sys%Mass(i-iTemp) = sys%Mass(i)
659        sys%Invmass(i-iTemp) = sys%Invmass(i)
660        sys%AndersonAmp(i-iTemp) = sys%AndersonAmp(i)
661     END DO
662     sys%Nmasses = sys%Nmasses - iTemp
663     sys%Length = sys%Length - iTemp

664     !!!!!!!!!!!!!!!!!!!!!!!!!!!!!!!!!!!!!!!!!!!
665     ! Adjust the locations in xImpurity to reflect any shift
666     !    in the system
667     !!!!!!!!!!!!!!!!!!!!!!!!!!!!!!!!!!!!!!!!!!!
668     DO i = 1, nImpurity
669       xImpurity(i) = xImpurity(i) - iTemp
670     END DO

671     eps = 1.
```

```
672     DO i = sys%Nmasses,sys%Nmasses-3*INT(lambda)/4,-1
673       IF (ABS(sys%y(i)) .LT. eps) THEN
674          iTemp = i
675          eps = ABS(sys%y(i))
676       END IF
677     END DO
678     IF (sys%Config .EQ. LINE) THEN
679       sys%Nmasses = iTemp - 1
680       sys%Length = iTemp
681       sys%Nright = sys%Nmasses + 1
682     ELSE IF (sys%Config .EQ. HOOP) THEN
683       sys%Nmasses = iTemp
684       sys%Length = iTemp
685       sys%Nleft = iTemp
686     ELSE IF (sys%Config .EQ. TAIL) THEN
687       sys%Nmasses = iTemp
688       sys%Length = iTemp
689       sys%Nright = sys%Nmasses
690     ELSE
691       PRINT *, 'ERROR: Unknown sys%Config in InitAnderson!'
692       PRINT *,' '
693       STOP
694     END IF
695     sys%y(sys%Length) = 0._double

696   END SUBROUTINE InitAnderson
```

fpu: Set() and Get()

```
!!!!!!!!!!!!!!!!!!!!!!!!!!!!!!!!!!!!!!!!!!!!!!!!!!!!!!!!!!!!!!!!
! User interface to Set() and Get() the integration interval dT
!!!!!!!!!!!!!!!!!!!!!!!!!!!!!!!!!!!!!!!!!!!!!!!!!!!!!!!!!!!!!!!!

SUBROUTINE SetdT(sys,dt)
  TYPE (FPUsystem), INTENT(INOUT)     :: sys
  REAL (double),    INTENT(IN)        :: dt

  sys%dT = dt
END SUBROUTINE SetdT

SUBROUTINE GetdT(sys,dt)
  TYPE (FPUsystem), INTENT(IN)        :: sys
  REAL (double),    INTENT(OUT)       :: dt

  dt = sys%dT
END SUBROUTINE GetdT
```

fpu: SetViscosity()

```
!!!!!!!!!!!!!!!!!!!!!!!!!!!!!!!!!!!!!!!!!!!!!!!!!!!!!!!!!!!!!!!!
!  Set viscosity
!   Nstart            (INTEGER)       starting mass
!   Nstop             (INTEGER)       stoping mass
!   Viscosity         (double)        set viscosity  for
!                                              Nstart<= i <= Nstop
!!!!!!!!!!!!!!!!!!!!!!!!!!!!!!!!!!!!!!!!!!!!!!!!!!!!!!!!!!!!!!!!

SUBROUTINE SetViscosity(sys,Nstart,Nstop,Viscosity)
  TYPE (FPUsystem),   INTENT(INOUT)   :: sys
  INTEGER,            INTENT(IN)      :: Nstart, Nstop
  REAL (double),      INTENT(IN)      :: Viscosity

  sys%viscosity(Nstart:Nstop) = Viscosity

END SUBROUTINE SetViscosity
```

fpu: Force()

```
723   !!!!!!!!!!!!!!!!!!!!!!!!!!!!!!!!!!!!!!!!!!!!!!!!!!!!!!!!!!!!
724   !  Calculate force on each mass.  Result is stored
725   !     in TYPE (FPUsystem)%F variable for later use in
726   !     Integrate()
727   !!!!!!!!!!!!!!!!!!!!!!!!!!!!!!!!!!!!!!!!!!!!!!!!!!!!!!!!!!!!

728   SUBROUTINE Force(sys)
729     TYPE (FPUsystem), INTENT(INOUT)     :: sys
730     INTEGER ::  i, N

731     N = sys%Nmasses

732     sys%eps(0:N) = sys%y(1:N+1) - sys%y(0:N)

733     sys%F(1:N) = sys%alpha(1)*(sys%eps(1:N) - sys%eps(0:N-1))

734     sys%disp = sys%eps
735     DO i = 2,sys%MaxExponent
736       sys%eps = sys%eps * sys%disp
737       sys%F(1:N) =sys%F(1:N) + sys%alpha(i)* &
738                           (sys%eps(1:N) - sys%eps(0:N-1))
739     END DO

740     !!!!!!!!!!!!!!!!!!!!!!!!!!!!!!!!!!!!!!!!!!!!!!!!!!!!!!!!!!!!
741     ! optional viscous damping
742     !!!!!!!!!!!!!!!!!!!!!!!!!!!!!!!!!!!!!!!!!!!!!!!!!!!!!!!!!!!!
743     sys%F(1:N) = sys%F(1:N) - sys%viscosity(1:N) * sys%v(1:N)
744   END SUBROUTINE Force
```

fpu: Integrate()

```
745   !!!!!!!!!!!!!!!!!!!!!!!!!!!!!!!!!!!!!!!!!!!!!!!!!!!!!!!!!!!!
746   !   Integrate FPU system using a symplectic integrator
747   !     algorithm.  User specifies the number of iterations
748   !     based on the previously established value of FPUsystem%dT
749   !
750   !    Iterations       (INTEGER)
751   !!!!!!!!!!!!!!!!!!!!!!!!!!!!!!!!!!!!!!!!!!!!!!!!!!!!!!!!!!!!

752   SUBROUTINE Integrate(sys,Iterations)
753     TYPE (FPUsystem), INTENT(INOUT)     :: sys
754     INTEGER, INTENT(IN)                 :: Iterations

755     INTEGER                             :: iter,i,N

756     N = sys%Nmasses

757     SELECT CASE (sys%IntegrationOrder)
758       CASE (4)
759         DO iter = 1, Iterations

760           sys%y(1:N) = sys%y(1:N) + An(1) * sys%v(1:N) * sys%dT
761           sys%y(0) = sys%y(sys%Nleft)
762           sys%y(N+1) = sys%y(sys%Nright)
763           DO i = 2, 4
764              CALL Force(sys)
765              sys%v(1:N) = sys%v(1:N) + &
766                        Bn(i)*sys%F(1:N)*sys%dT*sys%invmass(1:N)
767              sys%y(1:N) = sys%y(1:N) + An(i) * sys%v(1:N) * sys%dT
768              sys%y(0) = sys%y(sys%Nleft)
769              sys%y(N+1) = sys%y(sys%Nright)
770           END DO
771         END DO

772       CASE (6)
773         DO iter = 1, Iterations
774           DO i = 1, 7   ! Bn(8) = 0.
775             sys%y(1:N) = sys%y(1:N) + An(i)*sys%v(1:N)*sys%dT
776             sys%y(0) = sys%y(sys%Nleft)
777             sys%y(N+1) = sys%y(sys%Nright)
778             CALL Force(sys)
779             sys%v(1:N) = sys%v(1:N) + &
780                         Bn(i)*sys%F(1:N)*sys%dT*sys%invmass(1:N)
781           END DO
782           sys%y(1:N) = sys%y(1:N) + An(i)*sys%v(1:N)*sys%dT
```

```
783           sys%y(0) = sys%y(sys%Nleft)
784           sys%y(N+1) = sys%y(sys%Nright)
785         END DO

786       CASE (10)
787         DO iter = 1, Iterations
788           DO i = 1, 15  ! Bn(16) = 0.
789             sys%y(1:N) = sys%y(1:N) + An(i)*sys%v(1:N)*sys%dT
790             sys%y(0) = sys%y(sys%Nleft)
791             sys%y(N+1) = sys%y(sys%Nright)
792             CALL Force(sys)
793             sys%v(1:N) = sys%v(1:N) + &
794                          Bn(i)*sys%F(1:N)*sys%dT*sys%invmass(1:N)
795           END DO
796           sys%y(1:N) = sys%y(1:N) + An(i)*sys%v(1:N)*sys%dT
797           sys%y(0) = sys%y(sys%Nleft)
798           sys%y(N+1) = sys%y(sys%Nright)
799         END DO

800     END SELECT

801     sys%time = sys%time + Iterations * sys%dT

802   END SUBROUTINE Integrate
```

fpu: Energy()

```
803   !!!!!!!!!!!!!!!!!!!!!!!!!!!!!!!!!!!!!!!!!!!!!!!!!!!!!!!!!!!!
804   ! Energy() performs most of the useful statistics
805   !
806   !  Calculate total energy between
807   !    1 <= Nmin <= Nmax
808   !
809   !     and store
810   !    %R2E:    Energy R-squared
811   !    %R2E2:   Energy**2 R-squared
812   !    %R2Ec:   (1-Ec) R-squared
813   !    %H2:     Helfand moment for thermal conductivity
814   !
815   !!!!!!!!!!!!!!!!!!!!!!!!!!!!!!!!!!!!!!!!!!!!!!!!!!!!!!!!!!!!

816   !!!!!!!!!!!!!!!!!!!!!!!!!!!!!!!!!!!!!!!!!!!!!!!!!!!!!!!!!!!!
817   !   MPI:
818   !    In case the calculation is part of a bigger system (and
819   !    values of y() and v() overlap, Nmin and Nmax indicate
820   !    where to start counting.
821   !    The optional parameter Xmin gives the x-location of Nmin.
822   !
823   !!!!!!!!!!!!!!!!!!!!!!!!!!!!!!!!!!!!!!!!!!!!!!!!!!!!!!!!!!!!
824   REAL (double) FUNCTION Energy(sys,Nmin,Nmax,Xmin) RESULT (E)
825     TYPE (FPUsystem), INTENT(INOUT)             :: sys
826     INTEGER,          INTENT(INOUT)             :: Nmin,Nmax
827     INTEGER, OPTIONAL,INTENT(IN)                :: Xmin
828     INTEGER                                     :: Log10N
829     REAL (double)                               :: ScaleFactor, E2tot
830     REAL (double)                               :: Xo  ! smallest x
831     REAL (double), DIMENSION(:), ALLOCATABLE    :: x

832     INTEGER     :: i,N

833     N = sys%Nmasses
834     IF (Nmin.LT.1) Nmin = 1    ! avoid Nmin = 0
835     IF (Nmax.GT.N) Nmax = N
836     IF (Nmin.GT.Nmax) THEN
837        PRINT *, 'ERROR: Nmin > Nmax in Energy()'
838        PRINT *, ' '
839        STOP
840     END IF

841     ALLOCATE(x(Nmin:Nmax))
842     x = (/ (REAL(i), i=Nmin,Nmax) /)
```

```
843     IF (PRESENT(Xmin)) THEN
844        Xo = REAL(Xmin)
845     ELSE
846        Xo = 1._double
847     END IF

848     !!!!!!!!!!!!!!!!!!!!!!!!!!!!!!!!!!!!!!!!!!!!!!!!!!!!!!!!!!!!
849     ! Reduce roundoff error by scaling the length
850     !!!!!!!!!!!!!!!!!!!!!!!!!!!!!!!!!!!!!!!!!!!!!!!!!!!!!!!!!!!!
851     ScaleFactor = 1.
852     Log10N = INT(LOG10(Xo+REAL(Nmax-Nmin)))
853     IF (Log10N.GE.1) THEN
854        ScaleFactor = 10.**Log10N
855     END IF

856     x(Nmin:Nmax) = (Xo + x(Nmin:Nmax) - REAL(Nmin)) / ScaleFactor


857     sys%Ex(Nmin:Nmax) = 0.5_double * sys%mass(Nmin:Nmax) * &
858                                 sys%v(Nmin:Nmax)**2

859     sys%eps(0:N) = sys%y(1:N+1) - sys%y(0:N)
860     DO i = 1,sys%MaxExponent
861       sys%Ex(Nmin:Nmax) = sys%Ex(Nmin:Nmax) + &
862         0.5_double * (1./(i+1.)) * sys%alpha(i) * &
863         (sys%eps(Nmin-1:Nmax-1)**(i+1)+sys%eps(Nmin:Nmax)**(i+1))
864     END DO

865     sys%Etot =  SUM(sys%Ex(Nmin:Nmax))
866     E2tot =  SUM(sys%Ex(Nmin:Nmax)**2)


867     !!!!!!!!!!!!!!!!!!!!!!!!!!!!!!!!!!!!!!!!!!!!!!!!!!!!!!!!!!!!
868     ! cumulative energy Ec(x)
869     !!!!!!!!!!!!!!!!!!!!!!!!!!!!!!!!!!!!!!!!!!!!!!!!!!!!!!!!!!!!
870     DO i = Nmin, Nmax
871       sys%Ec(i) = SUM(sys%Ex(Nmin:i)) / sys%Etot
872     END DO

873     E = sys%Etot

874     sys%R2E  = SUM(sys%Ex(Nmin:Nmax) * &
875                 x(Nmin:Nmax)**2) * ScaleFactor**2 / E
876     sys%R2E2 = SUM(sys%Ex(Nmin:Nmax)**2 * &
```

```
                x(Nmin:Nmax)**2)*ScaleFactor**2/E2tot
   sys%R2Ec = SUM((1.-sys%Ec(Nmin:Nmax)) * &
                x(Nmin:Nmax)**2) * ScaleFactor**2



   !!!!!!!!!!!!!!!!!!!!!!!!!!!!!!!!!!!!!!!!!!!!!!!!!!!!!!!!!!!
   ! If the first time through Energy(), set sys%ExInit
   !!!!!!!!!!!!!!!!!!!!!!!!!!!!!!!!!!!!!!!!!!!!!!!!!!!!!!!!!!!
   IF (sys%FirstEx == .TRUE.) THEN
      sys%ExInit(Nmin:Nmax) = sys%Ex(Nmin:Nmax)
      sys%FirstEx = .FALSE.
   END IF

   !!!!!!!!!!!!!!!!!!!!!!!!!!!!!!!!!!!!!!!!!!!!!!!!!!!!!!!!!!!
   ! Helfand moment
   !!!!!!!!!!!!!!!!!!!!!!!!!!!!!!!!!!!!!!!!!!!!!!!!!!!!!!!!!!!
   sys%H2 = 0.
   DO i = Nmin, Nmax
      sys%H2 = sys%H2 + &
      SUM((x(Nmin:Nmax)-x(i))**2 * sys%Ex(Nmin:Nmax) *sys%ExInit(i))
   END DO
   sys%H2 = sys%H2 * ScaleFactor**2 / sys%Etot**2

   sys%Etime = sys%time

   DEALLOCATE(x)
END FUNCTION Energy
```

fpu: Co()

```
899   !!!!!!!!!!!!!!!!!!!!!!!!!!!!!!!!!!!!!!!!!!!!!!!!!!!!!!!!!!!!!!!!
900   !  Co returns the localization parameter
901   !!!!!!!!!!!!!!!!!!!!!!!!!!!!!!!!!!!!!!!!!!!!!!!!!!!!!!!!!!!!!!!!
902   REAL (double) FUNCTION Co(sys,Nmin,Nmax) RESULT (CoParam)
903     TYPE (FPUsystem),           INTENT(INOUT)   :: sys
904     INTEGER, OPTIONAL,          INTENT(IN)      :: Nmin, Nmax
905     INTEGER                                     :: N1, N2
906     REAL (double)                               :: Etemp

907     IF ( PRESENT(Nmin) .AND. PRESENT(Nmax) ) THEN
908       N1 = Nmin
909       N2 = Nmax
910     ELSE
911       N1 = 1
912       N2 = sys%Nmasses
913     END IF

914     IF ( sys%Etime .NE. sys%time ) THEN
915       Etemp = Energy(sys,N1,N2)
916     END IF

917     CoParam =  sys%Nmasses * SUM(sys%Ex(N1:N2)**2) / &
918                 (SUM(sys%Ex(N1:N2))**2)

919   END FUNCTION Co
```

fpu: FFTw()

```
920   !!!!!!!!!!!!!!!!!!!!!!!!!!!!!!!!!!!!!!!!!!!!!!!!!!!!!!!!!!!!
921   !  FFTw does the hard work of calculating the time/frequncy
922   !      FFT of a mass.
923   !  The subroutine can sample from multiple masses and will perform
924   !     the required time integration and sampling.
925   !!!!!!!!!!!!!!!!!!!!!!!!!!!!!!!!!!!!!!!!!!!!!!!!!!!!!!!!!!!!
926   SUBROUTINE FFTw(sys,w,yData,vData,Xsample,Nx,Log2FFTSamples,wMax)
927     TYPE (FPUsystem),      INTENT(INOUT)        :: sys
928     INTEGER, DIMENSION(:), INTENT(IN)   :: Xsample
929     REAL (double),DIMENSION(:),INTENT(OUT):: w
930     REAL (double),DIMENSION(:,:),INTENT(OUT):: yData, vData
931     INTEGER,               INTENT(IN)   :: Nx, Log2FFTSamples
932     REAL (double), OPTIONAL, INTENT(IN) :: wMax

933     INTEGER                             :: FFTSamples,FFTiters
934     REAL (double), DIMENSION(:),ALLOCATABLE     :: u,wSin,wCos,FFTemp
935     REAL (double)                       :: azero,OmegaMax

936     INTEGER :: i,j

937     FFTSamples = 2**Log2FFTSamples
938     ALLOCATE(FFTemp(4*FFTSamples+1))
939     ALLOCATE(u(FFTSamples))
940     ALLOCATE(wSin(FFTSamples))
941     ALLOCATE(wCos(FFTSamples))

942     IF (PRESENT(wMax)) THEN
943        OmegaMax = wMax
944     ELSE
945        OmegaMax = 2._double
946     END IF
947     FFTiters = MAX(INT(0.5 + PI / sys%dT / OmegaMax),1)
948     DO i = 1,FFTSamples/2
949       w(i) = TWO * i * PI/(1.*FFTSamples)/(sys%dT*FFTIters)
950     END DO

951     CALL EZFFTI(FFTSamples,FFTemp)

952     DO i = 1,FFTSamples
953        CALL Integrate(sys,FFTiters)
954        DO j = 1,Nx
955          yData(j,i) = sys%y(Xsample(j))
956          vData(j,i) = sys%v(Xsample(j))
957        END DO
```

```
958      END DO

959      DO j = 1,Nx
960         u(1:FFTSamples) = yData(j,1:FFTSamples)
961         CALL EZFFTF(FFTSamples,u,azero,wSin,wCos,FFTemp)
962  !      yData(j,1:FFTSamples/2) = &
963  !        SQRT(wSin(1:FFTSamples/2)**2 + wCos(1:FFTSamples/2)**2)

964         u(1:FFTSamples) = vData(j,1:FFTSamples)
965         CALL EZFFTF(FFTSamples,u,azero,wSin,wCos,FFTemp)
966         vData(j,1:FFTSamples/2) = &
967           SQRT(wSin(1:FFTSamples/2)**2 + wCos(1:FFTSamples/2)**2)

968         u(1:FFTSamples) = yData(j,1:FFTSamples)
969         CALL EZFFTF(FFTSamples,u,azero,wSin,wCos,FFTemp)
970         yData(j,1:FFTSamples/2) = &
971           SQRT(wSin(1:FFTSamples/2)**2 + wCos(1:FFTSamples/2)**2)

972      END DO

973      DEALLOCATE(FFTemp)
974      DEALLOCATE(u)
975      DEALLOCATE(wSin)
976      DEALLOCATE(wCos)
977    END SUBROUTINE FFTw
```

fpu: FFTk()

```
978   !!!!!!!!!!!!!!!!!!!!!!!!!!!!!!!!!!!!!!!!!!!!!!!!!!!!!!!!!!!!
979   !  FFTk performs an x/k FFT on a system.
980   !  A single FFT can be calculated, or the average over
981   !    Nsamples x iters
982   !!!!!!!!!!!!!!!!!!!!!!!!!!!!!!!!!!!!!!!!!!!!!!!!!!!!!!!!!!!!
983   SUBROUTINE FFTk(sys,k,yData,vData,Nsamples,iters)
984     TYPE (FPUsystem),      INTENT(INOUT)        :: sys
985     REAL (double),DIMENSION(:),INTENT(OUT):: k
986     REAL (double),DIMENSION(:,:),INTENT(OUT):: yData, vData
987     INTEGER, INTENT(IN)                 :: Nsamples,iters

988     REAL (double), DIMENSION(:), ALLOCATABLE :: kSin,kCos,FFTemp
989     REAL (double)               :: azero
990     INTEGER :: N, i

991     N = sys%Length

992     k = (/ (TWO*PI*i/N, i=1,N/2) /)

993     ALLOCATE(kSin(N))
994     ALLOCATE(kCos(N))
995     ALLOCATE(FFTemp(4*N))

996     CALL EZFFTI(N,FFTemp)



997     CALL EZFFTF(N,sys%y,azero,kSin,kCos,FFTemp)
998     yData(1,1:N/2) = &
999       SQRT(kSin(1:N/2)**2 + kCos(1:N/2)**2)

1000    CALL EZFFTF(N,sys%v,azero,kSin,kCos,FFTemp)
1001    vData(1,1:N/2) = &
1002      SQRT(kSin(1:N/2)**2 + kCos(1:N/2)**2)

1003    DO i = 2, Nsamples
1004      CALL Integrate(sys,iters)

1005      CALL EZFFTF(N,sys%y,azero,kSin,kCos,FFTemp)
1006      yData(i,1:N/2) = &
1007        SQRT(kSin(1:N/2)**2 + kCos(1:N/2)**2)

1008      CALL EZFFTF(N,sys%v,azero,kSin,kCos,FFTemp)
1009      vData(i,1:N/2) = &
1010        SQRT(kSin(1:N/2)**2 + kCos(1:N/2)**2)
```

```
1011      END DO

1012      DEALLOCATE(kSin)
1013      DEALLOCATE(kCos)
1014      DEALLOCATE(FFTemp)
1015    END SUBROUTINE FFTk
```

fpu: WriteSystem()

```
1016  !!!!!!!!!!!!!!!!!!!!!!!!!!!!!!!!!!!!!!!!!!!!!!!!!!!!!!!!!!!!
1017  !  WriteSystem() facilitates writing sufficient information to a
1018  !    file that the integration can resume from the present state.
1019  !!!!!!!!!!!!!!!!!!!!!!!!!!!!!!!!!!!!!!!!!!!!!!!!!!!!!!!!!!!!

1020  SUBROUTINE WriteSystem(sys,FileName,UnitNumber,Xstart)
1021    TYPE (FPUsystem), INTENT(IN)        :: sys
1022    CHARACTER(len=*), INTENT(IN)        :: FileName
1023    INTEGER, OPTIONAL, INTENT(IN)       :: UnitNumber
1024    INTEGER, OPTIONAL, INTENT(IN)       :: Xstart

1025    INTEGER     :: Unum=9, i, Xo=0

1026    IF (PRESENT(UnitNumber)) THEN
1027       Unum = UnitNumber
1028    ELSE
1029       Unum = 9
1030    END IF

1031    IF ( PRESENT(Xstart) ) THEN
1032      Xo = Xstart
1033    END IF

1034    OPEN(UNIT=Unum,FILE=FileName,STATUS='REPLACE')
1035     WRITE(Unum,LINE_1_FMT) FILE_VERSION
1036     WRITE(Unum,LINE_2_FMT) sys%Length, sys%Config, &
1037                                        sys%IntegrationOrder
1038     WRITE(Unum,LINE_3_FMT) sys%dT, sys%MaxFreq, sys%time
1039     WRITE(Unum,LINE_4_FMT) sys%MaxExponent
1040     WRITE(Unum,LINE_5_FMT) sys%alpha(1:sys%MaxExponent)
1041     WRITE(Unum,LINE_6_FMT) sys%MPI_Buffer,sys%MPI_Xleft
1042     DO i = 0, sys%Nmasses+1
1043       WRITE(Unum,LINE_N_FMT) i+Xo, sys%y(i), sys%v(i), sys%mass(i)
1044     END DO
1045    CLOSE(Unum)

1046  END SUBROUTINE WriteSystem
```

fpu: ReadSystem()

```
1047  !!!!!!!!!!!!!!!!!!!!!!!!!!!!!!!!!!!!!!!!!!!!!!!!!!!!!!!!!!!!
1048  !  ReadSystem() is the complementary subroutine to WriteSystem().
1049  !  sys should not have been initialized.  That is done here.
1050  !!!!!!!!!!!!!!!!!!!!!!!!!!!!!!!!!!!!!!!!!!!!!!!!!!!!!!!!!!!!

1051  SUBROUTINE ReadSystem(sys,FileName,UnitNumber)
1052    TYPE (FPUsystem), INTENT(INOUT)     :: sys
1053    CHARACTER(len=*), INTENT(IN)        :: FileName
1054    INTEGER, OPTIONAL, INTENT(IN)       :: UnitNumber
1055    INTEGER     :: Unum,i,j
1056    INTEGER     :: CheckVersion, Length, Configuration, IntOrder
1057    CHARACTER(len=128)                  :: DUMMY_STR

1058    IF (PRESENT(UnitNumber)) THEN
1059      Unum = UnitNumber
1060    ELSE
1061      Unum = 9
1062    END IF

1063    OPEN(UNIT=Unum,FILE=FileName,STATUS='OLD')
1064     READ (Unum,LINE_1_FMT) CheckVersion
1065     IF (CheckVersion.NE.FILE_VERSION) THEN
1066       IF (CheckVersion.LT.FILE_VERSION) THEN
1067         PRINT *,'WARNING: old system data file version.'
1068         PRINT *,' '
1069       ELSE
1070         PRINT *,'ERROR: Unknown system data file version!'
1071         PRINT *,' '
1072         STOP
1073       END IF
1074     END IF

1075     READ(Unum,LINE_2_FMT) Length, Configuration, IntOrder
1076     CALL Init(sys,Length,Configuration,IntOrder)

1077     READ(Unum,LINE_3_FMT) sys%dT, sys%MaxFreq, sys%time
1078     READ(Unum,LINE_4_FMT) sys%MaxExponent
1079     READ(Unum,LINE_5_FMT) sys%alpha(1:sys%MaxExponent)
1080     READ(Unum,LINE_6_FMT) sys%MPI_Buffer,sys%MPI_Xleft
1081     READ(Unum,LINE_7_FMT) DUMMY_STR
1082     DO i = 0, sys%Nmasses+1
1083       READ(Unum,LINE_N_FMT) j, sys%y(i), sys%v(i), sys%mass(i)
1084     END DO
1085    CLOSE(Unum)
```

```
1086      sys%invmass(1:sys%Nmasses) = 1._double/sys%mass(1:sys%Nmasses)
1087    END SUBROUTINE ReadSystem
```

fpu: Nmodes()

```
!!!!!!!!!!!!!!!!!!!!!!!!!!!!!!!!!!!!!!!!!!!!!!!!!!!!!!!!!!!!
!    Nmodes
!
!      Estiamte the number of modes participating in the
!           oscillations.
!    1. Copy the existing system
!    2. Integrate the pseudo-system
!    3. Calculate FFTw for harmonic mode components
!    4.     e(w) = E(w) / sum_w E(w)
!    5. Calculate entropy:   S = sum_w e(w) ln(e(w))
!    6. Nmodes = exp(S)
!
!!!!!!!!!!!!!!!!!!!!!!!!!!!!!!!!!!!!!!!!!!!!!!!!!!!!!!!!!!!!

SUBROUTINE Nmodes(NmodesSys,Log2FFTSamples,Nx,Xsample,Neff)
  TYPE (FPUsystem), INTENT(IN)        :: NmodesSys
  INTEGER, INTENT(IN)                 :: Log2FFTSamples, Nx
  INTEGER, DIMENSION(:), INTENT(IN)   :: Xsample
  REAL (double), DIMENSION(:), INTENT(OUT)    :: Neff

  TYPE (FPUsystem)                    :: CopySys
  REAL (double), DIMENSION(:), ALLOCATABLE    :: w
  REAL (double), DIMENSION(:,:), ALLOCATABLE  :: yData, vData
  REAL (double), DIMENSION(:), ALLOCATABLE    :: Ei
  REAL (double)                       :: S
  INTEGER                             :: FFTSamples, Ni

  INTEGER     :: i

  FFTSamples = 2**Log2FFTSamples
  ALLOCATE(w(FFTSamples))
  ALLOCATE(Ei(FFTSamples/2))
  ALLOCATE(yData(Nx,FFTSamples))
  ALLOCATE(vData(Nx,FFTSamples))

  !   CALL Copy(sys,CopySys)
  !   CALL FFTw(CopySys,w,yData,vData,Xsample,Nx,Log2FFTSamples)

  CALL FFTw(NmodesSys,w,yData,vData,Xsample,Nx,Log2FFTSamples)

  !   DO i = 1, FFTSamples/2
  !     PRINT *, w(i), yData(i), vData(i)
  !   END DO
```

```
1124      Ni = FFTSamples / 2
1125      DO i = 1, Nx
1126        Ei(1:Ni) = 0.5 * NmodesSys%mass(Xsample(i)) * &
1127                   (yData(i,1:Ni)**2 * w(1:Ni)**2 + vData(i,1:Ni)**2)
1128        Ei = Ei / SUM(Ei)
1129        S = - SUM(Ei * LOG(Ei))
1130        Neff(i) = EXP(S)
1131      END DO

1132      !   CALL Clear(CopySys)

1133      DEALLOCATE(w)
1134      DEALLOCATE(Ei)
1135      DEALLOCATE(yData)
1136      DEALLOCATE(vData)
1137    END SUBROUTINE Nmodes
```

fpu: Eflux()

```
1138    !!!!!!!!!!!!!!!!!!!!!!!!!!!!!!!!!!!!!!!!!!!!!!!!!!!!!!!!!!!!
1139    !  Eflux(sys,index) calculates the energy flux at site index
1140    !!!!!!!!!!!!!!!!!!!!!!!!!!!!!!!!!!!!!!!!!!!!!!!!!!!!!!!!!!!

1141    REAL (double) FUNCTION Eflux(sys,index) RESULT (flux)
1142      TYPE (FPUsystem), INTENT(IN)        :: sys
1143      INTEGER, INTENT(IN)                 :: index

1144      flux = sys%F(index) * sys%v(index)
1145    END FUNCTION Eflux


1146  END MODULE fpu
```

BIBLIOGRAPHY

[1] I. M. Lifshits, S. A. Gredeskul, and L. A. Pastur, *Introduction to the Theory of Disordered Systems* (Wiley & Sons, New York, 1988).

[2] P. Sheng, ed., *Scattering and Localization of Classical Waves in Random Media* (World Scientific, New Jersey, 1990).

[3] S. A. Gredeskul and Y. S. Kivshar, Phys. Rep. **216**, 1 (1992).

[4] W. Jones and N. H. March, *Theoretical Solid State Physics*, vol. 1 (Wiley-Interscience, London, 1973).

[5] P. W. Anderson, Phys. Rev. **109**, 1492 (1958).

[6] N. F. Mott, Rev. Mod. Phys. **40**, 677 (1968).

[7] F. Dominguez-Adame and V. A. Malyshev, Amer. J. Phys. **72**, 226 (2004).

[8] P. M. Morse and H. Feshbach, *Methods of Theoretical Physics* (McGraw-Hill, 1953).

[9] B. I. Halperin, Adv. Chem. Phys. **13**, 123 (1967).

[10] N. F. Mott and W. D. Twose, Adv. Phys. **10**, 107 (1961).

[11] R. E. Borland, Proc. Roy. Soc. Lond. A **274**, 529 (1963).

[12] H. Schmidt, Phys. Rev. **105**, 425 (1957).

[13] H. Matsuda and K. Ishii, Prog. Theor. Phys. Suppl. pp. 56–86 (1970).

[14] H. Furstenberg, Trans. Amer. Math. Soc. **108**, 377 (1963).

[15] K. Ishii, Prog. Theor. Phys. Suppl. pp. 77–138 (1973).

[16] B. Kramer and A. MacKinnon, Rep. Prog. Phys. **56**, 1469 (1993).

[17] E. Abrahams, P. W. Anderson, D. C. Licciardello, and T. V. Ramakrishnan, Phys. Rev. Lett. **42**, 673 (1979).

[18] E. N. Economou and C. M. Soukoulis, Phys. Rev. Lett. **46** (1981).

[19] D. S. Fisher and P. A. Lee, Phys. Rev. B **23**, 6851 (1981).

[20] D. J. Thouless, Phys. Rev. Lett. **47**, 972 (1981).

[21] R. Landauer, Philos. Mag. **21**, 863 (1970).

[22] P. W. Anderson, D. J. Thouless, E. Abrahams, and D. S. Fisher, Phys. Rev. B **22**, 3519 (1980).

[23] P. W. Anderson and P. A. Lee, Prog. Theor. Phys. Suppl. pp. 212–219 (1980).

[24] R. de L. Kronig and W. G. Penney, Proc. Roy. Soc. Lond. A **130**, 499 (1931).

[25] A. MacKinnon and B. Kramer, Phys. Rev. Lett. **47**, 1546 (1981).

[26] A. MacKinnon and B. Kramer, Z. Phys. B **53**, 1 (1983).

[27] G. Czycholl and B. Kramer, Z. Phys. B **39**, 193 (1980).

[28] D. C. Herbert and R. Jones, J. Phys. C **4**, 1145 (1971).

[29] D. J. Thouless, J. Phys. C **5**, 77 (1972).

[30] E. N. Economou, *Green's Functions in Quantum Physics* (Springer-Verlag, Berlin, 1983), 2nd ed.

[31] P. Devillard and B. Souillard, J. Stat. Phys. **43**, 423 (1986).

[32] P. Bougerol and J. Lacroix, *Random Products of Matrices with Applications to Schrödinger Operators* (Birkhaüser, Basel, Switzerland, 1985).

[33] B. Doucot and R. Rammal, Europhys. Lett. **3**, 969 (1987).

[34] D. L. Shepelyansky, Phys. Rev. Lett. **70**, 1787 (1993).

[35] E. Fermi, J. Pasta, and S. Ulam, Tech. Rep., Los Alamos Scientific Laboratory (1955).

[36] D. Beeman, J. Comput. Phys. **20**, 130 (1976).

[37] W. H. Press, B. P. Flannery, S. A. Teukolsky, and W. T. Vetterling, *Numerical Recipes* (Cambridge University Press, New York, 1988).

[38] J. Dormand, *Numerical Methods for Differential Equations* (CRC Press, 1996).

[39] J. Candy and W. Rozmus, J. Comput. Phys. **92**, 230 (1991).

[40] H. Yoshida, Phys. Lett. A **150**, 262 (1990).

[41] C. Kittel, *Introduction to Solid State Physics* (Wiley, 1986), sixth ed.

[42] L. Brillouin, *Wave Propagation in Periodic Structures* (Dover Publications, 1953).

[43] P. M. Morse and K. U. Ingard, *Theoretical Acoustics* (Princeton University Press, 1968).

[44] T. Dauxois, S. Ruffo, and A. Torcini, Phys. Rev. E **56**, R6229 (1997).

[45] S. Takeno, K. Kisoda, and A. J. Sievers, Prog. Theor. Phys. Suppl. **94**, 242 (1988).

[46] R. Khomeriki, S. Lepri, and S. Ruffo (2004), `cond-mat/0407134`.

[47] J. M. Ziman, *Models of Disorder* (Cambridge University Press, Cambridge, 1979).

[48] J. Hori, *Spectral Properties of Disordered Chains and Lattices* (Pergamon Press, Oxford, 1968).

[49] P. Dean, Proc. Roy. Soc. Lond. **254**, 507 (1960).

[50] P. Dean, Proc. Roy. Soc. Lond. **260**, 263 (1961).

[51] M. Tabor, *Chaos and Integrability in Nonlinear Dynamics: An Introduction* (John Wiley & Sons, New York, 1989).

[52] T. Cretegny, T. Dauxois, S. Ruffo, and A. Torcini, Physica D **121**, 106 (1998), `cond-mat/9709204`.

[53] T. Cretegny, T. Dauxois, S. Ruffo, and A. Torcini, *Localization and equipartition of energy in the beta-FPU chain : Chaotic breathers* (1997), `cond-mat/9709204`.

[54] J. D. Luca, A. J. Lichtenberg, and S. Ruffo, Phys. Rev. E **51**, 2877 (1995).

[55] J. D. Luca, A. J. Lichtenberg, and M. A. Lieberman, Chaos **5**, 283 (1995).

[56] R. Livi, M. Pettini, S. Ruffo, M. Sparpaglione, and A. Vulpiani, Phys. Rev. A **31**, 1039 (1985).

[57] R. Livi, M. Pettini, S. Ruffo, M. Sparpaglione, and A. Vulpiani, Phys. Rev. A **28**, 3544 (1983).

[58] C. E. Shannon and W. Weaver, *The Mathematical Theory of Communication* (University of Illinois Press, Urbana, Ill., 1949).

[59] L. Brillouin, *Science and Information Theory* (Academic Press, New York, 1956).

[60] G. Arfken, *Mathematical Methods for Physicists* (Academic Press, New York, 1970).

[61] Z. Rieder, J. L. Lebowitz, and E. Lieb, J. Math. Phys. **8**, 1073 (1967).

[62] A. Casher and J. L. Lebowitz, J. Math. Phys. **12**, 1701 (1971).

[63] A. J. O'Connor and J. L. Lebowitz, J. Math. Phys. **15**, 692 (1974).

[64] M. Bolsterli, M. Rich, and W. M. Visscher, Phys. Rev. A **1**, 1086 (1970).

[65] H. Yamada and K. S. Ikeda, Phys. Rev. E **65**, 046211 (2002).

[66] H. Yamada and K. S. Ikeda, Phys. Rev. E **59**, 5214 (1999).

[67] R. E. Peierls, *Quantum Theory of Solids* (Oxford University Press, London, 1955).

[68] S. Lepri, R. Livi, and A. Politi, Phys. Rev. Lett. **78**, 1896 (1997).

[69] D. N. Payton, M. Rich, and W. M. Visscher, Phys. Rev. **160**, 706 (1967).

[70] E. A. Jackson, J. R. Pasta, and J. F. Waters, J. Comput. Phys. **2**, 207 (1968).

[71] B. Li, H. Zhao, and B. Hu, Phys. Rev. Lett. **86**, 63 (2001).

[72] B. Hu, B. Li, and H. Zhao, Phys. Rev. E **57**, 2992 (1998).

[73] R. Bourbonnais and R. Maynard, Phys. Rev. Lett. **64**, 1397 (1990).

[74] R. Bourbonnais and R. Maynard, Int. J. Mod. Phys. C **1**, 233 (1990).

[75] M. Wagner, G. Zavt, J. Vazquez-Marquez, A. Lütze, T. Mougios, G. Viliani, W. Frizzera, O. Pilla, and M. Montagna, Philos. Mag. B **65**, 273 (1992).

[76] A. Rosas and K. Lindenberg, Phys. Rev. E **69** (2004).

[77] A. Sarmiento, R. Reigada, A. H. Romero, and K. Lindenberg, Phys. Rev. E **60**, 5317 (1999).

[78] L. Onsager, Phys. Rev. **37**, 405 (1931).

[79] L. Onsager, Phys. Rev. **38**, 2265 (1931).

[80] H. Mori, Phys. Rev. **112**, 1829 (1958).

[81] M. Green, J. Chem. Phys. **22**, 398 (1954).

[82] J. P. Boon and S. Yip, *Molecular Hydrodynamics* (Dover Publications, New York, 1991).

[83] E. Helfand, Phys. Rev. **119**, 1 (1960).

[84] D. J. Evans and G. P. Morriss, *Statistical Mechanics of Nonequilibrium Liquids* (Academic Press, London, 1990).

[85] F. Zhang, D. J. Isbister, and D. J. Evans, Phys. Rev. E **61**, 3541 (2000).

[86] A. Fillipov, B. Hu, B. W. Li, and A. Zeltser, J. Phys. A **31**, 7719 (1998).

[87] D. J. Evans, Phys. Lett. **91A**, 457 (1982).

[88] P. Sheng, B. White, Z.-Q. Zhang, and G. Papanicolaou, Phys. Rev. B **34**, 4757 (1986).

[89] M. Y. Azbel and P. Soven, Phys. Rev. Lett. **49**, 751 (1982).

[90] H. Goldstein, *Classical Mechanics* (Addison-Wesley, Reading, MA, 1980), 2nd ed.

[91] Y. S. Kivshar, S. A. Gredeskul, A. Sánchez, and L. Vázquez, Phys. Rev. Lett. **64**, 1693 (1990).

[92] J. Neter, W. Wasserman, and M. H. Kutner, *Applied Linear Statistical Models* (Irwin, Homewood, Ill., 1985).

[93] L. I. Deych, A. A. Lisyansky, and B. L. Altshuler, Phys. Rev. B **64**, 224202 (2001).

[94] BIPM, *Guide to the Expression of Uncertainty in Measurement* (International Organization for Standardization (ISO), Genève, Switzerland, 1993), ISBN 92-67-10188-9.

[95] M. Y. Azbel and P. Soven, Phys. Rev. B **27**, 831 (1983).

[96] M. Y. Azbel, Phys. Rev. B **28**, 4106 (1983).

[97] J. Ford, Phys. Rep. **213**, 271 (1992).

[98] L. Casetti, M. Cerruti-Sola, M. Pettini, and E. G. D. Cohen, Phys. Rev. E **55**, 6566 (1997).

[99] J. D. Luca and A. Lichtenberg, Phys. Rev. E **66**, 026206 (2002).

[100] P. A. Lee and T. V. Ramakrishnan, Rev. Mod. Phys. **57**, 287 (1985).

[101] S. Lepri, Phys. Rev. E **58**, 7165 (1998).

[102] T. Held, I. Pfeiffer, and W. Kuhn, Phys. Rev. B **55**, 231 (1997).

[103] S. Rohmfeld, M. Hundhausen, L. Ley, N. Schulze, and G. Pensl, Phys. Rev. Lett. **86**, 826 (2001).

[104] F. Widulle, J. Serrano, and M. Cardona, Phys. Rev. B **65**, 075206 (2002).

[105] I. Y. Solodov and B. A. Korshak, Phys. Rev. Lett. **88**, 014303 (2002).

[106] I. Solodov, J. Wackerl, K. Pfleiderer, and G. Busse, Appl. Phys. Lett. **84**, 5386 (2004).

[107] Technically speaking, the thermal conductivity as usually defined (as system size $\to \infty$) is zero. Here, we use the term 'thermal conductivity' in a more general sense.

[108] F. Piazza, S. Lepri, and R. Livi, J. Phys. A **34**, 9803 (2001).

[109] D. M. Leitner, Phys. Rev. B **64** (2001).

[110] J. Fabian and P. B. Allen, Phys. Rev. Lett. **77**, 3839 (1997).

[111] K. A. Snyder and T. R. Kirkpatrick, Phys. Rev. B **70**, 104201 (2004).

[112] J. Fröhlich, T. Spencer, and C. E. Wayne, J. Stat. Phys. **42**, 247 (1986).

[113] K. A. Snyder and T. R. Kirkpatrick, Ann. Phys. (Leipzig) **8**, SI 241 (1999).

[114] D. S. Saxon and R. A. Hunter, Philips Res. Rep. **4**, 81 (1949).

[115] J. M. Luttinger, Philips Res. Rep. **6**, 303 (1951).

[116] D. N. Payton and W. M. Visscher, Phys. Rev. **156**, 1032 (1967).

[117] D. N. Payton and W. M. Visscher, Phys. Rev. **154**, 802 (1967).

[118] H. Kinoshita, H. Yoshida, and H. Nakai, Celest. Mech. **50**, 59 (1991).

[119] L. D. Landau and E. M. Lifshitz, *Theory of Elasticity* (Pergamon Press, New York, 1986).

[120] C. J. Joachain, *Quantum Collision Theory*, vol. I and II (Elsevier Science, 1984).

[121] R. Shankar, *Principles of Quantum Mechanics* (Plenum Press, 1980).